3D SYNTHETIC APERTURE FOR CONTROLLED-SOURCE ELECTROMAGNETICS

by

Allison Knaak

ProQuest LLC.
789 East Eisenhower Parkway
P.O. Box 1346
Ann Arbor, MI 48106 - 1346

A thesis submitted to the Faculty and the Board of Trustees of the Colorado School of Mines in partial fulfillment of the requirements for the degree of Doctor of Philosophy (Geophysics).

Golden, Colorado

Date _____

Signed: _____
Allison Knaak

Signed: _____
Dr. Roel Snieder
Thesis Advisor

Golden, Colorado

Date _____

Signed: _____
Dr. Terry Young
Professor and Head
Department of Geophysics

ABSTRACT

Locating hydrocarbon reservoirs has become more challenging with smaller, deeper or shallower targets in complicated environments. Controlled-source electromagnetics (CSEM), is a geophysical electromagnetic method used to detect and derisk hydrocarbon reservoirs in marine settings, but it is limited by the size of the target, low-spatial resolution, and depth of the reservoir. To reduce the impact of complicated settings and improve the detecting capabilities of CSEM, I apply synthetic aperture to CSEM responses, which virtually increases the length and width of the CSEM source by combining the responses from multiple individual sources. Applying a weight to each source steers or focuses the synthetic aperture source array in the inline and crossline directions. To evaluate the benefits of a 2D source distribution, I test steered synthetic aperture on 3D diffusive fields and view the changes with a new visualization technique. Then I apply 2D steered synthetic aperture to 3D noisy synthetic CSEM fields, which increases the detectability of the reservoir significantly. With more general weighting, I develop an optimization method to find the optimal weights for synthetic aperture arrays that adapts to the information in the CSEM data. The application of optimally weighted synthetic aperture to noisy, simulated electromagnetic fields reduces the presence of noise, increases detectability, and better defines the lateral extent of the target. I then modify the optimization method to include a term that minimizes the variance of random, independent noise. With the application of the modified optimization method, the weighted synthetic aperture responses amplifies the anomaly from the reservoir, lowers the noise floor, and reduces noise streaks in noisy CSEM responses from sources offset kilometers from the receivers. Even with changes to the location of the reservoir and perturbations to the physical properties, synthetic aperture is still able to highlight targets correctly, which allows use of the method in locations where the subsurface models are built from only estimates. In addition to the technical work in this thesis, I explore the interface between

science, government, and society by examining the controversy over hydraulic fracturing and by suggesting a process to aid the debate and possibly other future controversies.

TABLE OF CONTENTS

ABSTRACT iii

LIST OF FIGURES AND TABLES ix

ACKNOWLEDGMENTS xvi

DEDICATION xix

CHAPTER 1 GENERAL INTRODUCTION 1

1.1 Thesis overview 4

CHAPTER 2 SYNTHETIC APERTURE WITH DIFFUSIVE FIELDS 9

2.1 Abstract 9

2.2 Introduction 9

2.3 3D Synthetic Aperture and Beamforming 11

2.3.1 Numerical Examples 13

2.4 3D Visualization 17

2.4.1 Numerical Examples 19

2.5 Discussion and Conclusions 27

2.6 Acknowledgments 27

CHAPTER 3 3D SYNTHETIC APERTURE FOR CSEM 28

3.1 Abstract 28

3.2 Introduction 28

3.3 Mathematical basis 30

3.4 Numerical examples 32

3.5 Visualizing steered fields in 3D 35
3.6 Conclusion 38
3.7 Acknowledgments 39
CHAPTER 4 OPTIMIZED 3D SYNTHETIC APERTURE FOR CSEM 40
4.1 Abstract 40
4.2 Introduction 41
4.3 Weighted synthetic aperture 42
4.4 Optimizing the weights for synthetic aperture 43
4.5 Synthetic examples 47
4.5.1 Increasing detectability 49
4.5.2 Increasing lateral detectability 53
4.6 Conclusion 57
4.7 Acknowledgments 57
CHAPTER 5 ERROR PROPAGATION WITH SYNTHETIC APERTURE 58
5.1 Introduction 58
5.2 Error propagation theory with synthetic aperture 59
5.3 Reducing error propagation with optimization 61
5.4 Synthetic example 65
5.5 Conclusion 76
5.6 Acknowledgments 77
CHAPTER 6 THE SENSITIVITY OF SYNTHETIC APERTURE FOR CSEM 78
6.1 Introduction 78
6.2 Testing sensitivity 79

6.2.1 Perturbing the model 80

6.2.2 Uncertainty in the location of the target 89

6.3 Conclusion 100

6.4 Acknowledgments 101

CHAPTER 7 FRACTURED ROCK, PUBLIC RUPTURES: THE HYDRAULIC FRACTURING DEBATE 102

7.1 Introduction 102

7.2 Participatory models 106

7.3 Background 109

7.3.1 Entrance of hydraulic fracturing and regulations 109

7.3.2 Key new technology 111

7.3.3 Current practices 112

7.3.4 Shale gas and major plays 113

7.3.5 Current regulations 116

7.4 The fracking debate 118

7.4.1 Hydraulic fracturing documentaries 122

7.5 Fracking as a post-normal technology 126

7.5.1 System uncertainties 126

7.5.2 Decision stakes 130

7.6 Importance of Deliberation 133

7.6.1 Challenges to a democratic approach 134

7.6.2 Extended peer communities/extended participation model 138

7.7 Summary 142

CHAPTER 8 GENERAL CONCLUSIONS 143

REFERENCES CITED 147

LIST OF FIGURES AND TABLES

Figure 1.1 A diagram showing the main components of synthetic aperture radar. Taken from Avery & Berlin. 3

Figure 1.2 A diagram depicting synthetic aperture implemented in ultrasound imaging. Taken from Jensen *et al.*. 4

Figure 2.1 The design of a traditional CSEM survey. The individual source, $\mathbf{s_1}$, is defined to be located at the origin. The steering angle, $\hat{\mathbf{n}}$, is a function of θ, the dip and φ which is either 0° or 90° to steer in the inline or crossline directions, respectively. 14

Figure 2.2 The point-source 3D scalar diffusive field log-transformed with the source at (0,0,0). 14

Figure 2.3 The unsteered 3D scalar diffusive field log-transformed. 15

Figure 2.4 The 3D scalar diffusive field log-transformed and steered at a 45° angle in the inline direction. The arrow shows the shift in the x-direction of the energy from the origin; without steering the maximum energy would be located at the center of the source lines (x= 0km). 16

Figure 2.5 The 3D scalar diffusive field log-transformed and steered at a 45° angle in the crossline direction. The arrow shows the shift in the energy from the centerline of the survey (y= 0km). The shift is less than in 16

Figure 2.6 The 3D scalar diffusive field log-transformed and steered at a 45° angle in the inline and crossline directions. The arrows demonstrate the shift in the energy in the x- and y- directions. 17

Figure 2.7 The unwrapped phase of a scalar diffusive field from a point-source located at (0,0,0). The colorbar displays radians. 19

Figure 2.8 The normalized gradient of a scalar diffusive field from a point-source location at (0,0,0). 20

Figure 2.9 The phase-binned gradient of a scalar diffusive field from a point-source located at (0,0,0). The change in direction occurs from the time-harmonic point-source. 20

Figure 2.10 The unwrapped phase of a scalar diffusive field with five lines of synthetic aperture sources. The colorbar displays radians. 21

Figure 2.11 The normalized gradient of a scalar diffusive field with five synthetic aperture sources. 21

Figure 2.12 The phase-binned gradient of a scalar diffusive field with five unsteered synthetic aperture sources. The movement of the energy is symmetric about both the x and y directions. 22

Figure 2.13 The phase-binned gradient of a scalar diffusive field with five synthetic aperture sources steered in the inline direction at a 45°. The energy is moving asymmetrically in the x-direction unlike the symmetric movement of the unsteered field. 23

Figure 2.14 The phase-binned gradient of a scalar diffusive field with five synthetic aperture sources steered in the crossline direction at 45°. The energy is moving asymmetrically in the negative y-direction in contrast to the symmetric movement of the unsteered field. 24

Figure 2.15 The phase-binned gradient of a scalar diffusive field steered in the inline and crossline directions at 45°. The combined inline and crossline steering produces a field whose energy moves out asymmetrically in both the x- and y-directions. 25

Figure 2.16 The y-z view of the unsteered diffusive field, panel a), and the combined inline and crossline steered diffusive field, panel b), at a phase of 3π. The oval highlights the change in the direction of the field caused by steering. 26

Figure 3.1 The model used to create the synthetic CSEM data. The values of ρ_H and ρ_V are the resistivity of the layer in the horizontal and vertical direction respectively given in Ohm-meters. 33

Figure 3.2 The geometry of the CSEM survey for the synthetic data. The seven towlines are shown as black lines. The reservoir is the black rectangle. The 3D box outlines the coverage of the sampling points. 33

Figure 3.3 The ratio of the absolute value of the inline electric component for a single source (panel a), a 2D synthetic aperture source (panel b), and a steered 2D synthetic aperture source (panel c). All three images depict the response at receivers located on the ocean floor. The footprint of the reservoir is outlined in black and the source is outlined in red. The area of expected reservoir anomaly is shown as the dashed black box. . . 36

Figure 3.4 The normalized, time-averaged Poynting vectors with z-component greater than zero for a single source (panel a), a 2D synthetic aperture source (panel b), and a steered 2D synthetic aperture source (panel c). The Poynting vectors from the 2km water layer (including the airwave) have been removed for clarity. All three images depict the footprint of the reservoir in black and the source in blue. 37

Figure 4.1 An illustration of the optimization problem depicted with 2D shapes. The squared absolute value of the difference is the equation for an ellipsoid and the weighting constraint is the equation for a sphere. The vector that lies along the principal axis of the ellipsoid is the vector of optimal weights. 46

Figure 4.2 An inline cross-section of the model used to generate the electromagnetic fields. The first layer is water with a depth of 200 m. There are five sediment layers with varying resistivity. The reservoirs are shown as the white rectangles. The vertical scale is exaggerated. . . . 48

Figure 4.3 The survey geometry used to create the synthetic CSEM data. The sources are shown as black dots and the receivers are the gray triangles. The locations of the reservoirs are outlined in black. 48

Figure 4.4 The normalized difference of the inline electric pay field and the inline electric wet field with 10^{-15} V/Am^2 independent random noise added for the original data (panel a), the optimal 2D steered synthetic aperture source array (panel b), and the optimal crossline steered synthetic aperture source array (panel c). 50

Figure 4.5 A map view of the amplitude (panel a) and the phase (panel b) of the optimal weights for the 2D synthetic aperture source array centered at -8.26 km for the responses from the receiver specified by the gray triangle. 53

Figure 4.6 A map view of the amplitude (panel a) and the phase (panel b) of the optimal weights for the 2D synthetic aperture source array centered at 3.08 km for the response from the receiver specified by the gray triangle. . 54

Figure 4.7 Panel a shows the phase of the optimal and calculated weights for a crossline synthetic aperture source array located at -17.44 km. Panel b shows the calculated focus point (the circle over the left reservoir) for the crossline synthetic aperture created from the five sources shown as black dots for a receiver located in the center of the survey. 56

Figure 5.1 The model used to create the synthetic CSEM data. The values of ρ_H and ρ_V are the resistivity of the layer in the horizontal and vertical directions, respectively, given in Ohm-meters. 66

Figure 5.2 The survey geometry used to create the synthetic CSEM data. The towlines are the black lines with the source locations marked as black dots and the receiver locations marked as the black triangles. The location of the reservoir is outlined in black. 66

Figure 5.3 Left panel: A pseudo cross-section displaying the normalized difference of the original inline electric response for the towline located at 6 km crossline and receivers located at 0 km crossline with 10^{-15} V/Am^2 independent, random noise added. Middle panel: The same original inline electric response as the first panel without noise. Right panel: The random independent noise present in the first panel found by taking the difference between the first two images. 68

Figure 5.4 A map view of the survey geometry with one location of the synthetic aperture source array shown as the red rectangle. 69

Figure 5.5 Left panel: A pseudo cross-section displaying the normalized difference of the unweighted 2D synthetic aperture response for the inline electric component with 10^{-15} V/Am^2 independent, random noise added. Middle panel: The same unweighted synthetic aperture response as the first panel without noise. Right panel: The random independent noise present in the first panel found by taking the difference between the first two images. 69

Figure 5.6 Left panel: A pseudo cross-section displaying the normalized difference of the weighted 2D synthetic aperture response for the inline electric component and $\gamma = 0$ with 10^{-15} V/Am^2 independent, random noise added. Middle panel: The same weighted synthetic aperture response as the first panel without noise. Right panel: The random independent noise present in the first panel found by taking the difference between the first two images. 70

Figure 5.7 Left panel: A pseudo cross-section displaying the normalized difference of the weighted 2D synthetic aperture response for the inline electric component and $\gamma = 1$ with 10^{-15} V/Am^2 independent, random noise added. Middle panel: The same weighted synthetic aperture response as the first panel without noise. Right panel: The random independent noise present in the first panel found by taking the difference between the first two images. 72

Figure 5.8 Left panel: A pseudo cross-section displaying the normalized difference of the weighted 2D synthetic aperture response for the inline electric component and $\gamma = 10$ with 10^{-15} V/Am^2 independent, random noise added. Middle panel: The same weighted synthetic aperture response as the first panel without noise. Right panel: The random independent noise present in the first panel found by taking the difference between the first two images. 73

Figure 5.9 A contour of the amplitude of the optimal weights with $\gamma = 0$ for the source array centered at 8.1 km inline and the receiver at 0 km shown on a map view of the survey geometry. 74

Figure 5.10 A contour of the amplitude of the optimal weights with $\gamma = 1$ for the source array centered at 8.1 km inline and the receiver at 0 km shown on a map view of the survey geometry. 74

Figure 5.11 A contour of the amplitude of the optimal weights with $\gamma = 10$ for the source array centered at 8.1 km inline and the receiver at 0 km shown on a map view of the survey geometry. 75

Figure 5.12 Left panel: A pseudo cross-section displaying the normalized difference of the weighted 2D synthetic aperture response for the inline electric component and $\gamma = 0$ with 10^{-15} V/Am^2 independent, random noise added. Middle panel: The weighted 2D synthetic aperture response for $\gamma = 1$ and the responses with negative largest eigenvalues masked with gray. Right panel: The weighted synthetic aperture response for $\gamma = 10$ and the negative eigenvalues masked out with gray. 76

Figure 6.1 An inline cross-section of the model used to generate the electromagnetic fields. The first layer is water with a depth of 200 m. There are five sediment layers with varying resistivity. The reservoirs are shown as the white rectangles. The vertical scale is exaggerated. . . . 79

Figure 6.2 The survey geometry used to create the synthetic CSEM data. The sources are shown as black dots and the receivers are the gray triangles. The locations of the reservoirs are outlined with black squares. 80

Figure 6.3 The normalized difference of the inline electric pay field and the inline electric wet field for the original data (panel a), the model with 50% increase in overburden resistivity (panel b), and the model with a 33% increase in anisotropy (panel c). 83

Figure 6.4 The normalized difference of the inline electric pay field and the inline electric wet field for the 2D weighted synthetic aperture response for the original data (panel a), the model with 50% increase in overburden resistivity (panel b), and the model with a 33% increase in anisotropy (panel c). 85

Figure 6.5 A contour of the phase of the optimal weights overlaid on a map of the survey geometry for the original data (panel a), the model with 50% increase in overburden resistivity (panel b), and the model with a 33% increase in anisotropy (panel c). 87

Figure 6.6 A contour of the amplitude of the optimal weights overlaid on a map of the survey geometry for the original data (panel a), the model with 50% increase in overburden resistivity (panel b), and the model with a 33% increase in anisotropy (panel c). 88

Figure 6.7 The normalized difference of the inline electric pay field and the inline electric wet field for the crossline weighted synthetic aperture response for original data (panel a), the model with 50% increase in overburden resistivity (panel b), and the model with a 33% increase in anisotropy (panel c). 90

Figure 6.8 The phase of the optimal weights for crossline synthetic aperture for the source array centered at -12.85 km and the receiver at 0 km for the unperturbed model, the 50% increase in overburden resistivity, and the 33% increase in anisotropy. 91

Figure 6.9 The amplitude of the optimal weights for crossline synthetic aperture for the source array centered at -12.85 km and the receiver at 0 km for the unperturbed model, the 50% increase in overburden resistivity, and the 33% increase in anisotropy. 91

Figure 6.10 A map view of the location of the reservoirs outlined as squares with the receivers shown as gray triangles for the original model (panel a), the reservoirs shifted 2.5 km to the right (panel b), and the reservoirs shifted 4.5 km to the right (panel c). 93

Figure 6.11 The normalized difference of the inline electric pay field and the inline electric wet field for the 2D weighted synthetic aperture response for no shift in the reservoir position (panel a), the response for the reservoir shifted 2.5 km to the left (panel b), and the response for the reservoir shifted 4.5 km (panel c). 95

Figure 6.12 A contour of the amplitude of the optimal weights for the 2D synthetic aperture source centered at -7.5 km and the receiver at 0 km inline overlaid on a map of the survey geometry for the unshifted reservoirs (panel a), the reservoirs shifted 2.5 km (panel b), and the reservoirs shifted 4.5 km (panel c). 96

Figure 6.13 A contour of the phase of the optimal weights for the 2D synthetic aperture source centered at -7.5 km and the receiver at 0 km inline overlaid on a map of the survey geometry for the unshifted reservoirs (panel a), the reservoirs shifted 2.5 km (panel b), and the reservoirs shifted 4.5 km (panel c). 97

Figure 6.14 The normalized difference of the inline electric pay field and the inline electric wet field for the crossline weighted synthetic aperture response for no shift in the reservoir position (panel a), the response for the reservoir shifted 2.5 km to the left (panel b), and the response for the reservoir shifted 4.5 km (panel c). 99

Figure 6.15 The phase of the optimal weights for crossline synthetic aperture for the source array centered at -7.5 km and the reservoirs shifted 0 km, 2.5 km, and 4.5 km. 100

Figure 6.16 The amplitude of the optimal weights for crossline synthetic aperture for the source array centered at -7.5 km and the reservoirs shifted 0 km, 2.5 km, and 4.5 km. 100

Figure 7.1 The locations of all the shale basins in the United States. Taken from Arthur *et al.*. 115

Table 7.1 A table detailing some of the common hydraulic fracturing fluid additives, their compounds, purposes, and common uses. Taken from DOE. 114

ACKNOWLEDGMENTS

I shall be telling this with a sigh
Somewhere ages and ages hence:
Two roads diverged in a wood, and I–
I took the one less traveled by,
And that has made all the difference.
–Robert Frost

The section above is the last stanza of Robert Frost's poem titled *The Road Not Taken*. I have often felt that my journey through graduate school is similar to this poem. It is a series of diverging paths that lead to unknown places. Every doctoral student takes the path less traveled, and hopefully, cuts a new trail. However, unlike Frost, who stands alone at the crossroads, I have many people who have helped me along my journey, which made the less-traveled path easier to take.

My years at the Colorado School of Mines in the Geophysics Department researching for the Center for Wave Phenomena have been some of the hardest, best, and most fulfilling of my life. I would like to thank all the Geophysics professors that pushed me to gain a better understanding of the physics and mathematics used to describe the subsurface, especially Dr. Yaoguo Li, Dr. Ilya Tsvankin, Dr. Paul Sava, and Dr. Dave Hale. I am grateful for my committee (Dr. Roel Snieder, Dr. Jen Schneider, Dr. Paul Sava, Dr. Rich Krahenbuhl, and Dr. John Berger) for their helpful comments and support throughout my journey. Much of my research and classwork were made clearer through discussions with other students in CWP and throughout the Geophysics Department. I am thankful for the encouragement and friendship from Filippo Broggini, Farhad Bazargani, Chinaemerem Kanu, Nishant Kamath, and Patricia Rodrigues.

I am grateful for the financial support from the Shell Gamechanger Project and the technical support from the Shell EM Research Team. I truly appreciate the insight, discussion, and industry perspective that I received from Dr. Liam Ó Súilleabháin, Dr. Mark Rosenquist, Dr. Yuanzhong Fan, and David Ramirez-Mejia.

The Geophysics Department would not function without significant support from Pam Kraus, Shingo Ishida, Diane Witters, Michelle Szobody, and Dawn Umpleby. I want to especially thank Diane for her help word-crafting my thesis text but also for being a friend and mentor through the ups and downs along the way. Your words of encouragement at those critical moments made such an impact!

I am thankful to have the opportunity to explore science communication, policy, and rhetoric as part of my minor Science, Technology, Engineering, and Policy in the Liberal Arts and International Studies Department. I want to especially thank Dr. Jen Schneider, Dr. Jon Leydens, Dr. Jessica Rolston, and Dr. Jason Delborne for exposing me to new ideas and facets of the world I only experienced through their classes. Jen, I truly appreciate the opportunity you gave me to write about an important energy issue. Without your guidance, I would not have been able to navigate the social science world.

I would not have accomplished anything without the support, love, and caring of my family. My mom and dad have always believed in me, encouraged me to do my best, and exposed me to new experiences. My sister (and legal counsel) has always been excited about my research and has given me new perspectives on what I saw as challenges. I am extremely grateful to have a partner in all my adventures, Sammy, who always tells me I can do it, talks me through what I think are impossible tests, and makes me laugh everyday.

I am grateful to have amazing guidance throughout my journey from my mentor, Dr. Roel Snieder. Without the advice, insight, and kindness from my advisor, I would not have been successful. Roel helped me grow from an unsure student to a confident researcher by reminding me often that it is not about getting the right answer but exploring the unknown. Not many advisors would see the value of their student taking classes and researching in

a subject outside of their field. I appreciate the opportunity to satiate my curiosity about the interface between industry and society. I have learned so many life lessons from Roel that have impacted how I view the world and my role as a scientist and as a human being. Possibly one of the most important lessons is that there is always time for a joke.

With the support and assistance from numerous people, I took the path less traveled by, and that has made all the difference.

To my family

"If I have seen further it is only by standing on the shoulders of giants" – Sir Isaac Newton

CHAPTER 1
GENERAL INTRODUCTION

Geophysics defines the structure of the subsurface through imaging techniques that can also characterize the physical properties of the Earth. In industrial applications, geophysical methods reveal the structure of the Earth and locations of minerals and hydrocarbons. One method developed to explore for and derisk hydrocarbon reservoirs in marine settings is controlled-source electromagnetics (CSEM). A boat tows an electric dipole source over receivers on the seafloor that record the electric and magnetic response. A horizontal dipole (typically around 300 m with a low frequency within 0.1-1 Hz) creates an electrical current in both the horizontal and vertical directions and generates galvanic effects in horizontal resistive bodies, which are sensitive to the lateral extent of the reservoir (Constable, 2010; Constable & Srnka, 2007). The signal from the source travels down through the conductive subsurface, through the resistive reservoir, and then up to the receiver. The method is able to detect the contrast between the conductive subsurface ($\sim$1 Ωm) and resistive hydrocarbon reservoirs ($\sim$30–100 Ωm) (Constable & Srnka, 2007; Edwards, 2005). Unlike seismic methods, CSEM is able to differentiate between the presence of hydrocarbons or brine in geologic structures. The recorded electric and magnetic responses are inverted to define areas with higher resistivity, indicating the presence of hydrocarbons. The method was initially developed in academia in the 1970's by Charles Cox (Constable & Srnka, 2007). The first successful CSEM survey was carried out in 2000 and since then, CSEM has been applied in numerous locations (Constable, 2010).

CSEM has been used for almost a decade and a half to verify if a hydrocarbon-saturated reservoir is present. The method has successfully identified reservoirs in multiple locations in shallow and deep-water (Ellingsrud *et al.*, 2002; Hesthammer *et al.*, 2010; Myer *et al.*, 2012). However, CSEM has several limitations that prevent it from being implemented in more

complicated settings. With the conductive subsurface and the low frequency of the source, the electromagnetic signals are diffusive and decay rapidly with time (Constable & Srnka, 2007). This property of the electromagnetic fields is described by the skin-depth, which is the distance where the signal has decayed to 37% of its original amplitude (Constable & Srnka, 2007). For CSEM, the skin-depth for a source with 0.2 Hz frequency, in a 1 Ωm resistive earth layer is 1.1 km. The presence of a hydrocarbon reservoir is typically indicated by only a 20% increase in the electromagnetic field (Constable & Srnka, 2007). Another limitation is the spatial resolution of CSEM, which is low when compared to other geophysical methods such as seismic imaging. In CSEM, the earth, water, and air are all excited by the signal and the receivers record the superposition of all these responses weighted by the distance to the receiver (Constable, 2010). Constable (2010) states that both the vertical and horizontal resolution of CSEM is around 5% of the depth of burial. For a reservoir at a depth of 3 km, the resolution is thus estimated to be 150 m. The depth and thickness of the reservoir limit the amount of signal that reaches the receivers. Currently, the method can detect reservoirs up to about 3.5 km in depth, provided the lateral extent of the reservoirs is several kilometers (Mittet & Morten, 2012). These drawbacks in the CSEM method led to investigating how to enhance the signal from the reservoir.

Synthetic aperture is the technique proposed to overcome some of the issues in CSEM. Synthetic aperture was first developed for applications in radar imaging (Barber, 1985). Cheney & Borden (2009) present an overview of synthetic aperture and the mathematical basis for its application. Signals from multiple locations of the radar are combined to produce a signal from a larger aperture radar, which increases the resolution of the images. Figure 1.1 depicts the general synthetic aperture radar (SAR) setup. The main idea of synthetic aperture is to virtually increase the length of the source. The formation of a synthetically increased aperture allows one to weight the responses from individual sources by applying a phase shift and amplitude. The weights allow one to steer or focus the beam from the synthetic source array by applying different phase shifts and amplitude terms. Van Veen

& Buckley (1988) describe the main beamformers developed for synthetic aperture radar and describe a process to solve for the optimal weights. The beamformers may be independent of the response from the sources (fixed) or the beamformers can adjust to the data received (adaptive) (Van Veen & Buckley, 1988). Weighted synthetic aperture has been applied in many different fields including sonar, medical imaging, nondestructive testing, and geophysics (Barber, 1985; Bellettini & Pinto, 2002; Jensen *et al.*, 2006). The method has increased the resolution in several areas of medical imaging, including ultrasounds. Figure 1.2 shows the process of applying synthetic aperture to an ultrasound-imaging device. Responses from several different sources are collected and summed to produce a high-resolution image (Jensen *et al.*, 2006).

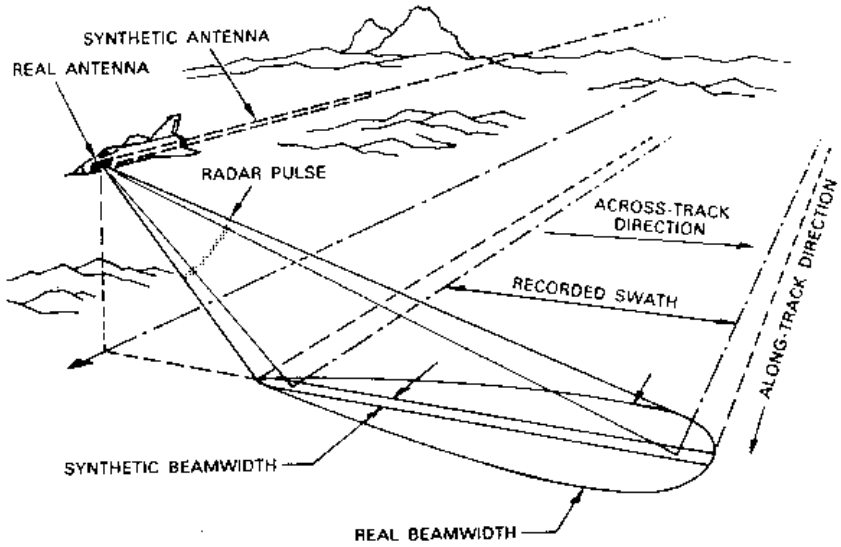

Figure 1.1: A diagram showing the main components of synthetic aperture radar. Taken from Avery & Berlin (1985).

For CSEM, the application of synthetic aperture virtually increases the length of the source after the acquisition of the electromagnetic responses from the typical length source. The electromagnetic signals are processed to behave as if they come from a several-kilometer-long source instead of a hundreds-meter-long source. Fan *et al.* (2010) first applied synthetic aperture to electromagnetic responses from a CSEM survey. The similarities between CSEM

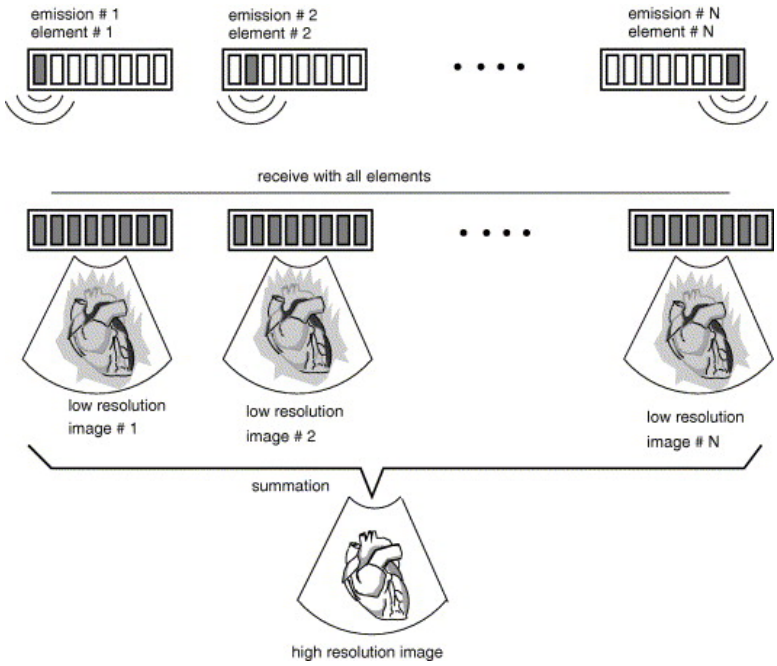

Figure 1.2: A diagram depicting synthetic aperture implemented in ultrasound imaging. Taken from Jensen *et al.* (2006).

fields at a single-frequency and the wave equation demonstrate that a diffusive field with a single frequency does have a direction of propagation (Fan *et al.*, 2010; Løseth *et al.*, 2006). This allows one to steer or focus the response from the synthetic aperture source creating constructive and destructive interference in the energy propagation of the response, which increases the illumination of the reservoir. The interference of diffusive fields has been previously used in physics for a variety of applications (Wang & Mandelis, 1999; Yodh & Chance, 1995). The combination of synthetic aperture and beamforming greatly improves the detectability of both shallow and deep targets (Fan *et al.*, 2011, 2012). Fan *et al.* (2012) tested synthetic aperture on a single towline of real electromagnetic fields demonstrating that the technique can increase the response from the reservoir.

1.1 Thesis overview

This thesis is composed of several research papers. The next five chapters detail the contributions I have made in applying synthetic aperture to controlled-source electromagnetics.

The seventh chapter details work I have done as part of my minor: Science, Technology, Engineering, and Policy.

In Chapter 2, I expand the application of synthetic aperture to the crossline direction, which allows for the creation of a two-dimensional (2D) synthetic aperture source array and steering in three-dimensions (3D). I describe the mathematical basis for the application of synthetic aperture to the 3D scalar diffusion equation. With synthetic diffusive fields, I demonstrate that coherent steering in the crossline direction is possible with sources spaced 2 km apart. To view the change in the diffusive fields caused by the application of synthetic aperture, the gradient of the diffusive fields is calculated. I show the temporal changes by phase-binning the gradient for a single source, an unsteered synthetic aperture source, and a steered synthetic aperture source.

In Chapter 3, I apply the theory developed in Chapter 2 to synthetic electromagnetic responses from a deep-water, layered, and anisotropic earth model. Exponential weights steer the synthetic aperture source, which radiates like a plane wave at a fixed steering angle. I search for the best steering angles and energy compensation coefficients within a range of reasonable values. The combination of coefficients that produces the highest detectability of the reservoir is chosen as the best steering parameters. For this synthetic model, I demonstrate that a synthetic aperture source steered in both the inline and crossline directions is able to increase the detectability of the reservoir by over 100%. In this chapter, I also show the benefits of viewing the direction of the electromagnetic fields with the Poynting vector, which is the energy flux density of the electromagnetic fields. An examination of the Poynting vector demonstrates the changes in the direction caused by the creation of a steered synthetic aperture source array. The response from the steered synthetic aperture source array sends more energy in the direction of the reservoir, thus increasing the detectability.

In Chapter 4, I describe an optimization method that calculates the optimal weights from the responses of the sources in the synthetic aperture array. I switch to using a single complex number to weight each source in the array, which gives more flexibility in steering

and focusing the source array. The benefits of the optimization method are that no user input is required to determine the weights, and the weights adjust automatically to highlight the desired information in the responses for each synthetic aperture array location. With the application of weighted synthetic aperture, I am able to increase the magnitude of the anomaly caused by the reservoir, decrease the random, independent noise, and better define the spatial location and extent of the reservoir. I demonstrate the ability of synthetic aperture to provide different types of information about the target using two different applications of synthetic aperture to electromagnetic responses from a synthetic model with two reservoirs laterally separated.

In Chapter 5, I investigate the ability of synthetic aperture to reduce the amount of noise propagation in the weighted synthetic aperture response while also increasing the detectability of the reservoir. The objective function in the optimization method in Chapter 4 is modified to include a term that requires the errors to be minimized. By implementing an optimization method that calculates the weights that reduce noise and increase the anomaly, the weighted synthetic aperture response reduces the noise floor, suppresses noise streaks, and increases the magnitude of the anomaly. I demonstrate these benefits with a synthetic CSEM example where the towlines are several kilometers away from the receivers. Without synthetic aperture, these responses are dominated by noise. The application of a weighted synthetic aperture array designed to reduce noise and increase the anomaly allows the signal from the reservoir to be extracted from the noisy responses and possibly allows for the use of CSEM in new areas where the towlines cannot be directly positioned over the receivers.

In Chapter 6, I test the sensitivity of synthetic aperture to the location of the target and to perturbations in the physical properties of the model. I input the responses from erroneous models into the optimization method developed in Chapter 4, which calculates the weights for the synthetic aperture source. I apply these incorrect weights to the unperturbed model. If the perturbations have no effect, then the anomaly from the reservoir should have the same magnitude and locations as when I use the correct weights. I show that even with weights

calculated from a model with a 50% increase in the background resistivity, the weighted synthetic aperture response still highlights the anomaly from the reservoirs and locates the anomaly in the correct position.

Chapter 7 addresses a different topic – that of my minor in Science, Technology, Engineering, and Policy from the Liberal Arts and International Studies Department. This choice of minor may at first appear unrelated to the subject area of geophysics, but I believe that scientists and engineers should be aware of the social impacts of their research and that investigating the implications of our research in this sphere is a valuable and needed component of becoming a Doctor of Philosophy. The chapter included in this thesis is a culmination of my investigations into the social affects of geophysics and energy extraction industries. The policy paper explores the controversial debate over the use of hydraulic fracturing in shale-rich areas. Hydraulic fracturing is a technique used to increase the production of oil and gas. Controversial debates about energy are relevant for every geophysicist because our research and activities directly relate to extracting many different types of energy and resources. I believe all scientists have the responsibility to communicate to the best of our ability. I show the controversy over hydraulic fracturing has escalated because parties, in an attempt to support their argument with facts that are often contested by experts on both sides, have ignored the complexities of the technology and debate. I call for an engagement approach to the debate over hydraulic fracturing that includes negotiation from all stakeholders.

Publications

Knaak, A., R. Snieder, L. Ó Súilleabháin, and Y. Fan, 2014. Error Propagation with synthetic aperture for CSEM: Geophysical Prospecting, *To be submitted.*

Knaak, A., R. Snieder, L. Ó Súilleabháin, Y. Fan, and D. Ramirez-Mejia, 2014. Optimized 3D synthetic aperture for CSEM: Geophysics, *Under Review.*

Knaak, A., R. Snieder, Y. Fan, and D. Ramirez-Mejia, 2013. 3D synthetic aperture and steering for controlled-source electromagnetics: The Leading Edge, 32, 8, 972-978.

Conference publications

Knaak, A. and R. Snieder, 2014. Optimized 3D synthetic aperture for CSEM: 84th Annual International Meeting, SEG, Expanded Abstracts, 691-696.

Knaak, A., R. Snieder, Y. Fan, and D. Ramirez-Mejia, 2013. 3D synthetic aperture and steering for controlled-source electromagnetics: 83rd Annual International Meeting, SEG, Expanded Abstracts, 744-749.

Knaak, A., J. Schneider, 2013. Fractured Rock, Public Ruptures: The hydraulic fracturing debate and *Gasland*: 73rd Annual Meeting of the Society for Applied Anthropology, 106.

CHAPTER 2

SYNTHETIC APERTURE WITH DIFFUSIVE FIELDS

2.1 Abstract

Controlled-source electromagnetics (CSEM), is a geophysical electromagnetic method used to detect hydrocarbon reservoirs in deep-ocean settings. CSEM is used as a derisking tool by the industry but it is limited by the size of the target, low-spatial resolution, and depth of the reservoir. Synthetic aperture, a technique that increases the size of the source by combining multiple individual sources, has been applied to CSEM fields to increase the detectability of hydrocarbon reservoirs. We apply synthetic aperture to 3D diffusive fields with a 2D source distribution to evaluate the benefits of the technique. We also implement beamforming to change the direction of propagation of the field, which allows us to increase the illumination of a specific area of the diffusive field. Traditional visualization techniques for electromagnetic fields, that display amplitude and phase, are useful to understand the strength of the electromagnetic field but they do not show direction. We introduce a new visualization technique utilizing the gradient and phase to view the direction of the diffusive fields. The phase-binned gradient allows a frequency-domain field to appear to propagate through time. Synthetic aperture, beamforming, and phase-binned gradient visualization are all techniques that will increase the amount of information gained from CSEM survey data.

2.2 Introduction

Diffusive fields are used in many different areas of science; in this paper we use diffusive fields as an approximation for electromagnetic fields to demonstrate the benefits of synthetic aperture, beamforming, and viewing fields with a visualization technique involving the phase and gradient. This work is motivated by the use of diffusive fields used in controlled-source electromagnetics (CSEM), a geophysical electromagnetic method for detecting hydrocarbon

reservoirs in deep-ocean settings. In CSEM, a horizontal antenna is towed just above the seafloor, where seafloor electromagnetic receivers are placed. CSEM was first developed in academia by Charles Cox in the 1970s and since then CSEM has been adopted by the industry and is used for derisking in the exploration of hydrocarbon reservoirs (Constable, 2010; Constable & Srnka, 2007; Edwards, 2005). The electromagnetic field in CSEM is predominantly diffusive because the source is low frequency and the signal propagates in a conducting medium. CSEM has some limitations that keep it from competing with other geophysical methods such as seismic. The size of the hydrocarbon reservoir must be large enough compared to the depth of burial to be detected and the signal that propagates through the reservoir is weak when compared to the rest of the signal (Constable & Srnka, 2007; Fan *et al.*, 2010). Also, CSEM has low spatial resolution compared to seismic methods (Constable, 2010). These drawbacks prompted an investigation into improving the signal received from the hydrocarbon reservoir through synthetic aperture, a method developed for radar and sonar that constructs a larger virtual source by using the interference of fields created by different sources (Barber, 1985; Bellettini & Pinto, 2002). Fan *et al.* (2010) demonstrated that the wave-based concept of synthetic aperture sources can also be applied to a diffusive field and that it can improve the detectability of reservoirs. The similarities in the frequency-domain expressions of diffusive and wave fields show that a diffusive field at a single frequency does have a specific direction of propagation (Fan *et al.*, 2010). Once synthetic aperture is applied, the field can be steered using beamforming, a technique used to create a directional transmission from a sensor array (see Van Veen & Buckley, 1988). The basic principles of phase shifts and addition can be applied to a diffusive field to change the direction in which the energy moves. These create constructive and destructive interference between the energy propagating in the field that, with a CSEM field, can increase the illumination of the reservoir (Fan *et al.*, 2012). Manipulating diffusive fields by using interference is not necessarily new; the interference of diffusive fields has been used previously in physics for a variety of applications (Wang & Mandelis, 1999; Yodh & Chance, 1995). Fan *et al.* (2010)

were the first to apply both concepts of synthetic aperture and beamforming to CSEM fields with one line of sources. Fan *et al.* (2012) demonstrate the numerous advantages of synthetic aperture steering and focusing to CSEM fields with a single line of sources; the detectability for shallow and deep targets greatly improves with the use of synthetic aperture. We extend this work by expanding the technique to a 2D source distribution. In this paper, we introduce the concept of 3D synthetic aperture for diffusive fields, provide examples of steered diffusive fields, present a new visualization technique, and provide examples demonstrating the benefits viewing diffusive fields with a phase-binned gradient.

2.3 3D Synthetic Aperture and Beamforming

Synthetic aperture was first applied to diffusive fields by Fan *et al.* (2010) with one line of sources. Before this new use, synthetic aperture was used for radar, sonar, medical imaging and other applications (Barber, 1985; Bellettini & Pinto, 2002; Jensen *et al.*, 2006). One reason synthetic aperture, a wave-based concept, has not been previously applied to diffusive fields is that it was thought diffusive fields could not be steered because they have no direction of propagation (Mandelis, 2000). Fan *et al.* (2010) showed that the 3D scalar diffusion equation has a plane wave solution at a single frequency with a defined direction of propagation, which allows the direction of the field to be manipulated by synthetic aperture. The 3D scalar homogeneous diffusion equation is an appropriate approximation of a CSEM field because at a low frequency and in conductive media, like the subsurface, CSEM fields are diffusive (Constable & Srnka, 2007). In the frequency domain, the 3D scalar diffusion equation in a homogeneous medium, under the Fourier convention $f(t) = \int F(\omega)e^{-i\omega t}d\omega$, is given by

$$D\nabla^2 G(\mathbf{r}, \mathbf{s}, \omega) + i\omega G(\mathbf{r}, \mathbf{s}, \omega) = -\delta(\mathbf{r} - \mathbf{s}), \tag{2.1}$$

where D is the diffusivity of the medium, δ is the Dirac-Delta function, ω is the angular frequency, and $G(\mathbf{r}, \mathbf{s}, \omega)$ is the Green's function at receiver position $\mathbf{r}$ and source location $\mathbf{s}$. For synthetic aperture, we start with a diffusive field created from one point-source. The

field from a point-source is given by

$$G(\mathbf{r},\mathbf{s},\omega) = \frac{1}{4\pi D \mid \mathbf{r}-\mathbf{s} \mid} e^{-ik|\mathbf{r}-\mathbf{s}|} e^{-k|\mathbf{r}-\mathbf{s}|}, \tag{2.2}$$

(Mandelis, 2000) where $G(\mathbf{r},\mathbf{s},\omega)$ is the Green's function at receiver position $\mathbf{r}$ and source location $\mathbf{s}$, ω is the angular frequency, and D is the diffusion constant. The wave number is given by $k = \sqrt{\omega/(2D)}$. The field from a point-source is the building block for synthetic aperture with diffusive fields. Multiple point-source fields can be summed to create one large source; the interference of the different sources combines to create a synthetic aperture source with greater strength than an individual point-source. The equation for synthetic aperture is given by

$$S_A(\mathbf{r},\omega) = \iint\limits_{sources} e^{-A} e^{-i\Delta\Psi} G(\mathbf{r},\mathbf{s},\omega) d\mathbf{s}, \tag{2.3}$$

where, for the source $\mathbf{s}$, $\Delta\Psi$ is the phase shift and A is an energy compensation coefficient. A traditional CSEM survey tows a source in parallel lines over receivers placed on the seafloor (Constable & Srnka, 2007); in the following we assume that the sources are towed along parallel lines that are parallel to the x-axis. Then we assume, also, that the y-axis is aligned with the crossline direction. The field is steered by applying a phase shift, for either inline steering or crossline steering, and energy compensation terms defined below:

$$\Delta\Psi = k\hat{\mathbf{n}}\boldsymbol{\Delta}\mathbf{s} \tag{2.4}$$

$$\hat{\mathbf{n}} = \begin{pmatrix} \cos\varphi \sin\theta \\ \sin\varphi \sin\theta \\ \cos\theta \end{pmatrix} \tag{2.5}$$

$$A = \Delta\Psi. \tag{2.6}$$

The phase shift, for an individual source, is shown in equation 2.4. The shift is a function of the wavenumber, the steering angle $\hat{\mathbf{n}}$, and a distance Δs. Equation 2.5 defines the steering direction which is controlled by two angles, θ and φ. The dip of the direction of the steering angle, represented by θ, is measured with respect to the vertical. The other angle, φ, represents the azimuthal direction. For inline steering, $\varphi = 0^\circ$ and for crossline steering,

$\varphi = 90°$; these are the only directions for φ considered in this work because they offer the best steering for a traditional CSEM survey set-up. The quantity, $\Delta s = \mid \mathbf{s_n} - \mathbf{s_1} \mid$ is the distance between an individual source, $\mathbf{s_n}$, and the source defined to be at the bottom left corner of the survey footprint, $\mathbf{s_1}$. In general, the phase shift is defined as $\Delta\Psi = k(n_x\Delta s_x + n_y\Delta s_y)$. For inline steering, the phase shift equation simplifies to $\Delta\Psi = k\sin\theta\Delta s_x$ and for crossline steering, the equation simplifies to $\Delta\Psi = k\sin\theta\Delta s_y$ where Δs_x is the distance between the two sources in the x-direction and Δs_y is the distance between the sources in the y-direction. Figure 2.1 demonstrates a traditional CSEM survey design with the steering angle and s_1 labeled. To achieve the final steered field, $G(r, s, \omega)$ is summed over all sources in each individual line and, then, summed over all lines, as shown in equation 2.3. The exponential weighting, shown in equation 2.6, is just one way to create the interference needed to steer diffusive fields (Fan *et al.*, 2012). For a homogeneous medium, the phase shift and energy compensation term are set to be equal because the decay of the field is proportional to the phase shift, and the attenuation coefficient in equation 2.2 is equal to the wave number (Fan *et al.*, 2011). For a CSEM field, the energy compensation term accounts for the diffusive loss, decreases the background field to create a window to view the secondary field and equalizes the interfering fields to create destructive interference (Fan *et al.*, 2011, 2012). We demonstrate the benefits of synthetic aperture and beamforming with numerical examples.

2.3.1 Numerical Examples

For all of the models shown in the next examples, the model volume is 20km×20km×4km to approximate the depth, width, and length of a traditional CSEM survey. We use parallel lines of sources, which are the standard survey set-up in industry; in these examples, the 2D source distribution used is constructed from five 5km long towlines that each contain 50 individual point-sources. The lines are spaced 2km apart which is a common spacing for receivers in the crossline direction. Diffusive fields are difficult to visualize with a linear scale because the field varies over many orders of magnitude. Therefore we use the transformation defined by Fan *et al.* (2010) to view the field's amplitude and sign with a logarithm to

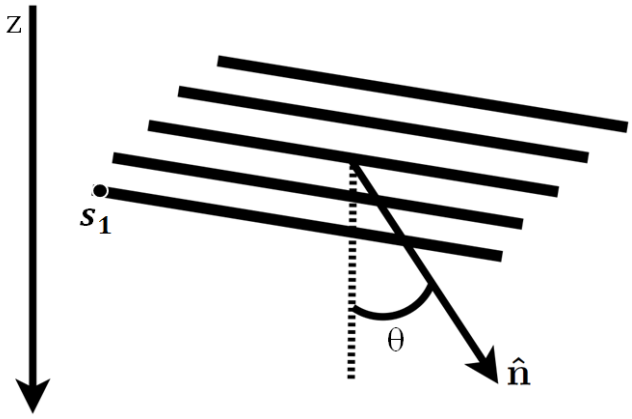

Figure 2.1: The design of a traditional CSEM survey. The individual source, $\mathbf{s_1}$, is defined to be located at the origin. The steering angle, $\hat{\mathbf{n}}$, is a function of θ, the dip and φ which is either 0° or 90° to steer in the inline or crossline directions, respectively.

account for the rapid decay of the field. The transform is shown below:

$$I_G = m * Im(S_A) \tag{2.7}$$

$$Z = sgn(I_G) log_{10} \mid I_G \mid . \tag{2.8}$$

The factor m, in equation 2.7, is a constant scaling factor which sets the smallest amplitude of $\mid S_A \mid$ equal to 10^0. The dimensionless Z field displays the log of I_G with a minus sign when I_G is negative. The diffusive field from a point-source is shown in Figure 2.2. All the

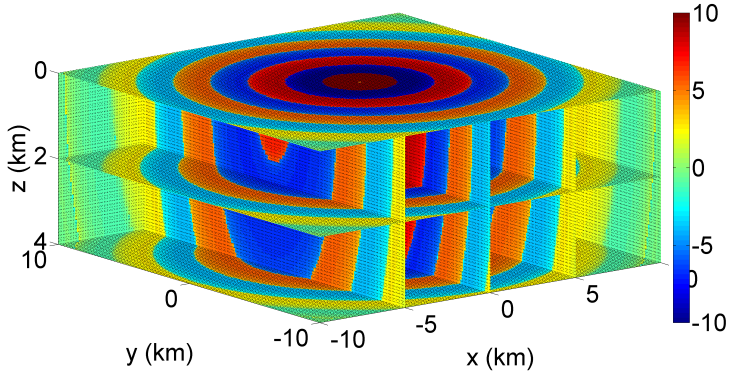

Figure 2.2: The point-source 3D scalar diffusive field log-transformed with the source at (0,0,0).

fields are created at a frequency of 0.25 Hz and a diffusivity $D = 2.4 \times 10^5$ m^2/s which is the

approximate diffusivity of an electromagnetic wave in seawater (Fan *et al.*, 2010). Figure 2.2 demonstrates how the field excited by a single point source diffuses through a 3D volume; the strength of the field decreases with increasing depth. We then apply synthetic aperture to the 2D source distribution in the inline and crossline directions. The unsteered field depicted in Figure 2.3 has five synthetic aperture sources each 5 km long. The sources in the five lines are summed, without any phase shifts and amplitude factors applied, in the x- and y-directions to produce a larger, longer source.

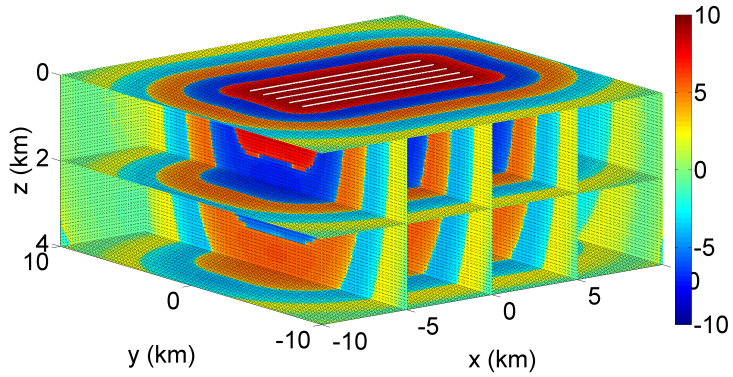

Figure 2.3: The unsteered 3D scalar diffusive field log-transformed.

In CSEM the longest source dipole is around 300 meters (Constable, 2010); with synthetic aperture, we can create a much longer source without requiring a boat to tow the extra-long source. Beamforming is applied to the field to change the direction of the energy. For inline steering, individual sources in each of the five lines are multiplied by a phase shift and an energy compensation term and then the sources are summed. The inline direction has more sources to use because the source is towed in the x-direction with samples taken every 100 meters. Figure 2.4 demonstrates how steering caused the field to be asymmetric towards negative x-values. The diffusive field is steered in the crossline direction much the same way as in the inline direction, but a different phase shift is applied to each synthetic aperture source with all the individual sources on one line multiplied by the same phase shift. As shown in Figure 2.5, this produces an asymmetric movement of the strength of the field in the negative y-direction. It is promising that even with five lines spaced 2km apart, we can

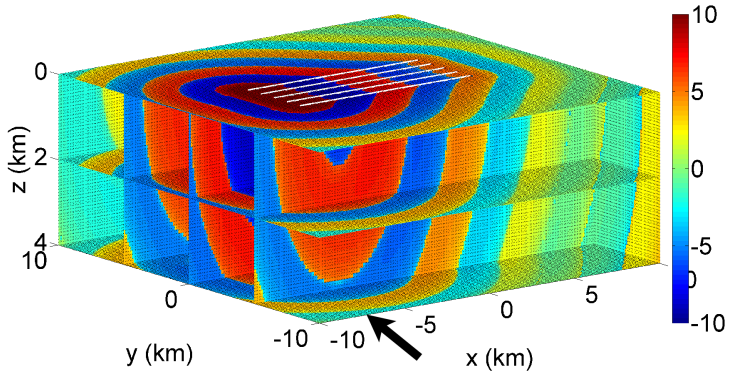

Figure 2.4: The 3D scalar diffusive field log-transformed and steered at a 45° angle in the inline direction. The arrow shows the shift in the x-direction of the energy from the origin; without steering the maximum energy would be located at the center of the source lines (x= 0km).

achieve a marked crossline steering of the field; the maximum of the field has been shifted to the right, away from the centerline of the survey (y = 0km). This leads us to believe that once applied to CSEM, crossline steering may direct the field toward a target. Inline and crossline steering can be combined to create a field that has energy shifted in the x- and y-directions (Figure 2.6). The combined steering creates a field that is asymmetric with respect to both axes, concentrating the energy in on area.

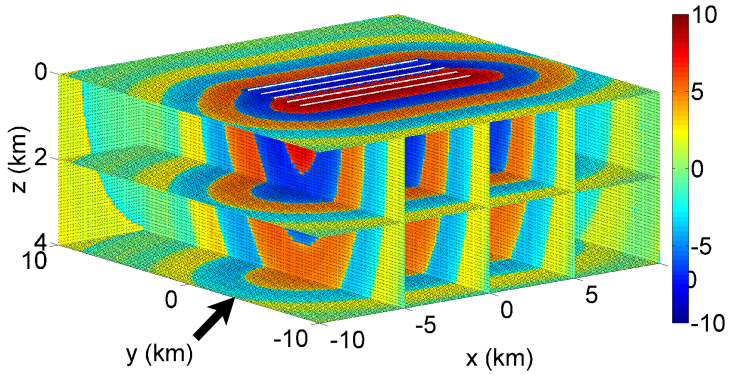

Figure 2.5: The 3D scalar diffusive field log-transformed and steered at a 45° angle in the crossline direction. The arrow shows the shift in the energy from the centerline of the survey (y= 0km). The shift is less than in Figure 2.4 because fewer sources are used.

Applying synthetic aperture to diffusive fields demonstrates the possibilities of using 3D synthetic aperture on real electromagnetic fields acquired from CSEM surveys. The inline

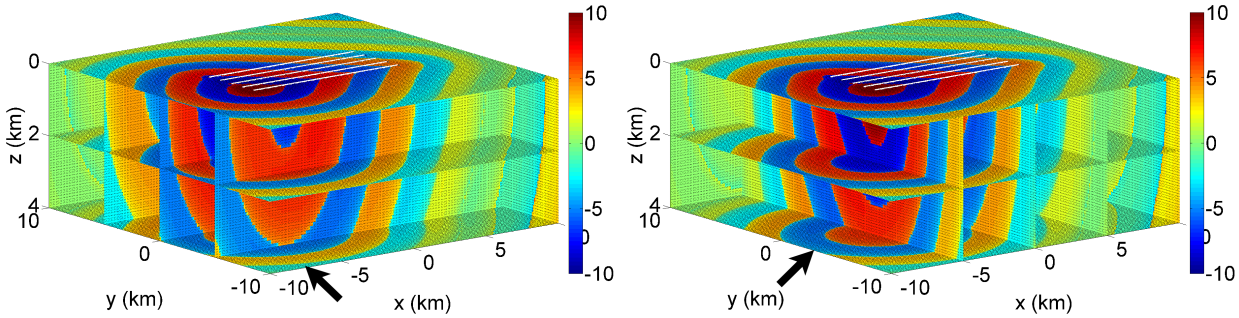

Figure 2.6: The 3D scalar diffusive field log-transformed and steered at a 45° angle in the inline and crossline directions. The arrows demonstrate the shift in the energy in the x- and y- directions.

and crossline steering of diffusive fields shows how the maximum can be shifted to a new area, which allows that area to be illuminated than without steering. The log-transform is a useful tool to view diffusive fields but it has some drawbacks. The only information communicated is the sign and normalized amplitude of the field. There is no information about the direction of the field or a sense of how it propagates in 3D space. We developed a new way to visualize the fields that shows the direction and propagation of the fields in the frequency-domain.

2.4 3D Visualization

The most common way to visualize electric and magnetic fields is through magnitude and phase plots but these lack the capability to show the direction the field is traveling (Constable, 2010). Additionally, the log-transformation employed in the previous figures only shows the sign and normalized amplitude of the field, but we need to visualize the direction of the field to identify the enhancement of the upgoing field from synthetic aperture and beamforming because the most important information from a CSEM survey is the electromagnetic signal that propagates down, through the reservoir, and then returns to the seafloor to be recorded by a receiver. This signal is difficult to identify because it is much weaker compared to the background field. The Poynting vector measures the direction in which the energy flux of the electromagnetic field is traveling; it is an effective way to examine how an electromagnetic

field propagates (Fan *et al.*, 2012). The energy flux density of the electromagnetic field is given by (Griffiths, 2008)

$$\mathbf{S} \equiv \frac{1}{\mu_o}\mathbf{E} \times \mathbf{B}, \tag{2.9}$$

where μ_o is the permeability of free space, $\mathbf{E}$, is the electric field, and $\mathbf{B}$ is the magnetic field. The diffusive field, an approximation of a diffusive electric field, we use is a scalar field and therefore the Poynting vector cannot be used. The gradient of a scalar field is, however, similar to the Poynting vector for an electromagnetic field: the Poynting vector is the energy flux density of the electromagnetic field which is similar to the heat flux density used in thermodynamics. The heat flux density is found by taking the gradient of temperature, which makes the gradient a useful measure of the energy flux for scalar diffusive fields (Schroeder, 1999). The gradient of a diffusive field is complex and only the real part is used to display the gradient, normalized to make the direction apparent. In addition to visualizing the direction of the field, it is useful to know the direction of the field in relation to the time over which the field has propagated; the use of the phase of the field in conjunction with the gradient allows a frequency-domain field to appear to propagate through time. A simple example demonstrates this concept. Consider a point-source field, e^{ikr} where k is the wavenumber and r is the distance from the source to another location in space. In that case, the phase is, then, equal to kr which smoothly increases with respect to r. A small phase corresponds to a location close to the source and a large phase corresponds to a location farther away from the source. Thus, when the phase is binned by multiplies of π the frequency-domain diffusive field appears to propagate outward in space the same way it propagates through time. The phase must not contain phase-jumps for use in our visualization method. To make the phase of the field increase smoothly, we use phase-unwrapping in 3D which corrects the phase-jumps of 2π that occur in the field. Phase unwrapping is applied in many fields including radar, medical, and geophysics; 3D phase unwrapping is an ongoing field of research (Itoh, 1982; Parkhurst *et al.*, 2011; Shanker & Zebker, 2010; Wang *et al.*, 2011). Phase unwrapping is simple for our noiseless scalar diffusive fields; we unwrap the phase one dimension at a

time to construct a smoothly increasing phase. Phase jumps determined to be larger than the tolerance value π are reduced by adding or subtracting 2π to until the jump is less than the tolerance value. Once the phase is unwrapped, we add a constant to the phase field to make the source phase equal to zero. Only the relative phase is needed to view a scalar diffusive field with this method. The source is time-varying with a period of four seconds, which creates a change in the direction of the field; to show only one type of direction on the image, the phase is binned by multiples of π. The gradient that corresponds to each phase bin is shown consecutively; as the phase increases the gradient is displayed at an increasing distance from the source.

2.4.1 Numerical Examples

As in the previous section, the volume of the diffusive field is 20km×20km×4km to represent a CSEM survey area. We first demonstrate the phase-binned gradient visualization technique with a simple point-source before applying the method to a field with a synthetic aperture source. The phase and gradient are shown in Figure 2.7 and Figure 2.8 to compare with the 3D phase-binned gradient in Figure 2.9.

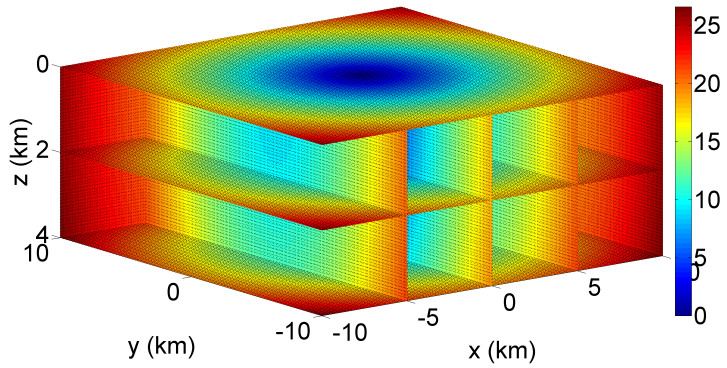

Figure 2.7: The unwrapped phase of a scalar diffusive field from a point-source located at (0,0,0). The colorbar displays radians.

The temporal evolution of the field cannot be viewed with the gradient or the phase. The advantage of the phase-binned gradient is that it displays the direction of the energy from

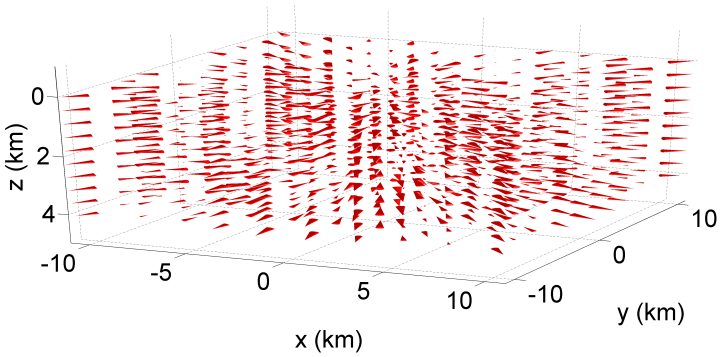

Figure 2.8: The normalized gradient of a scalar diffusive field from a point-source location at (0,0,0).

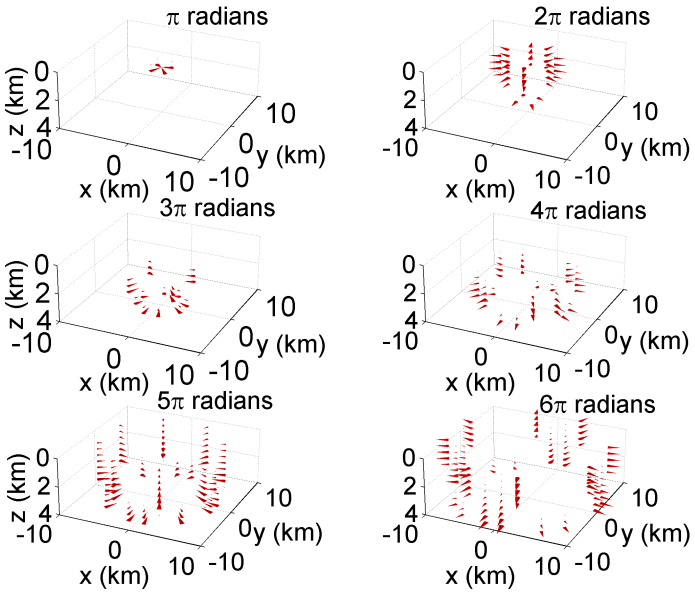

Figure 2.9: The phase-binned gradient of a scalar diffusive field from a point-source located at (0,0,0). The change in direction occurs from the time-harmonic point-source.

the origin outward to the edges of the model as a function of increasing phase. The direction of the field is displayed for different phase bins; a smaller phase corresponds to parts of the field closer to the source and a larger phase corresponds to parts of the field farther away from the source. This type of visualization becomes more useful when examining a field with synthetic aperture and steering, which are more complex than the point-source example. Figure 2.10 and Figure 2.11 display the unwrapped phase and gradient, respectively, of a scalar diffusive field with five 5km synthetic aperture sources.

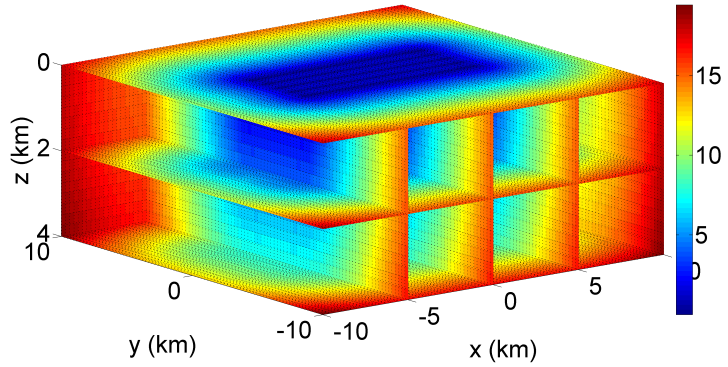

Figure 2.10: The unwrapped phase of a scalar diffusive field with five lines of synthetic aperture sources. The colorbar displays radians.

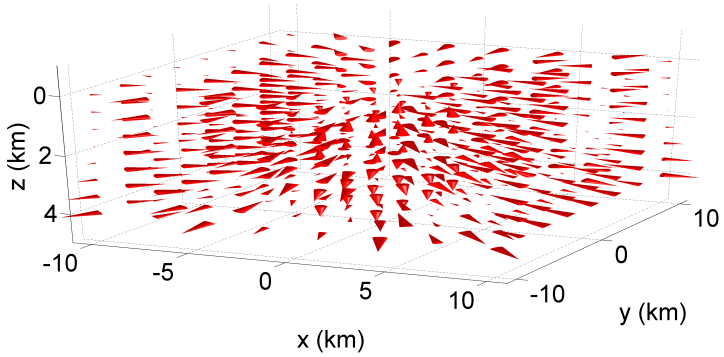

Figure 2.11: The normalized gradient of a scalar diffusive field with five synthetic aperture sources.

The phase of the unsteered diffusive field (Figure 2.10) created from synthetic aperture sources displays the change to a 2D source distribution when compared with the phase

of the point-source (Figure 2.7). However, it does not show the change in the direction as a result of the application of synthetic aperture because no steering is applied to this example. The gradient of the unsteered diffusive field, Figure 2.11, does display the direction of the field but it is difficult to see the differences between the unsteered synthetic aperture source and the point-source gradient, shown in Figure 2.8. The phase-binned gradient of the unsteered diffusive field allows the differences to be highlighted. Figure 2.12, in comparison to Figure 2.9, demonstrates the effect of synthetic aperture through the broadening of the pattern of arrows depicted in each phase, a result of the 2D distribution of the synthetic aperture source.

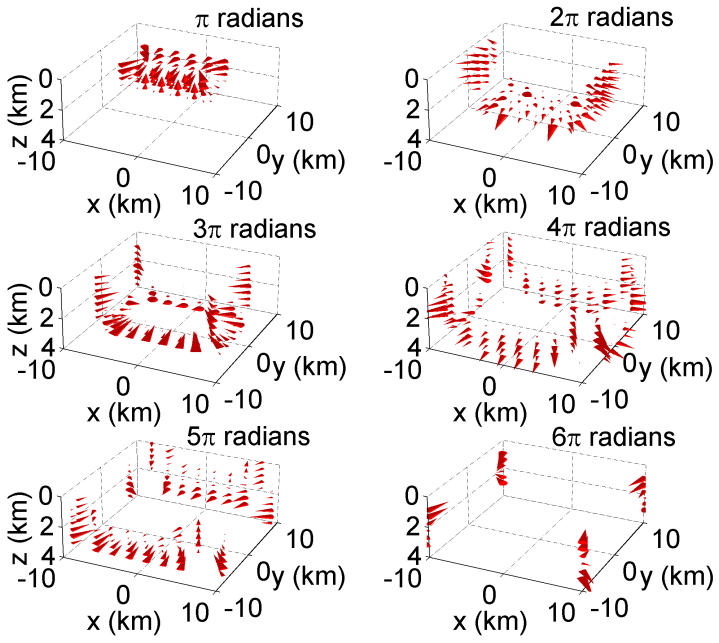

Figure 2.12: The phase-binned gradient of a scalar diffusive field with five unsteered synthetic aperture sources. The movement of the energy is symmetric about both the x and y directions.

The inline and crossline phase-binned gradient plots (Figure 2.13 and Figure 2.14) demonstrate how the direction of energy propagation changes with the use of beamforming. The inline field, shown in Figure 2.13, is steered at a 45° angle in the inline direction which causes constructive interference to occur at large x values compared to the unsteered field in Fig-

ure 2.12, which has the same amount of energy at all values of x. The interference is difficult to view with the log-transform, as previously shown in Figure 2.4, because the amplitude of the energy is small in the area 45° from the x-axis. The crossline field is steered at 45°

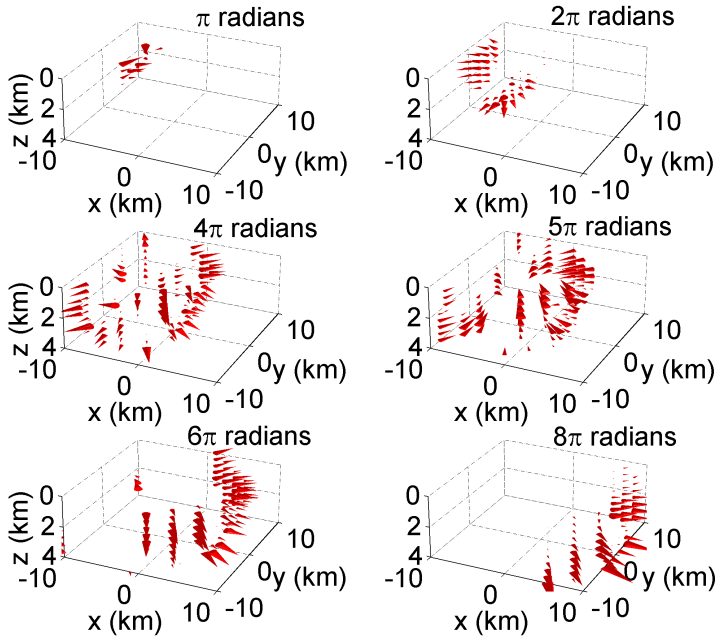

Figure 2.13: The phase-binned gradient of a scalar diffusive field with five synthetic aperture sources steered in the inline direction at a 45°. The energy is moving asymmetrically in the x-direction unlike the symmetric movement of the unsteered field.

which is visible in the lower right panels of Figure 2.14 as a preferential propagation in the crossline direction (large values of y). Rather than staying symmetric about the y-axis, the crossline steering causes the interference to occur at large y values in late phases. As with the inline field, this is difficult to visualize without the phase-binned display of the direction of propagation. The combination of inline and crossline steering produces a diffusive field with energy in one area of the model. In Figure 2.15, the concentration of energy to large x and y values is displayed in the later phases of the field. Without the phase-binned gradient technique the change in the direction due to beamforming is nearly impossible to visualize, especially with in a 3D volume. Figure 2.16 depicts an y-z view of the unsteered diffusive field gradient and the combined inline and crossline steered diffusive field gradient. The oval

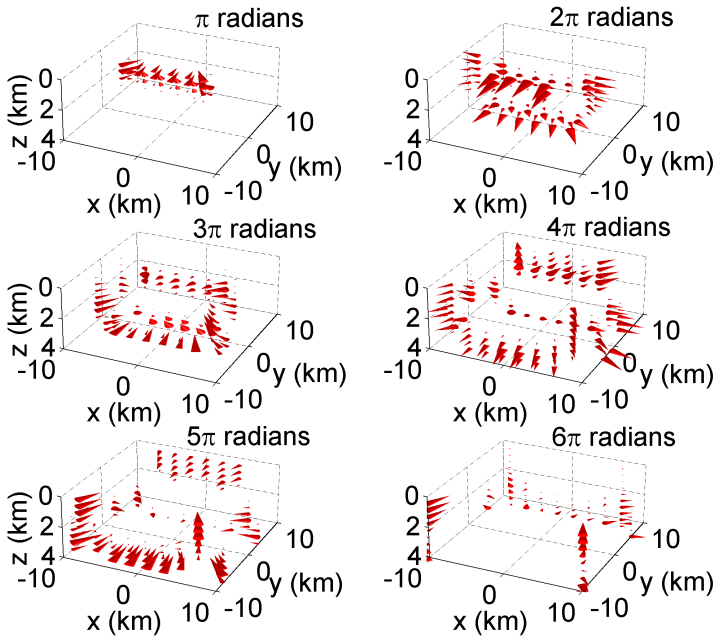

Figure 2.14: The phase-binned gradient of a scalar diffusive field with five synthetic aperture sources steered in the crossline direction at 45°. The energy is moving asymmetrically in the negative y-direction in contrast to the symmetric movement of the unsteered field.

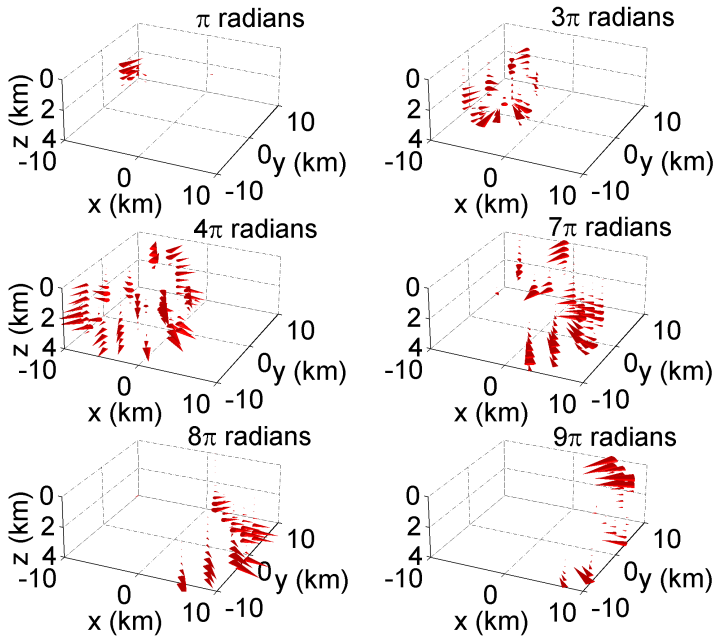

Figure 2.15: The phase-binned gradient of a scalar diffusive field steered in the inline and crossline directions at 45°. The combined inline and crossline steering produces a field whose energy moves out asymmetrically in both the x- and y-directions.

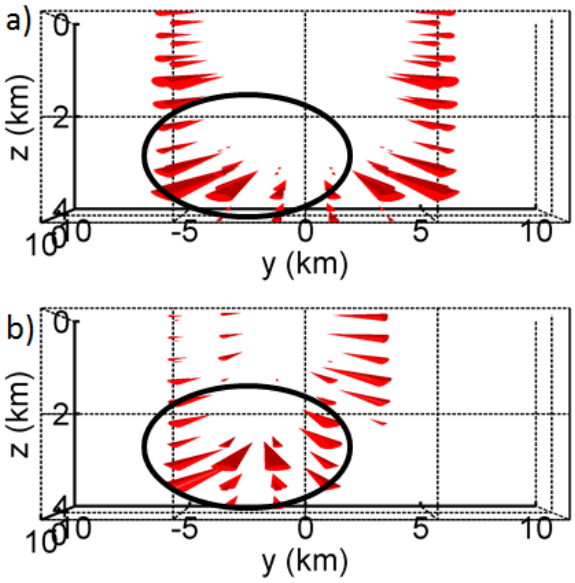

Figure 2.16: The y-z view of the unsteered diffusive field, panel a), and the combined inline and crossline steered diffusive field, panel b), at a phase of 3π. The oval highlights the change in the direction of the field caused by steering.

shape highlights the change in the direction of the field cause by steering. The unsteered field, panel a) of Figure 2.16, has mostly horizontal arrows. When steering is performed, panel b) of Figure 2.16, the arrows change to have an increased upward direction. CSEM measurements are effective for detecting reservoirs when the field propagates in the near vertical directions. Figure 2.16 demonstrates that with a diffusive field steering can modify the direction the energy propagates.

The differences in the direction of the diffusive fields can be used to determine if the synthetic aperture is steered optimally for a specific example. For CSEM fields, where the Poynting vectors are used instead of the gradient the goal is to increase the amount of upgoing energy that carries information about the reservoir. This visualization method will identify how the field propagates and how to optimize the beamforming parameters.

2.5 Discussion and Conclusions

The synthetic aperture technique offers a way to address some of the limitations of CSEM without requiring any changes in acquisition. Applying the technique to diffusive fields with 2D source distributions demonstrates the possibilities the technique has to increase the detectability of hydrocarbon reservoirs with CSEM fields. Steering the fields in both the inline and crossline directions causes the strength of the field to move to a localized area. Research is ongoing to apply this technique to synthetic CSEM fields to quantify the benefits of steering with a 2D source. The new visualization technique we introduce demonstrates how a frequency-domain field can appear to propagate as a function of increasing phase. The combined phase and gradient (or Poynting vector) provide a way to visualize how the steering modifies the upgoing field so that amount of information about the target is maximized. This is an improvement over other visualization methods that only show the amplitude or sign of the field. The implementation of these techniques increases the amount of information gleaned from data acquired from the CSEM survey, making CSEM a more valuable tool for industry. The next step is to apply the methods to electromagnetic fields with reservoirs. We will investigate what type of acquisition geometry maximizes the benefits of steering with synthetic aperture and how to optimize the steering.

2.6 Acknowledgments

We thank the Shell EM Research Team, especially Liam Ó Súilleabháin, Mark Rosenquist, Yuanzhong Fan, and David Ramirez-Mejia, for research suggestions and industry perspective. We are grateful for the financial support from the Shell Gamechanger Program of Shell Research, and thank Shell Research for the permission to publish this work.

CHAPTER 3

3D SYNTHETIC APERTURE FOR CSEM

Allison Knaak,[1] Roel Snieder,[1] Yuanzhong Fan,[2] and David Ramirez-Mejia[2]

Published in *The Leading Edge* (2013): 32, 972-978

3.1 Abstract

Controlled-source electromagnetics (CSEM) is a geophysical electromagnetic method used to detect hydrocarbon reservoirs in marine settings. Used mainly as a derisking tool by the industry, the applicability of CSEM is limited by the size of the target, low-spatial resolution, and depth of the reservoir. Synthetic aperture, a technique that increases the size of the source by combining multiple individual sources, has been applied to CSEM fields to increase the detectability of hydrocarbon reservoirs. We apply synthetic aperture to a 3D synthetic CSEM field with a 2D source distribution to evaluate the benefits of the technique. The 2D source allows steering in the inline and crossline directions. We present an optimized beamforming of the 2D source, which increases the detectability of the reservoir. With only a portion of three towlines spaced 2 km apart, we enhance the anomaly from the target by 80%. We also demonstrate the benefits of using the Poynting vector to view CSEM fields in 3D. Synthetic aperture, beamforming, and Poynting vectors are tools that will increase the amount of information gained from CSEM survey data.

3.2 Introduction

Controlled-source electromagnetics (CSEM) is a geophysical electromagnetic method used for detecting hydrocarbon reservoirs in marine settings. First developed in academia in the 1970s, a CSEM survey involves towing a horizontal antenna just above the seafloor, where electromagnetic receivers are placed. The oil industry has used CSEM for almost two

[1]Center for Wave Phenomena, Colorado School of Mines, Golden, CO
[2]Shell International Exploration & Production, Houston, TX

decades as a derisking tool in the exploration of hydrocarbon reservoirs (Constable, 2010; Constable & Srnka, 2007; Edwards, 2005). CSEM is often used in conjunction with other geophysical methods such as seismic but it has limitations that prevent it from gaining more widespread use in industry. The limitations come from the fact that the electromagnetic field in CSEM is a predominantly diffusive field. For the reservoir to be detectable, the lateral extent of the reservoir must be large enough compared to the depth of burial, and enough of the weak signal from the reservoir must reach the receivers (Constable & Srnka, 2007; Fan *et al.*, 2010). Also compared to seismic methods, the spatial resolution of CSEM is low (Constable, 2010).

These drawbacks prompted an investigation of how to improve the signal received from the reservoir through synthetic aperture, a method developed for radar and sonar that constructs a larger virtual source by using the interference of fields created by different sources (Barber, 1985; Bellettini & Pinto, 2002). Fan *et al.* (2010) demonstrate for a 1D array of sources that the wave-based concept of synthetic aperture sources can also be applied to CSEM fields and that it can be used to improve the detectability of reservoirs. The similarities in the frequency-domain expressions of diffusive and wave fields show that a diffusive field at a single frequency does have a specific direction of propagation (Fan *et al.*, 2010). Synthetic aperture allows for the use of beamforming, a technique used to create a directional transmission from a source or sensor array (see Van Veen & Buckley, 1988). One can apply the basic principles of phase shifts and addition to electromagnetic fields to change the direction in which the energy moves. The shifts create constructive and destructive interference between the energy propagating in the field that, with a CSEM field, can increase the illumination of the reservoir (Fan *et al.*, 2012). Manipulating diffusive fields by using interference is not necessarily new; physicists have previously used the interference of diffusive fields for a variety of applications (Wang & Mandelis, 1999; Yodh & Chance, 1995). Fan *et al.* (2010) applied the concepts of synthetic aperture and beamforming to CSEM fields with one line of sources. They demonstrated the advantages of synthetic aperture steering and focusing to

CSEM fields; the main improvement is to the detectability of targets shallower and deeper than the typical range of depths for CSEM.

In this paper, we introduce the concept of 3D synthetic aperture for electromagnetic fields; the source distribution is expanded from sources along a line to 2D with multiple parallel lines allowing the fields to be steered in 3D. We also briefly discuss a visualization tool to view 3D electromagnetic fields.

3.3 Mathematical basis

Fan *et al.* (2010) first applied synthetic aperture to controlled-source electromagnetic fields with one line of sources. Synthetic aperture was used earlier for radar, sonar, medical imaging, and other applications (Barber, 1985; Bellettini & Pinto, 2002; Jensen *et al.*, 2006). One reason synthetic aperture, a wave-based concept, has not been previously applied to CSEM fields is that it was assumed diffusive fields could not be steered because they have no direction of propagation (Mandelis, 2000). Fan *et al.* (2010) showed that the 3D scalar diffusion equation has a plane wave solution at a single frequency with a defined direction of propagation, which allows the direction of the field to be manipulated by synthetic aperture. The equation for synthetic aperture is given by

$$S(\mathbf{r},\omega) = \iint\limits_{sources} e^{-A(\mathbf{s})} e^{-i\Delta\Psi(\mathbf{s})} F(\mathbf{r},\mathbf{s},\omega) d\mathbf{s}, \tag{3.1}$$

where, for each source $\mathbf{s}$, $\Delta\Psi$ is a phase shift and A is an energy compensation coefficient. $F(\mathbf{r},\mathbf{s},\omega)$ is a general field; it could any component the electric or magnetic field at receiver $\mathbf{r}$ and source $\mathbf{s}$. For a plane wave synthetic aperture source, the field is steered by applying a phase shift and energy compensation terms defined by

$$\Delta\Psi(\mathbf{s}) = k(\hat{\mathbf{n}} \cdot \boldsymbol{\Delta}\mathbf{s}) \tag{3.2}$$

$$\hat{\mathbf{n}} = \begin{pmatrix} \cos\varphi \sin\theta \\ \sin\varphi \sin\theta \\ \cos\theta \end{pmatrix} \tag{3.3}$$

$$A(\mathbf{s}) = k(\boldsymbol{\Delta}\mathbf{s} \cdot \mathbf{a}) \tag{3.4}$$

The shift $\Delta\Psi(\mathbf{s})$ is a function of the wavenumber, the steering angle $\hat{\mathbf{n}}$, and a location vector $\mathbf{\Delta s}$. The unit vector $\hat{\mathbf{n}}$ in equation 3.3 defines the steering direction of the phase shift which is controlled by angles θ and φ. The dip of the direction of the steering angle, represented by θ, is measured with respect to the vertical. The angle φ represents the azimuthal direction. The quantity $\mathbf{\Delta s} = \mathbf{s_n} - \mathbf{s_1}$ is the relative location of an individual source $\mathbf{s_n}$ and the source defined to be at the bottom left corner of the survey footprint $\mathbf{s_1}$. The energy compensation term $A(\mathbf{s})$ in equation 3.4 is the dot product of the distances in $\mathbf{\Delta s}$ and the vector $\mathbf{a}$ which is composed of $[a_i\ a_c\ a_d]$. These three values define the weighting components for the inline direction, crossline direction, and depth, respectively.

In a traditional CSEM survey one tows a source along parallel lines (inline direction) over receivers on the seafloor; the source and receiver geometry in the examples in this paper follow the traditional design (Constable & Srnka, 2007). The exponential weighting (equation 3.4) equalizes the amplitudes and creates interference needed to steer diffusive fields; other methods of weighting exist (Fan *et al.*, 2012). For a homogeneous medium, the phase shift and energy compensation term are set to be equal because the decay of the field is proportional to the phase shift, and the attenuation coefficient in equation 3.1 is equal to the wave number (Fan *et al.*, 2011). For a realistic CSEM field, the background is heterogeneous and the phase shift and energy compensation terms are not equal. In this case, the energy compensation term accounts for the diffusive loss, decreases the background field to create a window to view the secondary field, and equalizes the interfering fields to create destructive interference (Fan *et al.*, 2011, 2012).

The proper choice for the energy compensation term and the phase shift for a CSEM field are determined by maximizing a quantity of the CSEM field that indicates the presence of a reservoir. For this paper, we choose to use the ratio of the absolute value of the inline component of the electric field with and without the reservoir; we call this value the *detectability ratio*. This measure is commonly used in industry to quantify the anomaly from hydrocarbon reservoirs (Constable & Srnka, 2007). In future research, we will investigate

other types of metrics for the quality of the synthetic aperture source. The optimization of the steering parameters of the synthetic aperture source finds the values of four parameters: θ, ϕ, a_i, a_c that control steering. The a_d component of the weighting term is not included because the depth component of $\mathbf{\Delta s}$ is zero for this survey; if sources in a survey are located at different depth then this term becomes relevant. We selected a range for each variable and combinations of the parameters were put into the steering equation until the combination was found that produced the maximum average detectability ratio between the inline component of the electric field with a reservoir and the field without a reservoir. The outcome from the steering and optimization is discussed in the next section.

3.4 Numerical examples

We use synthetic controlled-source electromagnetic fields to demonstrate the benefits of steering with 3D synthetic aperture. We computed a synthetic dataset using a code from the CEMI group at University of Utah (Hursán & Zhdanov, 2002). The synthetic data contains all three components of both the electric and magnetic fields. The model contains seven towlines 2km apart and 15km long over a 4km x 4km x 50m reservoir located at 3.5km depth. All of the parameters are within the ranges for a typical CSEM survey. The source is a 300m horizontal dipole with a frequency of 0.2Hz. The resistivity of the earth model varies with depth and direction; the model is shown in Figure 3.1. The reservoir has a resistance of 35Ωm. Because of the large water depth (2km), the airwave is weak at the acquisition level (sea bottom). The fields are sampled at points on the seafloor and at several depths in the subsurface. The sampling points in the subsurface give information about the flow of energy around and near the reservoir. The points span -7km to 7km in the inline direction and -4km to 4km in the crossline direction spaced every 250m. In depth, the sample points range from 0km to 4km and occur at a sampling interval of 200m. Figure 3.2 displays the survey geometry.

We create a 2D synthetic aperture source to demonstrate inline and crossline steering. The source extends from -6.6km to -1.8km in the inline direction and is 4km wide in the

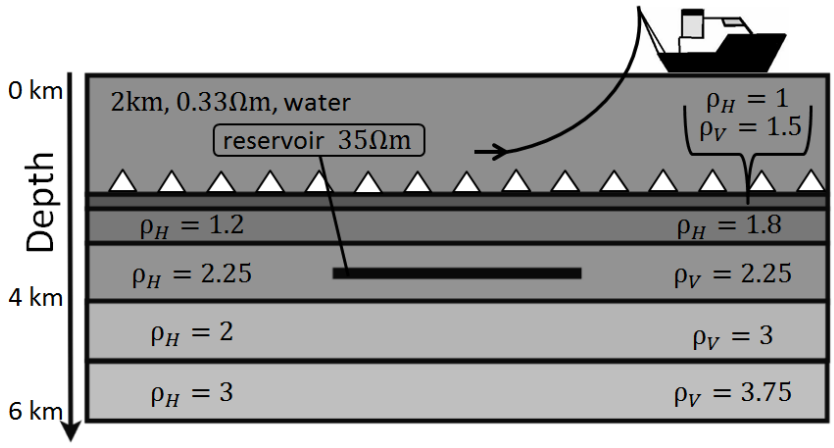

Figure 3.1: The model used to create the synthetic CSEM data. The values of ρ_H and ρ_V are the resistivity of the layer in the horizontal and vertical direction respectively given in Ohm-meters.

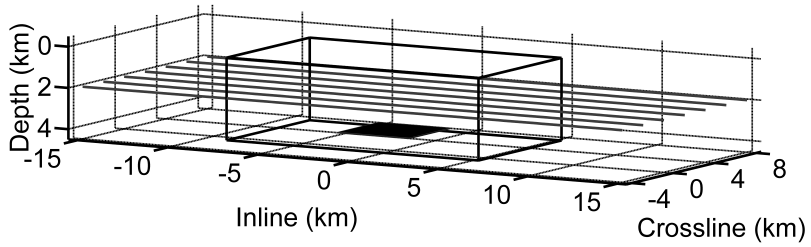

Figure 3.2: The geometry of the CSEM survey for the synthetic data. The seven towlines are shown as black lines. The reservoir is the black rectangle. The 3D box outlines the coverage of the sampling points.

crossline direction. The individual sources are sparsely spaced in the crossline direction, 2km apart, and more densely spaced in the inline direction, 300m apart. The choice of location of the 2D source region is offset from the reservoir to test the strength of the inline and crossline steering. The optimization discussed above finds the optimum steering angles θ and φ and two components of the energy compensation terms a_i and a_c. For these examples, the range of the steering angles θ and ϕ is from zero to $\pi/2$. The range for the energy compensation terms, a_i and a_c is zero to one. The increase in the detectability of the reservoir needs to occur over an area, not just a single point, to ensure the signal is recorded by a receiver placed in the region of interest. We include this spatial requirement by defining an area where we would expect to find the anomaly from the reservoir. We use the detectability ratio of a single source located in the middle of our proposed 2D source to determine the area of expected increased anomaly. Then the detectability ratio in the defined area is averaged and the maximum average detectability ratio defines the best steering. We defined the area of expected increased anomaly to be 0km to 4km in the inline and crossline direction for this synthetic model (the dashed box in Figure 3.3).

The maximum average detectability ratio in that area results in these values for the specified 2D source: $\theta = 64°$, $\varphi = 83°$, $a_i = 0.125$, $a_c = 0.875$. The steering angles are reasonable for the geometry of the source relative to the reservoir in that the steered source sends the energy down and toward the energy. Figure 3.3 depicts the detectability ratio of the inline electric field with and without the reservoir at the sea floor for a single source (panel a), an unsteered 2D synthetic aperture source (panel b), and a steered 2D synthetic aperture source (panel c). The average detectability ratio between the field with and without the reservoir for a single source (located at -4.5km in the inline direction and -2km in the crossline direction) in the area we expect the anomaly is 1.11 meaning there is an 11% anomaly from the presence of the reservoir. After we apply synthetic aperture to the 2D source the average detectability ratio becomes 1.19. When the 2D synthetic aperture source is steered with the parameters found by the optimization, the average detectability ratio

becomes 2.06. This corresponds to a 100% anomaly from the reservoir. From combining and steering sources from parts of three towlines, we increased the detectability of the reservoir from a small indication of its presence to a level where its existence is certain. The maximum of the average ratio between the inline electrical component with and without the reservoir is not the only choice for a measure of the improvement obtained with steering. Future research will focus on developing a more robust optimization scheme possibly including more parameters such as number of sources and placement of sources. Maximizing the average ratio of the inline electric component with and without the reservoir demonstrates the increases in detectability that synthetic aperture can achieve.

3.5 Visualizing steered fields in 3D

To visualize the impact the steering has on the direction of the energy transport, we use the Poynting vector. The most common way to visualize electric and magnetic fields is through magnitude and phase plots but these lack the capability to show the direction the field is propagating (Constable, 2010). The Poynting vector measures the direction in which the energy flux of the electromagnetic field is traveling; it is an effective way to examine how an electromagnetic field propagates (Fan *et al.*, 2012). The energy flux density of the electromagnetic field is given by

$$\mathbf{P} = \mathbf{E} \times \mathbf{H}, \tag{3.5}$$

where $\mathbf{E}$ is the electric field and $\mathbf{H}$ is the magnetic field (Jackson, 1999). For frequency domain fields, the Poynting vectors must be averaged over time to eliminate the oscillation of the source. The time-averaged Poynting vector is given by (Jackson, 1999)

$$\bar{\mathbf{P}} = 1/2Re(\mathbf{E} \times \mathbf{H}^*). \tag{3.6}$$

The synthetic CSEM dataset presented in this paper is sampled in three dimensions, which enables the Poynting vector of the field to be viewed in 3D as well. The resulting Poynting vector field is too dense to view all of the vectors at once. It is more demonstrative to show the downward propagating field from the source. Figure 3.4 shows the Poynting vectors with

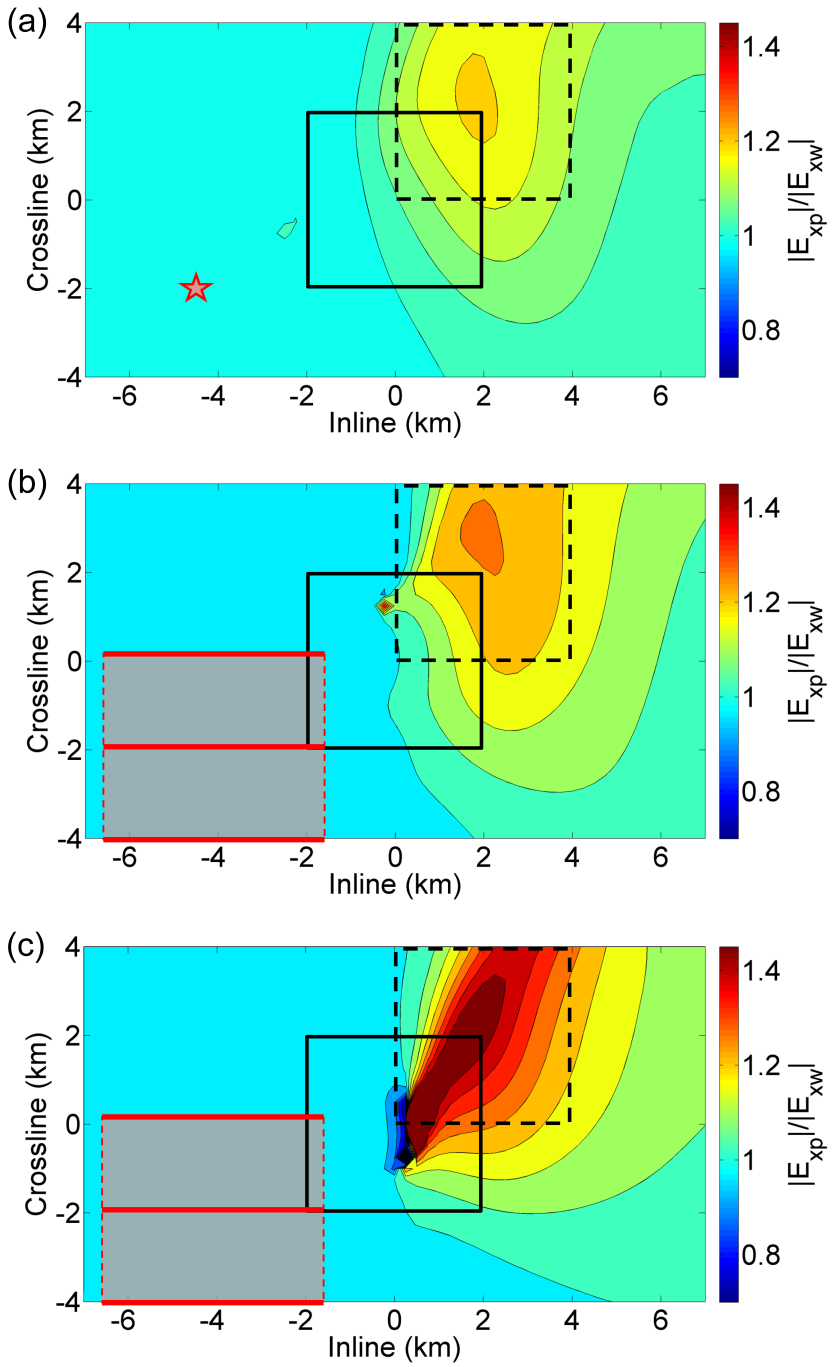

Figure 3.3: The ratio of the absolute value of the inline electric component for a single source (panel a), a 2D synthetic aperture source (panel b), and a steered 2D synthetic aperture source (panel c). All three images depict the response at receivers located on the ocean floor. The footprint of the reservoir is outlined in black and the source is outlined in red. The area of expected reservoir anomaly is shown as the dashed black box.

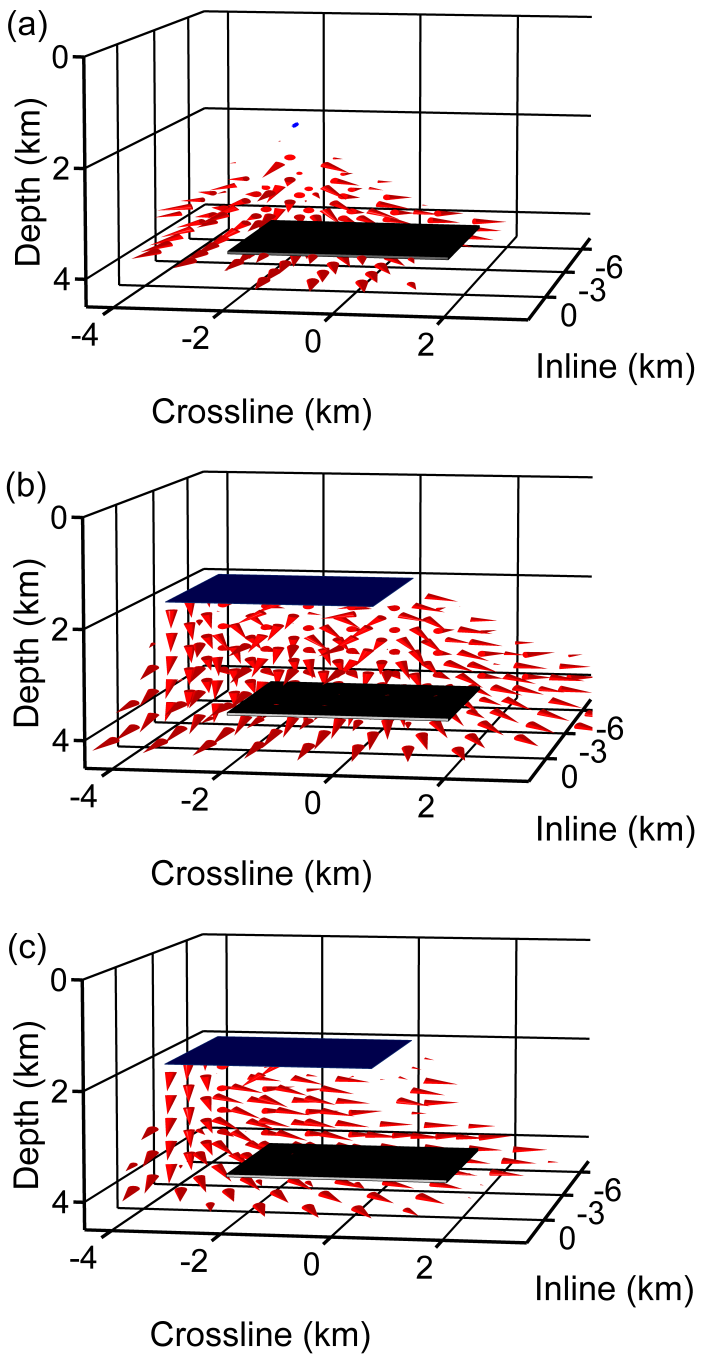

Figure 3.4: The normalized, time-averaged Poynting vectors with z-component greater than zero for a single source (panel a), a 2D synthetic aperture source (panel b), and a steered 2D synthetic aperture source (panel c). The Poynting vectors from the 2km water layer (including the airwave) have been removed for clarity. All three images depict the footprint of the reservoir in black and the source in blue.

z-component greater than zero for a single source, the 2D synthetic aperture source, and the steered 2D synthetic aperture source. The Poynting vectors from the 2km water layer, which includes the airwave, are not shown to make the subsurface interactions of the field visible. The message of Figure 3.4 is the difference in direction of the Poynting vectors from the steered source when compared to the other sources. The steered source shifts the energy towards the reservoir in the crossline direction (panel c) while the energy of the single source (panel a) and unsteered 2D synthetic aperture source (panel b) radiate downward and away from the reservoir. Our ability to steer in the crossline direction, shown in Figure 3.3(c), is promising because even though the towlines are sparsely spaced, 2km apart in the crossline direction, we are still able to achieve coherent steering of the energy with just three towlines. The Poynting vectors show an organization in the crossline direction that is not present in the vectors of the other sources. These vectors may assist in refining the optimization by defining the change in the direction of the energy propagating through the reservoir. The Poynting vector is a useful tool to view all parts of the electromagnetic energy propagating through the earth.

3.6 Conclusion

The synthetic aperture technique offers a way to address some of the limitations of CSEM without requiring any changes in acquisition. Applying the technique to synthetic CSEM data demonstrates the possible increase to the detectability of hydrocarbon reservoirs. Steering the fields in both the inline and crossline directions sends more energy toward the reservoir rather than propagating out symmetrically. The implementation of these techniques increases the amount of information gleaned from data acquired from the CSEM survey, making CSEM a more valuable tool for industry. Research is ongoing to optimize the synthetic aperture source and to investigate the implications of synthetic aperture to the design of CSEM surveys.

3.7 Acknowledgments

We acknowledge the use of synthetic data generated from INTEM3D, a modeling code developed by the CEMI consortium at the University of Utah. We are grateful for the financial support from the Shell Gamechanger Program of Shell Research, and thank Shell Research for the permission to publish this work.

CHAPTER 4

OPTIMIZED 3D SYNTHETIC APERTURE FOR CSEM

Allison Knaak[1], Roel Snieder[1], Liam Ó Súilleabháin[2], Yuanzhong Fan[2], and David Ramirez-Mejia[2]

Submitted to *Geophysics*

4.1 Abstract

Locating hydrocarbon reservoirs has become more challenging with smaller, deeper or shallower targets in complicated environments. Controlled-source electromagnetics (CSEM) is one geophysical method used by industry to find and derisk reservoirs in marine settings. The diffusive nature of CSEM fields means the signal from the target is only a small part of the total field. To reduce the impact of the complicated settings and improve the detecting capabilities of CSEM, we apply synthetic aperture to CSEM data. Synthetic aperture virtually increases the length and width of the CSEM source by combining the responses from multiple individual sources. Applying a weight to each source steers or focuses the synthetic aperture source array in the inline and crossline directions. We introduce an optimization method to find the optimal weights for synthetic aperture arrays that adapts to the information in the CSEM data. To demonstrate the benefits of weighted synthetic aperture, we apply a 2D synthetic aperture array and a crossline only synthetic aperture array to noisy, simulated electromagnetic fields. Both synthetic aperture arrays reduce the noise and increase the anomaly from the reservoir. The crossline only synthetic aperture array enhances the inline resolution of the measurements.

[1]Center for Wave Phenomena, Colorado School of Mines, Golden, CO
[2]Shell International Exploration & Production, Houston, TX

4.2 Introduction

Controlled-source electromagnetics (CSEM) is a geophysical method used primarily for finding oil reservoirs in marine settings (Constable, 2010; Constable & Srnka, 2007; Edwards, 2005). CSEM was first proposed in academic research and was implemented in industry over a decade ago (see Constable, 2010; Constable & Srnka, 2007; Edwards, 2005 for history and overview). Industry now uses the method widely to derisk and discover offshore reservoirs (Constable & Srnka, 2007). The method involves towing an electric dipole source over receivers placed on the ocean floor, which record the electric and magnetic fields. The dipole source, operating at low frequencies (typically around 0.1-1 Hz), emits a signal, which travels down through the conductive subsurface creating diffusive fields (Constable & Srnka, 2007). The diffusive fields decay quickly which means that the signal from the reservoir is only a small part of the total field. The difficulty of identifying the signal from the reservoir is exacerbated in complicated environments. Finding and derisking reservoirs with CSEM has become more challenging because CSEM is applied to targets that are shallower, deeper, smaller, and in more complex settings. We apply synthetic aperture to reduce the impact of these issues and improve the detecting capabilities of CSEM. Researchers in the radar field first developed synthetic aperture and now many different fields, including medical imaging and geophysics, apply the technique (Jensen *et al.*, 2006; Van Veen & Buckley, 1988). Synthetic aperture utilizes the information from multiple individual sources to create a source array with a longer aperture. Fan *et al.* (2010) first applied synthetic aperture to CSEM fields using sources from a single towline to create a source array several kilometers long. The use of synthetic aperture has expanded to include sources from multiple towlines, which allows for the creation of a 2D source array. We give a weight to each source in the synthetic aperture source array to maximize the signal from the reservoir. The weighting is analogous to beamforming with synthetic aperture radar and allows us to steer or focus the energy in the inline, crossline or both directions. In this paper, we first review the application of weighted synthetic aperture to CSEM. Then we introduce a method to find the optimal

weighting parameters for a synthetic aperture source array. Finally, we present two examples of applying the optimal weighted synthetic aperture to synthetic electromagnetic fields with noise added.

4.3 Weighted synthetic aperture

We review the theory and history of weighted synthetic aperture and present a new weighting formulation for applications to CSEM. Fan *et al.* (2010) first applied synthetic aperture to CSEM fields; however, the technique was developed earlier for radar (Barber, 1985). Currently, many fields use the technique, including radar, sonar, medical imaging, to increase resolution or detectability (Barber, 1985; Jensen *et al.*, 2006; Van Veen & Buckley, 1988). The technique virtually increases the length of the aperture of a source by summing responses from multiple individual sources. To create a beam to steer or focus, one weights the sources in the synthetic aperture source array; there are numerous algorithms from the radar field to determine the appropriate weights for a specific type of beam (Van Veen & Buckley, 1988). Synthetic aperture was only recently applied to CSEM fields because it was thought diffusive fields could not be steered (Mandelis, 2000). Løseth *et al.* (2006) demonstrated that electromagnetic fields can be described by both wave and diffusion equations. A solution to the 3D scalar diffusion equation is a plane wave at single frequency with a defined direction of propagation (Fan *et al.*, 2010; Løseth *et al.*, 2006). The equation for synthetic aperture in the frequency domain at a single frequency is given by

$$S(\mathbf{r}) = \sum_j a_j F_j(\mathbf{r}), \tag{4.1}$$

where a_j is a complex weighting term and $F_j(\mathbf{r})$ is the response of any component of the electric or magnetic field for each source j at the location $\mathbf{r}$. For CSEM, implementing synthetic aperture is a post-acquisition step and does not require any changes to the acquisition design. Because the synthetic aperture source array is composed of multiple individual sources, the direction of radiation can be steered or focused by weighting the individual sources. Fan *et al.* (2011, 2012) demonstrate steering and focusing with CSEM fields with

a single towline. Generalizing to using sources from several towlines, one can choose the weights to steer the source array in the inline direction (along the towline), the crossline direction (perpendicular to the towline), or in both directions. Previously, we used exponential weighting where we chose a single value for the amplitude term and a steering angle for the phase shift (Fan *et al.*, 2011, 2012; Knaak *et al.*, 2013). This type of weighting is analogous to a fixed beamformer for radar where the weighting is independent of the signal (Van Veen & Buckley, 1988). The phase shift and amplitude terms for exponential weighting are linear in the spatial coordinates, which essentially forces the source array to radiate a plane wave. This type of weighting is not ideal for every situation. For example, a 2D source array centered over a reservoir would be more effective with weights that focus the energy towards the center. To achieve a less restrictive formulation, we define the weight as a complex number for each source. The new weighting creates an adaptive, weighted synthetic aperture source array where the weight is allowed to take on any value. With this formulation, the number of weights corresponds to the number of sources in the synthetic aperture array. Previously, we tested different combinations of phase shifts and amplitude terms to find the best steering parameters, with the range of steering angles and amplitudes set by what seemed reasonable based on the geometry. Testing combinations is impractical given the large number of weights in the new formulation. Also with a 2D source array, the functional form of the weights is not easily known. Focusing may be optimal for some source locations while steering works better for others. To determine the optimal weights for a 2D source array, a new solving method is needed. In the next section, we introduce an optimization method used to find the optimal weights for the synthetic aperture source array.

4.4 Optimizing the weights for synthetic aperture

To ensure that weighted synthetic aperture highlights the reservoir optimally for every source array location, we use optimization to solve for the weights used to steer the synthetic aperture source. The goal of applying synthetic aperture to CSEM data is to increase

the detectability of the reservoir and/or increase the spatial resolution. We measure the detectability as the magnitude of the difference between the pay field and the wet field. The pay field is the electromagnetic field recorded from a CSEM survey or the fields generated from a model including a reservoir. The wet field is the background field without the reservoir. To implement this method with real data, one needs an estimate of the response without the reservoir or the response from a nearby location without a reservoir. We apply weighted synthetic aperture to both the pay and wet fields, as in equation 4.1, to determine the increase in the signal from the reservoir. The equations for the weighted synthetic aperture pay field and wet field are given below:

$$S^p(\mathbf{r}) = \sum_j a_j F_j^p(\mathbf{r}) \tag{4.2}$$

$$S^w(\mathbf{r}) = \sum_j a_j F_j^w(\mathbf{r}), \tag{4.3}$$

where $F_j^p(\mathbf{r})$ and $F_j^w(\mathbf{r})$ are any component of the electric or magnetic field at receiver $\mathbf{r}$ from the pay field and wet field respectively and a_j is the weight for the source j. One way to measure the anomaly from the reservoir is to take the difference between the pay and wet fields. The difference gives the contribution from the secondary field created by the presence of the reservoir. This is the measure we use in the optimization scheme to determine the optimal weights. The difference between the weighted synthetic aperture pay and wet responses is given by:

$$\Delta S(\mathbf{r}) = S^p(\mathbf{r}) - S^w(\mathbf{r}). \tag{4.4}$$

The optimal weights are those that maximize the difference between the two steered synthetic aperture responses. One way to create a large difference between the responses is to use a set of weights equal to a large scalar value, which amplifies the magnitude of the response from each source in the synthetic aperture array. This type of weighting effectively increases the amount of energy radiating by the source array instead of increasing the signal from the reservoir. To ensure the energy radiated by the source array is fixed, we place the following

constraint on the weights a_j:

$$\sum_j |a_j|^2 = 1, \tag{4.5}$$

These weights normalize the energy that is radiated by the synthetic aperture source. The following constrained optimization problem maximizes the difference between the pay and wet fields while constraining the total energy radiated:

$$\max |\Delta S(\mathbf{r})|^2 \text{ subject to } \sum_j |a_j|^2 = 1. \tag{4.6}$$

We define the optimal weights as those that create the maximum difference ΔS in the weighted synthetic aperture pay and wet responses at receiver location $\mathbf{r}$. The optimization gives higher amplitude to the sources with more information about the reservoir. We select the quadratic objective function in equation 4.6, rather than the ratio between the pay and wet fields, because it gives a linear system of equations for the weight a_j. The optimization method we outline above is similar to linear constrained optimization beamformers for synthetic aperture radar (Van Veen & Buckley, 1988). The common way to solve this type of constraint optimization problem is to use Lagrangian multipliers (Aster *et al.*, 2005; Boas, 1983). However, because of the linearity of the objective function, we apply a different solving method. The quadratic term $|\Delta S(\mathbf{r})|^2$ in equation 4.6 is the equation for an ellipsoid, which the constraint, $\sum_j |a_j|^2$ describes as a sphere. The optimal weights occur at the intersection of the sphere and the ellipsoid, which is the largest principal axis of the ellipsoid. Figure 4.1 depicts the geometry with 2D shapes. We can rewrite the inversion problem in quadratic form as

$$\max \mathbf{a}^\top \mathbf{H} \mathbf{a}^*, \tag{4.7}$$

where $*$ denotes the complex conjugate, $\mathbf{a}$ is the vector of optimal weights, and $\mathbf{H}$ is a Hermitian matrix, where the eigenvectors $\mathbf{u}$ of $\mathbf{H}$ are the columns of the matrix $\mathbf{U}$. The components of $\mathbf{H}$ are $\Delta F_j \Delta F_k^*$, the difference between the unweighted pay and wet fields, for $j = 1, ..., n$ and $k = 1, ..., n$ with n equal to the number of sources in the synthetic aperture source array. The matrix is diagonalized to rotate to the principal axes of the ellipsoid by

decomposing the Hermitian matrix into $\mathbf{H} = \mathbf{U}\mathbf{\Lambda}\mathbf{U}^{\top}$. The eigenvector $\mathbf{u}_j$ corresponding to the largest eigenvalue $\lambda_{\max}$ is the vector of optimal weights $\mathbf{a}$. We meet the weighting constraint by normalizing the vector of weights. One characteristic of this method is that the vector of weights multiplied by a constant phase shift remains a valid solution. This does give a known phase shift to the steered source, but it does not effect the overall steering created by the change in phase between sources.

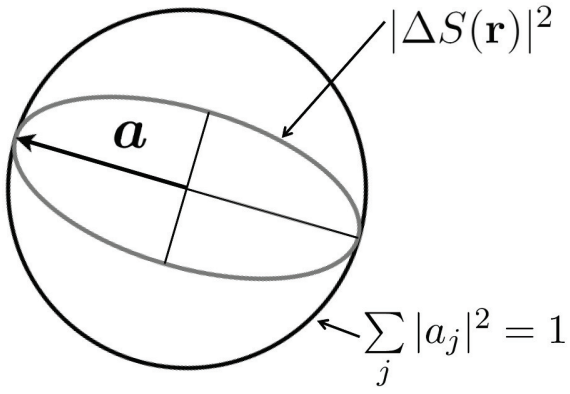

Figure 4.1: An illustration of the optimization problem depicted with 2D shapes. The squared absolute value of the difference is the equation for an ellipsoid and the weighting constraint is the equation for a sphere. The vector that lies along the principal axis of the ellipsoid is the vector of optimal weights.

The difference between wet and pay fields is equivalent to the imprint of the reservoir on the response. The amplitude of this signal is several magnitudes larger at small source-receiver offsets than at larger source-receiver offsets. The inversion focuses on the locations with higher magnitude in the difference of the response because the goal is to maximize the difference. However, there is valuable information in the signal at larger offsets. To force the inversion to value all the differences between responses evenly, the responses are weighted by the inverse of the amplitude of the wet field $F_j^w(\mathbf{r})$ as shown below:

$$W_j(\mathbf{r}) = 1/|F_j^w(\mathbf{r})|. \tag{4.8}$$

We apply the weighting to each response from a source in the synthetic aperture array. This type of weighting is commonly used in inversion of CSEM data to equalize the amplitudes (Weitemeyer *et al.*, 2010). The difference with evenly valued data is given by

$$\Delta S_j(\mathbf{r}) = W_j(\mathbf{r})(S_j^p(\mathbf{r}) - S_j^w(\mathbf{r})). \tag{4.9}$$

Now the optimization scheme finds the optimal weights that highlight the reservoir for each individual source, even those at large offsets. The optimization method solves for data-dependent weights that create an adaptive beamformer to maximize the signal from the reservoir encoded in the electromagnetic fields. The only inputs are a component of the electric or magnetic fields of the sources in the synthetic aperture array. The user decides on the length and width of the source array, which allows the method to work with any survey geometry. The optimization also independently switches from steering to focusing, depending on the geometry, without additional information from the user. To show the impact of these characteristics of the optimization method and the benefits of weighted synthetic aperture, we present two examples from modeled electromagnetic fields of two shallow reservoirs in a marine setting.

4.5 Synthetic examples

We present examples from a synthetic model to demonstrate the benefits of an optimized, steered synthetic aperture source array. The synthetic electromagnetic fields were generated with the IBCEM3D code, modeling software for 3D electromagnetic fields (Endo & Zhandanov, 2009). We modeled a shallow water situation (water depth of 200 m) with two reservoirs that are laterally separated. The model has an anisotropic layered background with typical vertical resistivities found in shallow water locations, shown in Figure 4.2. The two reservoirs are both 1.5 km below the seafloor and 50 m thick with a resistivity of 50 Ωm. The two reservoirs are separated 1.5 km laterally as shown in Figure 4.2. The source is a 270 m horizontal electric dipole with a frequency of 0.2 Hz. The survey has five towlines spaced 1.5 km apart, each with 186 source locations. The 61 receivers are along one line,

centered in the crossline direction, and spaced 500 m apart in the inline direction. A map view of the survey design is shown in Figure 4.3. To make our examples more realistic, we add a typical noise floor of 10^{-15} V/Am^2 independent random noise to the simulated electromagnetic fields (Constable, 2010). A benefit of the outlined weighted synthetic aperture

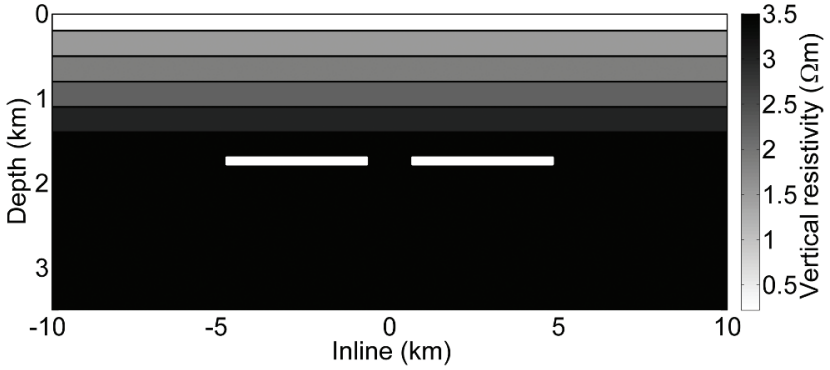

Figure 4.2: An inline cross-section of the model used to generate the electromagnetic fields. The first layer is water with a depth of 200 m. There are five sediment layers with varying resistivity. The reservoirs are shown as the white rectangles. The vertical scale is exaggerated.

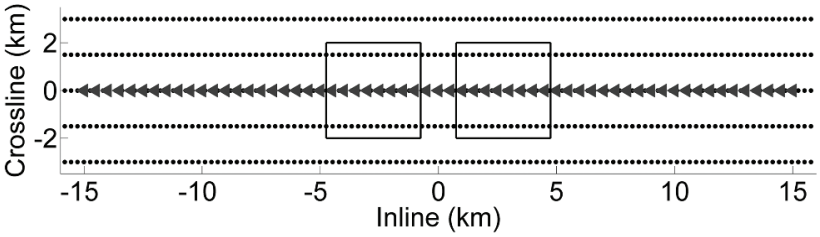

Figure 4.3: The survey geometry used to create the synthetic CSEM data. The sources are shown as black dots and the receivers are the gray triangles. The locations of the reservoirs are outlined in black.

technique is the flexibility of the method to work for several different applications. Here we present two different applications of weighted synthetic aperture. The first example is for a situation where a higher level of detectability is required. To increase the magnitude of the recorded anomaly, we apply a 2D weighted synthetic aperture source array. The second example is for a situation where more information about the structure is needed. Resolving the two reservoirs in the model is best done with crossline steering only because the

inline steering spatially averages the two anomalies. For these examples, we use only the inline component of the electric field. To view the electromagnetic fields, we use common midpoint versus offset plots, which show data points with common offsets along the same horizontal line. Displaying the response from the synthetic aperture array this way creates a pseudo-depth section (Silva Crepaldi *et al.*, 2011). The difference is the measure of the response in the optimization method; however, it is more informative to view the normalized difference, which is the difference divided by the absolute value of the background field. Figure 4.4 shows the normalized difference of the modeled inline electric pay and wet fields with noise added for no synthetic aperture (panel a), 2D steered synthetic aperture (panel b), and steered crossline only synthetic aperture (panel c). For the original data, the anomaly from the reservoir appears at 7 km offset and the maximum of the anomaly is 27%, which includes the signal from the reservoir but also noise. A typical criterion for detectability in CSEM surveys is a normalized difference of around 20% (Constable, 2010). With a 2D weighted synthetic aperture source array (shown in Figure 4.4(b)), the anomaly increases in magnitude and spatial area. However, the structural information about the two reservoirs is obscured. Applying synthetic aperture only in the crossline direction preserves the two anomalies (Figure 4.4(c)). The details of each example are described in the sections below.

We apply synthetic aperture to increase the anomaly from a reservoir in imaging. However, the only way to recover a model of the subsurface from CSEM data is through inversion. Figure 4.4(b) obscures the true structure of the model in the image, but an inversion of the weighted 2D synthetic aperture source may produce a more accurate model of the subsurface than the original data. Future work will focus on the effects of synthetic aperture to inversion of CSEM data.

4.5.1 Increasing detectability

If the goal of applying synthetic aperture is to increase the signal from the reservoir then the best method is to use a 2D source array because information from both the crossline and inline directions is included. To apply 2D synthetic aperture and find the optimal weights,

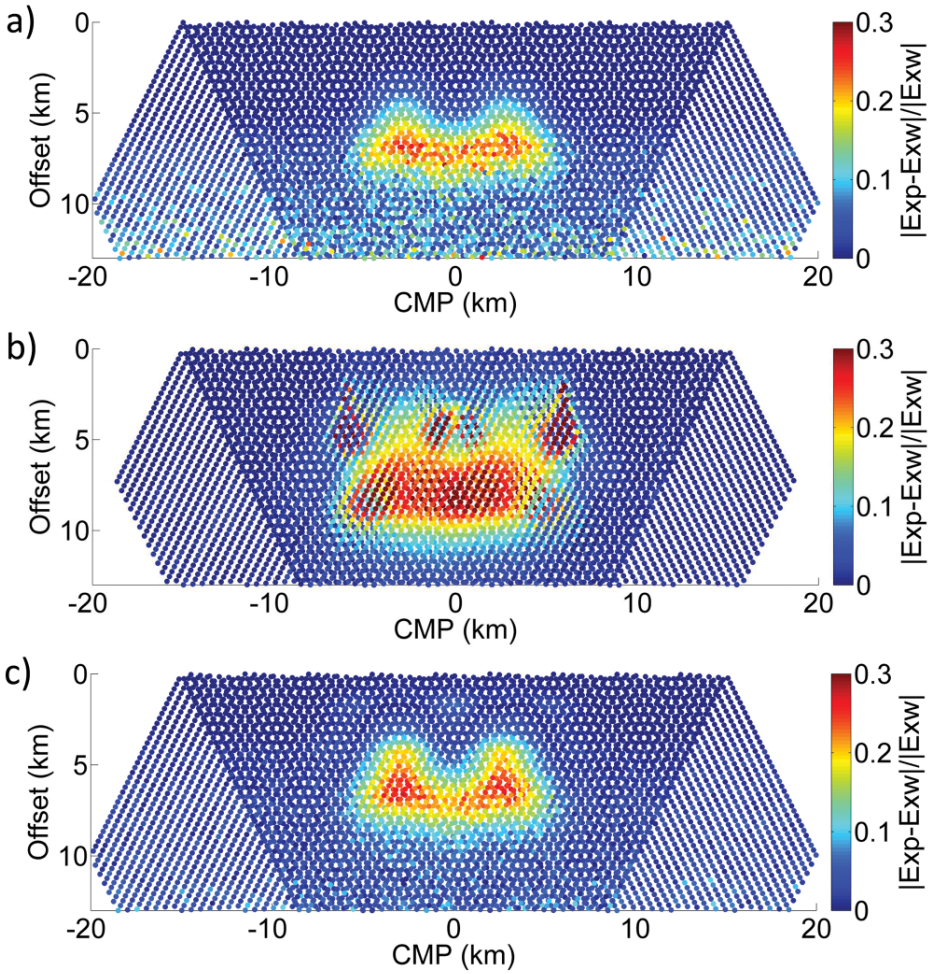

Figure 4.4: The normalized difference of the inline electric pay field and the inline electric wet field with 10^{-15} V/Am^2 independent random noise added for the original data (panel a), the optimal 2D steered synthetic aperture source array (panel b), and the optimal crossline steered synthetic aperture source array (panel c).

we first decide on a length and width for the 2D synthetic aperture source. A larger source array creates higher detectability but the averaging in the inline direction also increases, which can obscure structure. For this example, we arbitrarily use 21 sources in the inline direction and all five sources in the crossline direction. The resulting synthetic aperture source array is 5.7 km long and 6 km wide. The source spacing in the inline direction (270 m apart) is denser than the spacing in the crossline direction (1.5 km apart). Even with this discrepancy, we achieve coherent focusing in the crossline direction. We apply the optimization scheme to find the 105 weights that maximize the difference between the pay and wet fields for one source array location. We move the synthetic aperture source array around the entire survey footprint to simulate towing the 2D synthetic aperture source array. We make the assumption that, for a real data situation, the optimization scheme would use data generated from models of the expected structure, and hence the electromagnetic fields would not contain noise. Thus inputs into the optimization method are the inline electrical response from each source included in the synthetic aperture array without noise. The optimization method finds the optimal weights for each source array location and for all receivers. We then apply the optimal weights to the noisy inline electrical pay and wet fields for each source in the 2D synthetic aperture array. The normalized difference of the inline electric fields for the 2D steered synthetic aperture source is shown in Figure 4.4(b). With the application of the optimal weighted 2D synthetic aperture source, the anomaly from the reservoir has increased in magnitude and spatial extent. The maximum normalized difference is 46%, which is an increase from the 27% anomaly in the original noisy data. Additionally, the noise, shown in the large offsets in the image without synthetic aperture, Figure 4.4(a), does not appear in the normalized difference of the noisy inline electric fields from the steered 2D synthetic aperture source. There is still some noise in the image but the addition of multiple sources in the synthetic aperture source array increases the magnitude of the coherent signal and almost completely stacks out the random noise.

To understand the adaptive nature of the optimization scheme, it is useful to look at the optimal weights for the 2D synthetic aperture source array from different locations. The optimal weights for one source array location and receiver can be viewed in phase and amplitude plots. Figure 4.5(a) and Figure 4.5(b) display contour plots of the amplitude and phase, respectively, of the steering coefficients for the source array centered at -8.26 km and the receiver located in the center of the survey between the two reservoirs. The optimal weights for this location steer the field toward the center by giving a higher phase shift to the source farther away in the inline direction. In the crossline direction, the weights focus toward the center with a parabolic phase shift where the outer towlines are weighted higher. The amplitude plot (Figure 4.5(a)) shows that the sources closer to the nearest reservoir, for this source array position, have a higher weight. The sources given lower amplitude weight contain less information about the reservoirs than those weighted higher. Figure 4.6(a) and Figure 4.6(b) display contour plots of the amplitude and phase, respectively, for the source array centered at 3.08 km. This source array location is directly over one reservoir, and the amplitude plot shows that more emphasis is placed on the source locations with larger offsets. Less emphasis on the sources over the reservoir is congruent with the expected weighting because small source-receiver offsets are dominated by the background signal (Constable, 2010). The phase shifts (Figure 4.6(b)) are similar to those from the other source array location but with a larger phase shift across the source array in the inline direction. Figure 4.5(a) and Figure 4.6(a) show there is a section of the synthetic aperture array that has amplitude weighting close to zero, which demonstrates that the sources in that part of the source array are not contributing to the increase in the anomaly from the reservoir. The optimization method essentially implemented a smaller synthetic aperture for these two source array locations, which indicates we could have chosen a smaller synthetic aperture length. However, because the method is able to recognize when to reduce the length, there is no detriment from the longer synthetic aperture.

The optimal 2D weighted synthetic aperture source array increases the magnitude and spatial area of the anomaly. However, 2D steering averages the two anomalies into one large anomaly, which conceals the fact that there are two reservoirs present. The ability to discern if two reservoirs are present is difficult in CSEM data. To increase the anomaly and retain the information about the structure, we apply a different steering method.

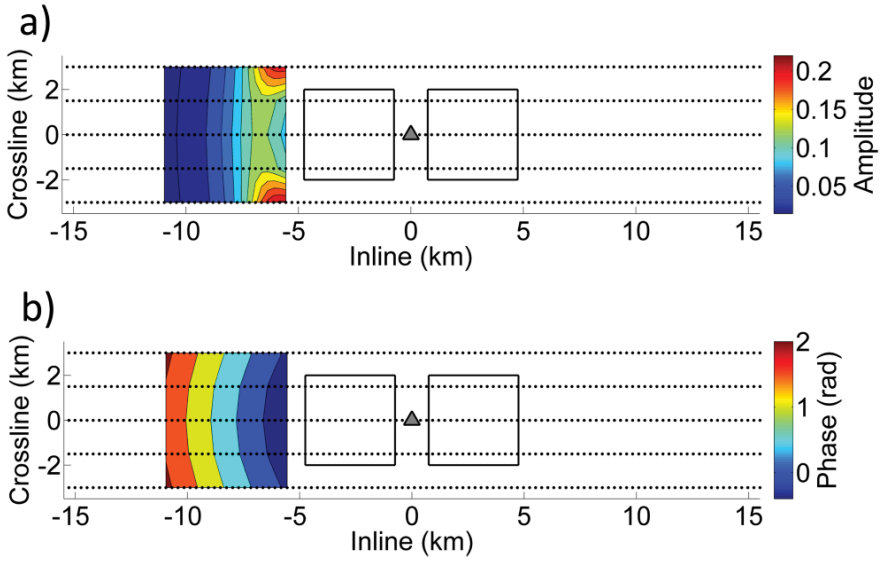

Figure 4.5: A map view of the amplitude (panel a) and the phase (panel b) of the optimal weights for the 2D synthetic aperture source array centered at -8.26 km for the responses from the receiver specified by the gray triangle.

4.5.2 Increasing lateral detectability

It is often difficult with CSEM field responses to determine if a reservoir consists of one unit or two separate reservoirs. If the goal is to differentiate two bodies, then crossline synthetic aperture is the best choice because the inline steering averages the two anomalies from the two receivers and the anomaly appears to be from one reservoir. We use sources from all five towlines to create a 6 km wide synthetic aperture source in the crossline direction. We apply the optimization method for the crossline synthetic aperture source array for all source array locations and receivers. The process is the same as for the 2D source array but now we solve for five optimal weights for each source array instead of 105. We apply the

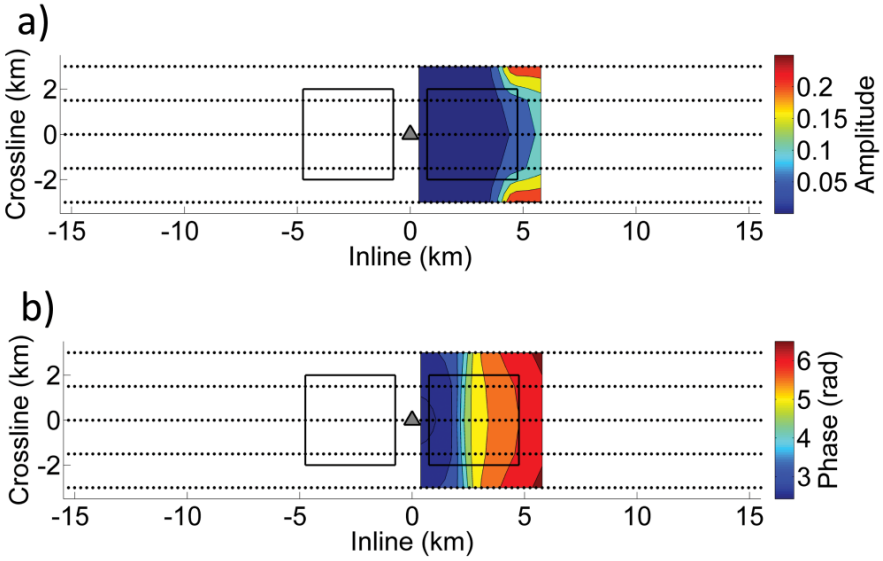

Figure 4.6: A map view of the amplitude (panel a) and the phase (panel b) of the optimal weights for the 2D synthetic aperture source array centered at 3.08 km for the response from the receiver specified by the gray triangle.

optimal weights to the inline electrical component of the pay and wet fields for each source in the crossline source array.

Figure 4.4(c) shows the normalized difference of the crossline weighted inline electric fields. The two reservoirs are more discernible with crossline weighted synthetic aperture than in the original data (Figure 4.4(a)) or the normalized difference of the 2D steered inline electric fields (Figure 4.4(b)). The crossline only synthetic aperture increases magnitude and spatial localization of each individual reservoir and does not blur the two separate anomalies into one large anomaly. To quantify the improvement, we take the spatial average of the normalized difference from 6 km to 8 km offset and 0.5 km to 4 km CMP. The average normalized difference for the crossline weighted synthetic aperture field in this area is 21%; while the same spatial average of the original field is 17%. The noise is more visible in the crossline synthetic aperture fields (Figure 4.4(c)) than in the 2D steered fields (Figure 4.4(b)) because fewer sources are in the synthetic aperture source array, but the noise level is smaller than it is for the original data (Figure 4.4(a)). The optimal weights in the crossline direction create a focus by giving the sources farthest away larger phase shifts

and amplitudes. Figure 4.7(a) shows the parabolic phase shifts for the optimal weights for the crossline source array located at -17.44 km. We did not require the optimization to create a focus, but the inversion found the best weights for the situation. We can verify if these weights are reasonable by analytically calculating the phase shifts for each of the five sources to focus the field on the reservoir. The equation for a phase shift to create a focus is given by (Fan *et al.*, 2011):

$$\Phi(x, y, z) = k(\sqrt{(x - x_f)^2 + (y - y_f)^2 + (z - z_f)^2} - D), \tag{4.10}$$

where (x_f, y_f, z_f) is the location of focus, k is the wavenumber, and D is the distance from the focal point to the nearest end of the synthetic aperture, which normalizes the phase shift. To use equation 4.10, we assume a homogeneous field and a single resistivity. We calculate the wavenumber for the survey frequency, 0.2 Hz, and a resistivity equal to 3 Ωm (the resistivity of the second-to-last layer in our model) and set the depth of the focus at 1.51 km, which is the depth of the reservoirs. The focus point varies for each source array location. We choose one source array location (-17.44 km) to compare the optimal focusing with the calculated focusing. The calculated focus point that produces a curvature matching the optimal weights is $(x_f, y_f, z_f) = (-2.21 \text{ km}, 0 \text{ km}, 1.51 \text{ km})$. The phases of the optimal weights and the calculated weights are shown in Figure 4.7(a), and the location of the sources and calculated focus point are shown in Figure 4.7(b). The focus point is only an estimate of where the optimal weights focus point is located because we assume in the calculation a homogeneous resistivity model for the calculation. We find the phase for the calculated focus point that almost identically matches the curvature of the phase of the optimal weights and the spatial location of calculated focus point is reasonable for the geometry of the survey, which demonstrates the optimal weights agree with the analytical focusing. The optimization method thus solves for the weights that correspond to the optimal focus point for each source array location without any additional inputs from the user. In this example, there are five towlines symmetric about the reservoirs, which make focusing the best weighting option.

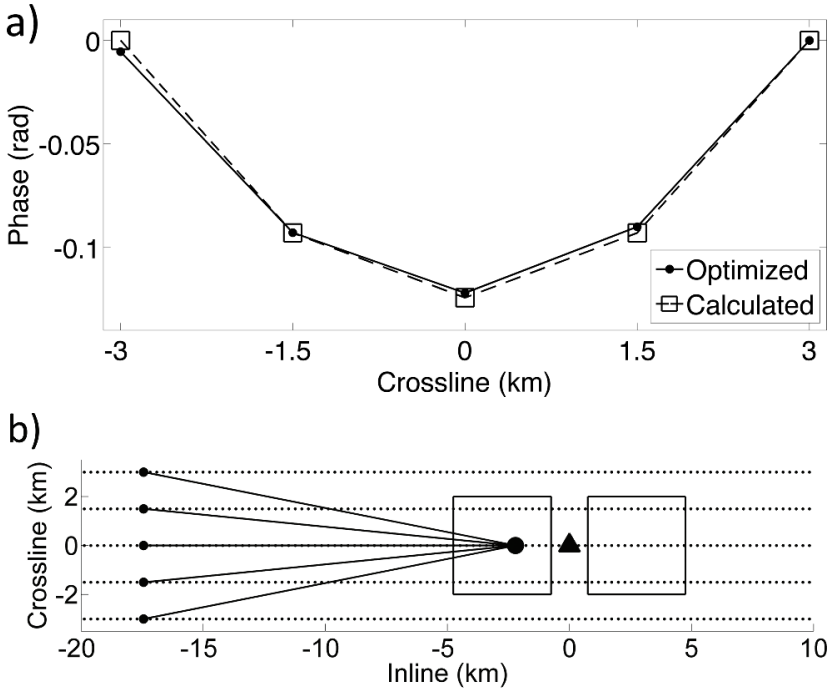

Figure 4.7: Panel a shows the phase of the optimal and calculated weights for a crossline synthetic aperture source array located at -17.44 km. Panel b shows the calculated focus point (the circle over the left reservoir) for the crossline synthetic aperture created from the five sources shown as black dots for a receiver located in the center of the survey.

The steering or focusing created by the optimal weights depends on the geometry of the survey, the information within the responses, and the size of the array.

4.6 Conclusion

Locating smaller, deeper or shallower targets with CSEM in complicated environments is becoming more challenging. We demonstrated the benefits of applying the technique of synthetic aperture, which virtually increases the length, and/or width of the source. Applying weights to the synthetic aperture source array allows us to steer or focus the array in the inline and crossline directions. With complex settings and more intricate survey geometries, the best type of weighting is no longer intuitive. We presented a method to optimize the weights for synthetic aperture source arrays, which acts as an adaptive beamformer by adjusting to the information about the reservoir encoded in the CSEM data. A 2D synthetic aperture source array applied to CSEM data increases the detectability of the reservoir and reduces noise but may obscure structure. We found that applying crossline weighting to noisy inline electric fields from a model with two laterally separated reservoirs preserved the structure, increased the magnitude of the anomalies from the reservoirs, and reduced the noise. However, the impact of weighted synthetic aperture on inversion results is unknown; a 2D source array may have more information about the structure when inverted. Future work will explore if applying weighted synthetic aperture before inversion increases the accuracy of the recovered model. We will also continue to work with synthetic aperture for the forward problem by testing the technique on more complicated models.

4.7 Acknowledgments

We acknowledge the use of synthetic data generated from IBCEM3D, a modeling code developed by the CEMI consortium at the University of Utah. We are grateful for the financial support from the Shell Gamechanger Program of Shell Research, and thank Shell Research for the permission to publish this work.

CHAPTER 5

ERROR PROPAGATION WITH SYNTHETIC APERTURE

Allison Knaak[1], Roel Snieder[1], Liam Ó Súilleabháin[2], and Yuanzhong Fan[2]

To be submitted to *Geophysical Prospecting*

5.1 Introduction

Controlled-source electromagnetics (CSEM) is a geophysical method used to find resistive reservoirs in the conductive subsurface in marine settings. A boat tows a horizontal electric dipole source over receivers placed on the ocean floor, which record electric and magnetic responses. Because the source operates at a low frequency and the subsurface is conductive, the electromagnetic fields are diffusive. The signal from the source decays rapidly over time and only a small part of the signal, which is easily obscured by noise, contains information about the reservoir. There are a variety of noise sources that affect a CSEM survey: natural radiation, swells, seawater currents, and navigation and calibration errors (Maaø & Nguyen, 2010; Mittet & Morten, 2012). These create multiplicative and additive noise in the electromagnetic responses. Efforts are made to reduce the noise in the survey design, equipment technology, and processing of CSEM (Constable, 2010; Maaø & Nguyen, 2010; Mattsson *et al.*, 2012; Myer *et al.*, 2012; Ziolkowski & Wright, 2010). Reducing the effects of noise and increasing the accuracy of CSEM would allow the use of the technology in more areas such as for monitoring reservoirs or CO_2 storage over time (Orange *et al.*, 2009).

One technique that reduces the effect of noise in CSEM responses is synthetic aperture, a technique first developed for radar applications. In this technique, one adds responses from multiple source locations to virtually increase the length and width of the source. Fan *et al.* (2010) first demonstrated how synthetic aperture applied to CSEM responses increased the

[1]Center for Wave Phenomena, Colorado School of Mines, Golden, CO
[2]Shell International Exploration & Production, Houston, TX

detectability of the reservoir. The addition of multiple sources allows one to apply weights and steer or focus the synthetic aperture array in the inline, crossline, or both directions. In a previous paper, we developed and implemented an optimization method that finds the optimal weights for each source in the synthetic aperture array (see Chapter 4). The large reduction in uncorrelated noise from weighted synthetic aperture prompted us to investigate if we could design a source array that reduces the noise even further. In this paper, we use error propagation theory to amend our optimization method to design weights that increase the anomaly from the reservoir but also reduce the noise propagation. We describe the implementation of this new optimization method and demonstrate the benefits to CSEM responses with towlines offset from the location of the receivers and reservoir thus, enabling the side-looking capabilities of CSEM.

5.2 Error propagation theory with synthetic aperture

To describe the uncertainty in electromagnetic responses from additive noise after applying synthetic aperture, we employ error propagation theory. Mittet & Morten (2012) characterize many of the uncertainties arising in CSEM and build a framework to determine which experiment components limit the detection and imaging of the reservoir. They found that one of the experimental uncertainties that restricts the detection of the reservoir the most in CSEM surveys is the receiver noise level (Mittet & Morten, 2012). Typical electric responses from a CSEM survey have a noise floor of 10^{-15} V/Am^2 which comes mostly from the limited sensitivity of the instruments (Constable, 2010). In this work, we only consider additive noise. Mittet & Morten (2012) conclude that if the receiver noise decreases by a factor of 10, then the detectable depth of burial doubles. Our goal in this paper is to design an optimally weighted synthetic aperture that reduces additive noise and increases the anomaly from the reservoir.

To understand the propagation of this noise into the new responses created from synthetic aperture, we first describe the noise in the recorded responses. For a source j and receiver location $\mathbf{r}$, we denote the complex response of one electric or magnetic field component for

a single frequency as $F_j(\mathbf{r})$. One measure of the characteristics of the noise is the covariance matrix. The covariance between responses from different sources at a single receiver location is (Bevington & Robinson, 2002)

$$C^F_{mn} = \langle (F_m - \langle F_m \rangle)(F_n - \langle F_n \rangle)^* \rangle, \tag{5.1}$$

where $\langle F_m \rangle$ is the expected value of F_m, which is the response of any component of the electric or magnetic field from the source m at a single receiver location, and the indices m and n range from 1 to N, with N equal to the number of sources. The symbol $*$ denotes the complex conjugate which is needed because the field responses are complex. The noise we are analyzing is random, independent noise, so we assume the noise in the responses is uncorrelated between different sources. Hence, elements of $\mathbf{C}^F$ with $m \neq n$ vanish and the only nonzero elements are the variances $\sigma^2_{F_m}$ of the response F_m along the diagonal:

$$C^F_{mn} = \sigma^2_{F_m} \delta_{mn}, \tag{5.2}$$

where $\sigma^2_{F_m}$ is the variance of the response F_m and δ_{mn} is the Kronecker delta. The variance of each response is determined from the estimated uncertainty of the measurements.

To reduce the noise level in synthetic aperture data, we first need to understand how the noise changes when we apply synthetic aperture to noisy electromagnetic responses. Synthetic aperture uses multiple responses from individual sources to simulate the response from a larger source. We apply the technique to CSEM responses acquired with the traditional CSEM survey setup. Previously, we have shown how weighted synthetic aperture increases the detectability and resolution of hydrocarbon reservoirs. Fan *et al.* (2012) demonstrate the increase in detectability for a single towline of real data. The equation for synthetic aperture for a single frequency is given below:

$$S(\mathbf{r}) = \sum_j a_j F_j(\mathbf{r}), \tag{5.3}$$

where $F_j(\mathbf{r})$ is any component of the electric or magnetic response at receiver location $\mathbf{r}$ for the source j, and a_j is a complex weight for the source j. For a single receiver location $\mathbf{r}$, synthetic aperture is a linear combination of the responses F_j multiplied by the weights

a_j. The error propagation equation for a weighted linear function with uncorrelated noise is (Bevington & Robinson, 2002)

$$\sigma_S^2 = \mathbf{a}^\top \mathbf{C}^F \mathbf{a}^*, \tag{5.4}$$

where σ_S^2 is the variance of the response from the synthetic aperture source array $S(\mathbf{r})$, $\mathbf{C}^F$ is the covariance matrix of the electromagnetic responses as detailed in equation 5.2, and $\mathbf{a}$ is the vector of complex weights for the source array. If we give each source in the synthetic aperture array a uniform weight, then the variance of the synthetic aperture response will be a summation of the variances in the responses corresponding to the individual sources. We can find a vector of weights that optimally reduces the contribution of the noise in the synthetic aperture response. In the next section, we explain how we use this description of the error propagation in synthetic aperture to discover the optimal weights that reduce the noise and increase the anomaly.

5.3 Reducing error propagation with optimization

In previous work, we developed an optimization method that calculates the optimal weights for synthetic aperture source arrays that highlight the target in a CSEM survey. Without any user input, other than the size of the synthetic aperture array, the optimization scheme identifies the optimal weights, that adjust from steering to focusing depending on the information in the responses, for each synthetic aperture source array location (as shown in Chapter 4). Then we incorporate the error propagation theory into the optimization method to increase the anomaly from the reservoir while also reducing the imprint of the noise on the synthetic aperture data. First, we review our original optimization method and then we explain how we merge the noise reduction into our objective function.

The goal of using optimization for our problem is to increase the detectability of the target by finding the weights that maximize a detectability measure. The detectability measure we use is the difference between the synthetic aperture response with the reservoir present and the synthetic aperture response without the reservoir. The difference between the two

responses leaves the secondary field generated from the presence of the reservoir. We use this measure, rather than others such as the ratio, because it results in a linear system of equations. We denote the synthetic aperture response from the field responses with the reservoir present, also called the pay field, as $S^p(\mathbf{r})$; we denote the synthetic aperture response from the field responses without the reservoir, also called the wet field, as $S^w(\mathbf{r})$ as shown below:

$$S^p(\mathbf{r}) = \sum_j a_j F_j^p(\mathbf{r}) \tag{5.5}$$

$$S^w(\mathbf{r}) = \sum_j a_j F_j^w(\mathbf{r}), \tag{5.6}$$

and we denote the difference between the two fields as

$$\Delta S(\mathbf{r}) = S^p(\mathbf{r}) - S^w(\mathbf{r}). \tag{5.7}$$

In practice, there is no reference field response from a CSEM survey. We assume the background response has been simulated or statistically estimated from the recorded responses. The objective function for the optimization scheme maximizes the absolute squared difference of the wet and pay responses:

$$\max |\Delta S(\mathbf{r})|^2. \tag{5.8}$$

Because this objective function increases quadratically with the weights, we need to place a constraint on the amplitude of the weights. The following constraint ensures that the synthetic aperture source radiates a fixed amount of energy:

$$\sum_j |a_j|^2 = 1. \tag{5.9}$$

The constrained optimization problem is stated as

$$\max |\Delta S(\mathbf{r})|^2 \text{ subject to } \sum_j |a_j|^2 = 1. \tag{5.10}$$

Linear constrained optimization problems are usually solved with Lagrangian multipliers (Aster *et al.*, 2005; Boas, 1983). We propose a different method that utilizes the quadratic property of the problem to determine the optimal weights for each synthetic aperture source

array location. The objective function rewritten as a quadratic function of the vector $\mathbf{a}$ becomes

$$\max \mathbf{a}^{\top}\mathbf{H}\mathbf{a}^{*}, \tag{5.11}$$

where $\mathbf{a}$ is the vector of optimal weights, and $\mathbf{H}$ is a Hermitian matrix with $H_{ij} = \Delta F_i \Delta F_j^{*}$, where $i, j = 1, ..., N$ with N equal to the number of sources in the synthetic aperture source array. The constraint (equation 5.9) placed on the weights is a sphere and the objective function (equation 5.8) is an ellipsoid. The optimal weights occur where the ellipsoid touches the sphere. To find the optimal weights, we need to identify the largest principal axis of the ellipsoid. We rotate the Hermitian matrix $\mathbf{H}$ to its principal axes by decomposing the matrix into $\mathbf{U}\mathbf{\Lambda}\mathbf{U}^{\top}$ with eigenvalue decomposition. The matrix $\mathbf{U}$ contains the eigenvectors that correspond to the eigenvalues on the diagonal of the matrix $\mathbf{\Lambda}$. The largest eigenvalue defines the direction of the largest axis of the ellipsoid, and the eigenvector matching that eigenvalue is the vector of optimal weights. We satisfy the constraint by normalizing the vector. The optimization scheme repeats this process for every receiver and synthetic aperture source location.

The electric and magnetic responses from a CSEM survey decay exponentially as the distance between the source and receiver increases. We normalize the responses by the absolute value of the background or wet field to ensure that the lower magnitude responses at larger offsets are valued equally with the higher magnitude responses at smaller offsets:

$$W_j(\mathbf{r}) = 1/|F_j^{w}(\mathbf{r})| \tag{5.12}$$

This type of weighting is commonly used in CSEM inversions (Weitemeyer *et al.*, 2010). The difference between the pay and wet fields with the weighting term becomes:

$$\Delta S(\mathbf{r}) = W_j(\mathbf{r})(S^{p}(\mathbf{r}) - S^{w}(\mathbf{r})) \tag{5.13}$$

The optimization scheme finds the weights that maximize the anomaly in the responses. The user specifies only the length and width of the synthetic aperture source array. We show in a previous paper how the optimization adapts the steering, focusing (or both) of

the weights to the responses and location of the source array (see Chapter 4). The weights from the optimization scheme create the expected steering or focusing based on the location of the source. For example, towlines symmetrically spaced over the reservoir in the crossline direction receive weights with a parabolic phase which focuses the responses toward the location of the reservoir. The summation, used to create the synthetic aperture source, averages the noise resulting in a lower noise level in the synthetic aperture response compared to the original response from a single towline. However, we wondered if we could design an optimization scheme that purposely reduces the noise at each source array location while also maximizing the anomaly.

The new goal is to define an optimization scheme that finds the optimal weights that maximize the detectability of the reservoir but also reduce the random, independent noise. To incorporate the noise reduction into our objective function, we use the error propagation theory defined in the previous section to minimize the variance of the constructed synthetic aperture source array σ_S^2. The objective function is defined as

$$\min \sum_j |a_j|^2 \sigma_{F_j}^2, \tag{5.14}$$

where a_j is the weight for the source j, and $\sigma_{F_j}^2$ is the variance of the original electromagnetic response as defined in equation 5.2. We must normalize the variances to have the same dimension as the electromagnetic responses before inserting them into our original objective function. We use the same weighting term applied to the wet and pay fields, equation 5.12, but we square the weighting to make the responses and the variance the same dimension as the norm of the detectability, as shown below:

$$C_{mn}^F(\mathbf{r}) = W_m^2(\mathbf{r}) \sigma_{F_m}^2 \delta_{mn}, \tag{5.15}$$

where $C_{mn}^F(\mathbf{r})$ is the covariance matrix for all sources m and n at receiver location $\mathbf{r}$, $W_m(\mathbf{r})$ is the same weighting function in equation 5.12, $\sigma_{F_m}^2$ is the variance for the response F_m, and δ_{nm} is the Kronecker delta. In order to incorporate the normalized error term into our optimization, we subtract the error objective function (equation 5.14) from the norm of

the differences between the pay and wet responses, which is our original objective function (equation 5.8). The new objective function maximizes the difference of the norm of the detected signal and the norm of the noise:

$$\max\ (|\Delta S|^2 - \gamma \sum_j |a_j|^2 \sigma_j^2). \tag{5.16}$$

In matrix form, the problem becomes

$$\max\ \mathbf{a}^\top (\mathbf{H} - \gamma \mathbf{C}^F) \mathbf{a}^*, \tag{5.17}$$

where $\mathbf{H}$ is the same Hermitian matrix from equation 5.11, $\mathbf{C}^F$ is the covariance matrix from equation 5.4, and $\mathbf{a}$ is the vector of optimal weights. We control the influence of the noise reduction with a weighting factor γ. When $\gamma = 1$, the matrices are equally weighted because both the Hermitian matrix and the covariance matrix are normalized by the background field and source-dipole moment. A higher value of γ places more importance on reducing the noise than on increasing the anomaly from the reservoir. In the following section, we apply this new optimization scheme to synthetic electromagnetic responses from a model with the source towlines several kilometers away from the receivers to demonstrate the improvements of the new optimization scheme.

5.4 Synthetic example

To show the benefits of applying a steered synthetic aperture source that highlights the reservoir and reduces noise, we apply our optimization method to synthetic CSEM fields. The synthetic data was generated with a 3D CSEM modeling code, IBCEM3D (Endo & Zhandanov, 2009). The model represents a typical deep-water marine setting with a single reservoir. The background is a layered, anisotropic earth model with vertical and horizontal resistivities shown in Figure 5.1. The reservoir, with a resisitivity of 35 Ωm, is 50 m thick, 4 km long in the inline and crossline directions and located 1.5 km below the seafloor. The source is a 300 m horizontal electric dipole with a frequency of 0.25 Hz. Figure 5.2 shows a map view of the survey geometry of three towlines and a single line of receivers. The

towlines, each with 100 source locations, are located at 4, 6, and 8 km away from the line of receivers. There are 29 receivers spaced 500 m apart centered over the reservoir in the crossline direction. We use towlines that are offset from the reservoir to represent a situation where the reservoir is not centered under the towlines; we choose this geometry because these offset towlines are more susceptible to noise than towlines directly over the receivers. We add independent, random noise at a level of 10^{-15} V/Am^2 to the synthetic responses to simulate the additive noise in real data.

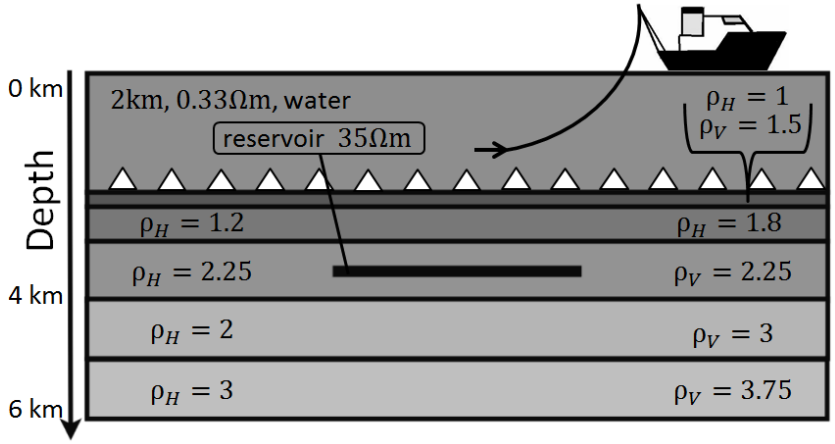

Figure 5.1: The model used to create the synthetic CSEM data. The values of ρ_H and ρ_V are the resistivity of the layer in the horizontal and vertical directions, respectively, given in Ohm-meters.

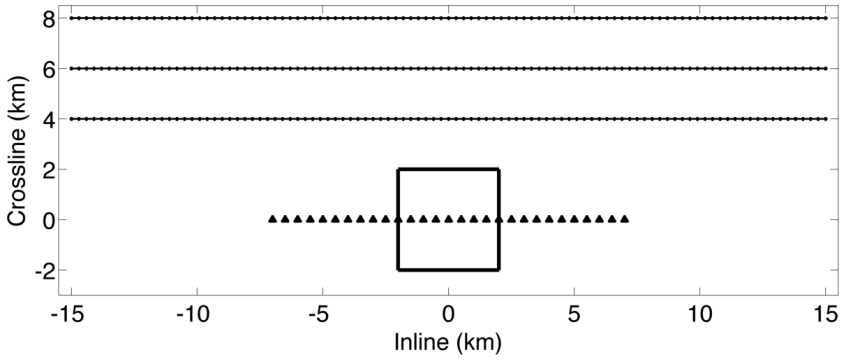

Figure 5.2: The survey geometry used to create the synthetic CSEM data. The towlines are the black lines with the source locations marked as black dots and the receiver locations marked as the black triangles. The location of the reservoir is outlined in black.

We display the simulated response in three images shown in Figure 5.3. The left panel shows the normalized difference (defined as the absolute value of the difference between the pay and wet fields divided by the absolute value of the wet field) of the original inline electric response with 10^{-15} V/Am^2 of independent, random noise added for the towline located at 6 km. The image depicts the response for all receivers and sources from the towline as a pseudo cross-section by plotting the responses at the common midpoint of the source and receiver versus their offset. This is a common way to view one component of the CSEM response (Silva Crepaldi *et al.*, 2011). The middle panel of Figure 5.3 shows the same normalized difference without noise. The right panel shows the difference between the first two panels which is the contribution from the additive noise. The anomaly from the reservoir, which begins at 5 km offset, is centered at 0 km CMP as shown in the center panel of Figure 5.3. The maximum normalized difference of the anomaly without noise is 0.234, which means there is a 23.4% change in the response from the presence of the reservoir. The noise dominates the electromagnetic response, and the anomaly from the reservoir is completely obscured (left panel of Figure 5.3) because the large distance between the source and receiver causes the magnitude of signal reaching the receiver to be almost at the detection limits of the receivers. One would not use the response from this towline for imaging or detection of the reservoir because the noise is too high.

To show the amount of improvement to the noise level from only the addition of multiple source responses, we first apply unweighted synthetic aperture to the electromagnetic responses, which is equivalent to setting the weights in equation 5.3 to be constant. The unweighted synthetic aperture response establishes a baseline for the noise reduction from a synthetic aperture source; we expect the weighted synthetic aperture response to reduce the noise better than the unweighted synthetic aperture response. We arbitrarily choose the 2D synthetic aperture source to be 6.3 km long in the inline direction and 4 km in the crossline direction. The source array uses 63 sources: 21 sources from the three towlines located at 4 km, 6 km, and 8 km. One synthetic aperture source array location is shown as a red rectangle

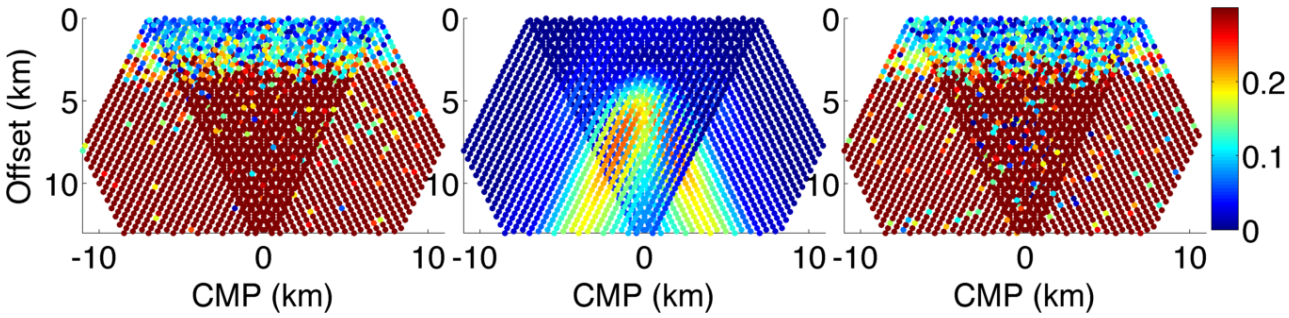

Figure 5.3: Left panel: A pseudo cross-section displaying the normalized difference of the original inline electric response for the towline located at 6 km crossline and receivers located at 0 km crossline with 10^{-15} V/Am^2 independent, random noise added. Middle panel: The same original inline electric response as the first panel without noise. Right panel: The random independent noise present in the first panel found by taking the difference between the first two images.

on a map view of the survey geometry in Figure 5.4. We move the source array in the inline direction to simulate the towing of the larger aperture source. Figure 5.5 shows the noisy normalized difference response from the unweighted synthetic aperture response (left panel), the noiseless response (middle panel), and the difference between the two responses (right panel). The addition of multiple source locations greatly reduces the amount of noise when compared to the original response (Figure 5.3) because the addition averages the incoherent noise. The noise floor in the unweighted synthetic aperture response is reduced from 0 km offset in the original response (left panel of Figure 5.3) to around 5 km offset. However, there is still noise present between 5 km and 10 km offset where the signal from the target appears (right panel of Figure 5.5). The anomaly from the reservoir is still difficult to discern from the unweighted synthetic aperture response.

We next apply our optimization scheme (equation 5.16) to find the optimal weights that maximize the anomaly from the reservoir without including the error term ($\gamma = 0$). First, we choose the length and width of the synthetic aperture source array. We use the same synthetic aperture length and width as the unweighted synthetic aperture. Then for each source array location, we input the responses from the source array into the optimization, which forms the Hermitian matrix and finds the largest eigenvalue. The vector of optimal

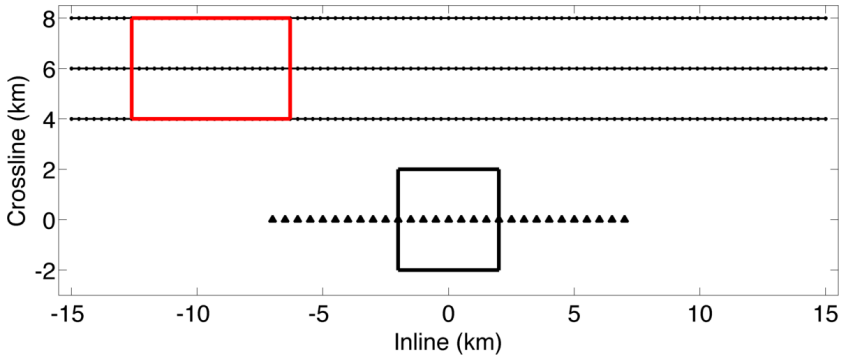

Figure 5.4: A map view of the survey geometry with one location of the synthetic aperture source array shown as the red rectangle.

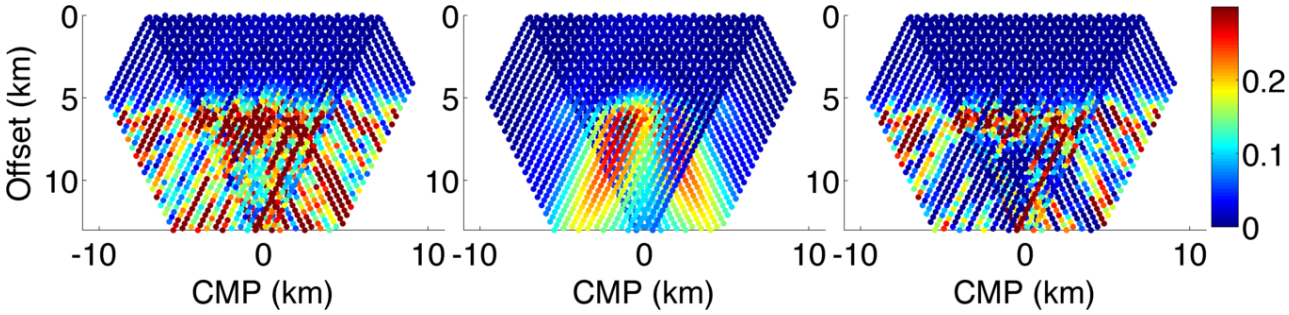

Figure 5.5: Left panel: A pseudo cross-section displaying the normalized difference of the unweighted 2D synthetic aperture response for the inline electric component with 10^{-15} V/Am^2 independent, random noise added. Middle panel: The same unweighted synthetic aperture response as the first panel without noise. Right panel: The random independent noise present in the first panel found by taking the difference between the first two images.

weights is the eigenvector that corresponds to the largest eigenvalue. Finally, we apply the optimal weights to the responses from the sources within the source array and create the weighted synthetic aperture response. The process is repeated for every receiver and source array location. Figure 5.6 shows the weighted synthetic aperture response for $\gamma = 0$. The application of weighted synthetic aperture increases the signal from the reservoir especially at smaller offsets, from 3 km to 5 km, which is an improvement over the unweighted synthetic aperture response that shows no signal from the target at those offsets (Figure 5.5). The weighted synthetic aperture response reduces the imprint of the noise where the anomaly appears, between 3 km and 10 km offset, and so the signal from the reservoir is more evident in the noisy response from the optimally weighted synthetic aperture response than either in the original data (Figure 5.3) or in the unweighted synthetic aperture response (Figure 5.5). The noise dominates the weighted synthetic aperture response for offsets greater than about 10 km. The right panel of Figure 5.6 shows a noise floor lower than the original response and the unweighted synthetic aperture response; however, there are streaks of noise at the edges of the image. The anomaly from the reservoir increases with the application of the optimization scheme with the objective function including only the norm of the difference between responses, as we expect. The noise floor decreases, without the inclusion of the error term, because of the summation of coherent signal which averages the noise.

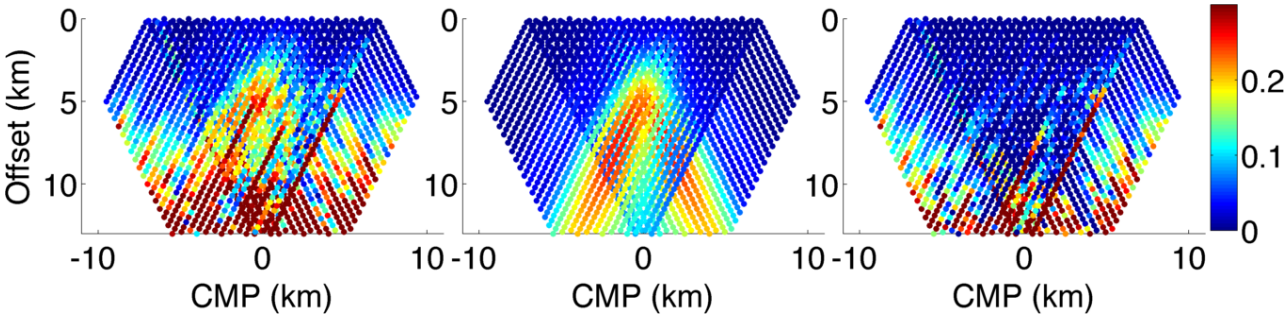

Figure 5.6: Left panel: A pseudo cross-section displaying the normalized difference of the weighted 2D synthetic aperture response for the inline electric component and $\gamma = 0$ with 10^{-15} V/Am^2 independent, random noise added. Middle panel: The same weighted synthetic aperture response as the first panel without noise. Right panel: The random independent noise present in the first panel found by taking the difference between the first two images.

We next implement the optimization scheme with the objective function that includes both the norm of the differences and the norm of the variance to design a synthetic aperture source array that increases the anomaly from the reservoir while decreasing the noise. With the inclusion of the error term in the objective function, the optimization scheme now designs weights that decrease the noise while increasing the anomaly. We use the same process to find the optimal weights and create the weighted synthetic aperture response for all receivers and all source array locations. There are changes in the response from the weighted synthetic aperture response with weights determined from the optimization that included the error term (Figure 5.7). But we first note that the anomaly from the reservoir did not degrade with the inclusion of the error term. In fact, the anomaly is slightly stronger in the response from the weighted synthetic aperture with $\gamma = 1$ (Figure 5.7) than with $\gamma = 0$ (Figure 5.8). Part of the increase in magnitude at the location of the anomaly comes from noise, as shown in the right panel of Figure 5.7. The weighted synthetic aperture response causes a fortuitous positive interference of the noise with the anomaly. The noise floor of the response with $\gamma = 1$ lowers slightly but is almost equal to the noise floor from the response with $\gamma = 0$. One large change in the response from the weighted synthetic aperture with $\gamma = 1$ is at the edges of the image. The noise streaks present in the weighted synthetic aperture response with $\gamma = 0$ are suppressed in the edge of the response with $\gamma = 1$ reducing the presence of noise in the image above 5 km offset. There are changes to the noise floor and noise streaks when $\gamma = 1$ but the overall impact to the ability to view the anomaly from the reservoir is minimal.

With only slight improvements when $\gamma = 1$, it may seem reasonable to expect that a higher value of γ will reduce the effect of the noise even further. We test this idea by setting $\gamma = 10$ and finding the optimal weights from the optimization scheme. We apply the weights and show the weighted synthetic aperture response for $\gamma = 10$ in Figure 5.8. First, note that the anomaly from the response with $\gamma = 10$ (the middle panel of Figure 5.8) decreases at 4.5 km offset and 1.5 km CMP when compared to the anomalies from the responses with $\gamma = 0$ and $\gamma = 1$. The optimization decreases the noise more than it maximizes the signal from

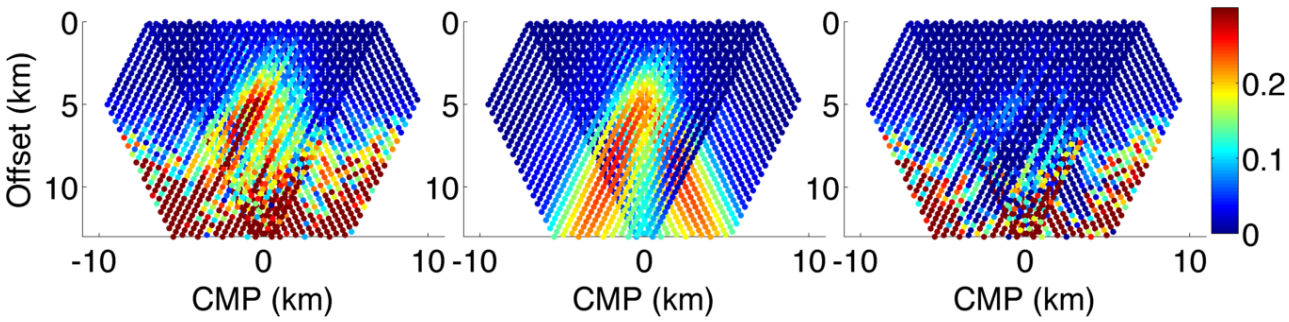

Figure 5.7: Left panel: A pseudo cross-section displaying the normalized difference of the weighted 2D synthetic aperture response for the inline electric component and $\gamma = 1$ with 10^{-15} V/Am^2 independent, random noise added. Middle panel: The same weighted synthetic aperture response as the first panel without noise. Right panel: The random independent noise present in the first panel found by taking the difference between the first two images.

the reservoir because we use a high γ. Also with $\gamma = 10$, the noise begins to dominate the response at 7.5 km offset, which is higher than the 10 km noise floor of the response with $\gamma = 1$. There are no streaks of noise at the edges of the image as with the $\gamma = 1$ image, but the noise floor in the $\gamma = 10$ response is at the level of the streaks in the $\gamma = 0$ response. Overall, the response from the weighted synthetic aperture source with $\gamma = 10$ is worse than the response from the other values of γ because it decreases the signal from the reservoir and has a higher noise floor. With $\gamma = 1$, the norms of the field anomaly and of the errors are weighted equally. However, when a large value of γ is used, the optimization places a higher importance on reducing the noise rather than increasing the anomaly from the reservoir.

We explain why the changes in the anomaly, noise floor, and noise streaks occur for different values of γ by examining the amplitude of the weights. Figure 5.9-Figure 5.11 show contour plots of the amplitudes of the optimal weights for the source array centered at 8.1 km inline and the receiver located at 0 km for $\gamma = 0$, $\gamma = 1$, and $\gamma = 10$, respectively. When $\gamma = 0$ (Figure 5.9), the amplitude of the optimal weights is almost equal for all sources in the synthetic aperture source array. The anomaly from the reservoir increases because the weights combine the responses to maximize the anomaly. Also, with almost equal amplitude for all the weights, there are more sources of coherent signal, which averages the incoherent

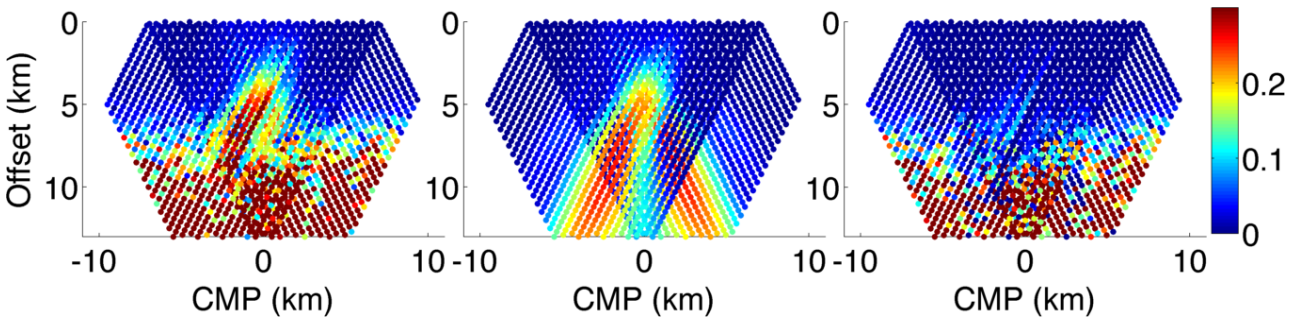

Figure 5.8: Left panel: A pseudo cross-section displaying the normalized difference of the weighted 2D synthetic aperture response for the inline electric component and $\gamma = 10$ with 10^{-15} V/Am^2 independent, random noise added. Middle panel: The same weighted synthetic aperture response as the first panel without noise. Right panel: The random independent noise present in the first panel found by taking the difference between the first two images.

noise resulting in a lower noise floor. However, if a single response is particularly noisy, then that noise affects the overall response from the synthetic aperture array in multiple locations because the noisy response is included in multiple source arrays causing a streak of noise. When $\gamma = 1$ (Figure 5.10), the amplitude is higher for sources closer to the receiver. Even with fewer sources receiving nonzero weights, the anomaly from the reservoir still increases. The sources with higher amplitude contain the most information about the reservoir. The noise floor is also lowered because enough sources with coherent signal are averaged to reduce the noise. The noise streaks disappear because the synthetic aperture response is formed from a subset of the source responses in the synthetic aperture source array. A very noisy source response given a nonzero weight in one source array location could receive a zero weight in the next source array location, which imprints the noise on only one array location instead of multiple locations as with $\gamma = 0$. When $\gamma = 10$ (Figure 5.11), only two out of a total of 63 sources have significant amplitudes (for the source array location shown); thus the synthetic aperture response only uses information from two sources. The higher noise floor occurs for $\gamma = 10$ because higher amplitude is placed on only a couple of responses, which results in less cancellation of incoherent noise. Also, there are no streaks because a noisy response has zero weight in the next source array location. From the amplitudes of the

weights, we consider the response with $\gamma = 1$ to have the best balance between suppressing the noise and increasing the anomaly.

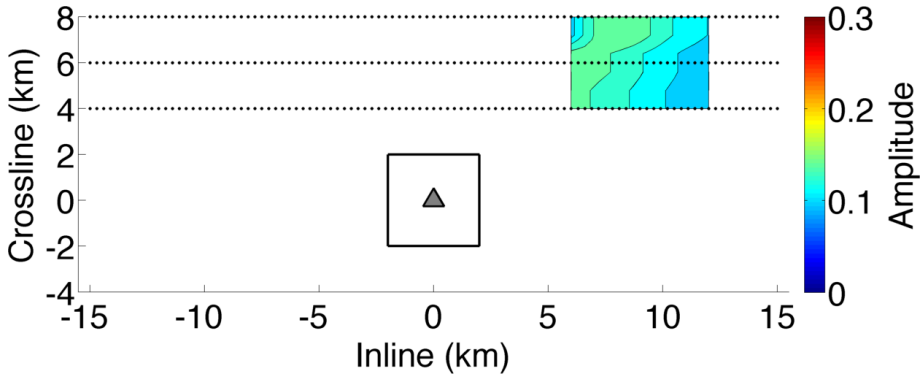

Figure 5.9: A contour of the amplitude of the optimal weights with $\gamma = 0$ for the source array centered at 8.1 km inline and the receiver at 0 km shown on a map view of the survey geometry.

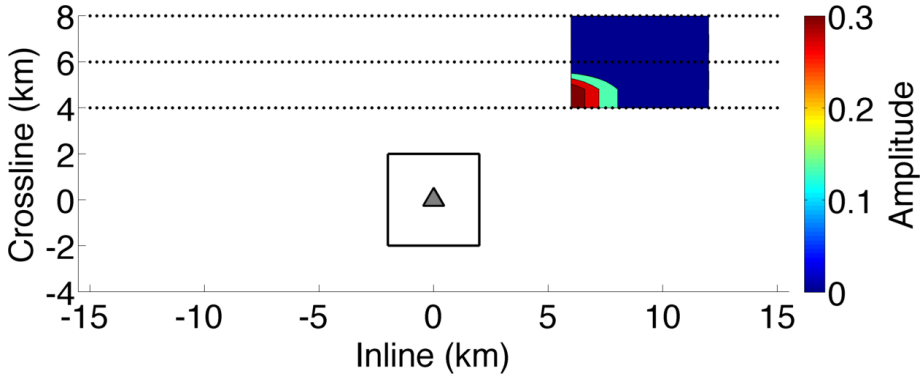

Figure 5.10: A contour of the amplitude of the optimal weights with $\gamma = 1$ for the source array centered at 8.1 km inline and the receiver at 0 km shown on a map view of the survey geometry.

When reducing the noise in electromagnetic responses is realized at the expense of diminishing the signal from the reservoir, then this reduction is no longer useful. To understand the tradeoff between noise reduction and increasing the signal from the reservoir, we examine the largest eigenvalue from each synthetic aperture source array location. The eigenvalue determines the direction of the largest axis of the ellipsoid as we discuss when we describe our optimization method above. Using a large value of γ causes some of the eigenvalues

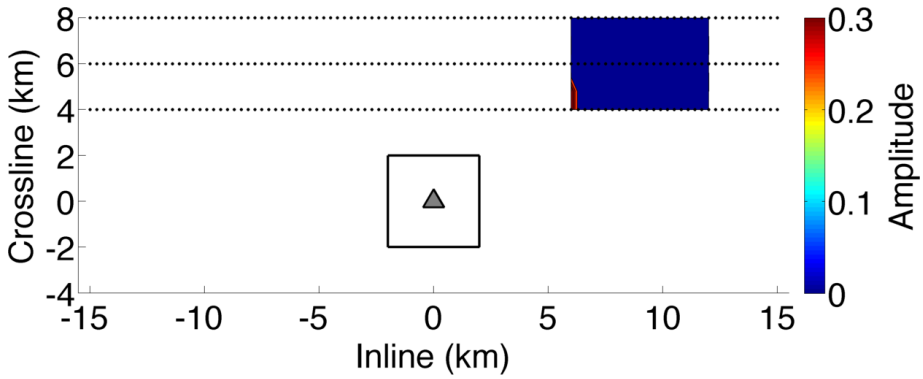

Figure 5.11: A contour of the amplitude of the optimal weights with $\gamma = 10$ for the source array centered at 8.1 km inline and the receiver at 0 km shown on a map view of the survey geometry.

to become negative because the norm of the variance of the synthetic aperture response is larger than the difference between the pay and wet fields of the synthetic aperture response. Negative eigenvalues imply that the optimization gives more weight to reducing the data than to increasing the signal. We map these negative eigenvalues to view where the error term dominates. Figure 5.12 displays the response from the weighted synthetic aperture source for $\gamma = 0$, 1, and 10 with the response with negative eigenvalues muted in gray. For $\gamma = 0$, there are no negative eigenvalues because the norm of the difference between the pay and wet fields creates a Hermitian matrix which always has positive eigenvalues. For $\gamma = 1$, large offsets and the receivers farthest away from the reservoir have negative eigenvalues. These are areas where the variance of the synthetic aperture response is larger than the coherent signal. The responses with negative eigenvalues for an entire receiver location (the first and last three receivers in the middle panel of Figure 5.12) are completely dominated by noise. When $\gamma = 10$, the area of negative eigenvalues increases because now the norm of the variance is ten times larger than the difference between the pay and wet fields. More receivers have negative eigenvalues; comparing these areas to the responses shown in Figure 5.7, one sees that the magnitude of the anomaly for those receivers decreases. Examining the negative eigenvalues demonstrates which source array locations of the weighted synthetic aperture response are dominated by noise and thus where the response does not

contain any useful information about the reservoir. It confirms that the γ value that best balances between reducing the noise and increasing the signal is $\gamma = 1$.

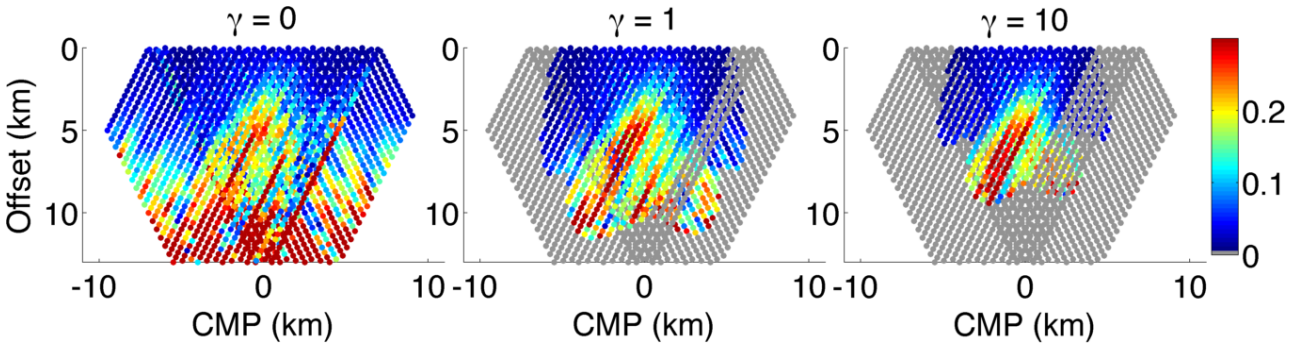

Figure 5.12: Left panel: A pseudo cross-section displaying the normalized difference of the weighted 2D synthetic aperture response for the inline electric component and $\gamma = 0$ with 10^{-15} V/Am^2 independent, random noise added. Middle panel: The weighted 2D synthetic aperture response for $\gamma = 1$ and the responses with negative largest eigenvalues masked with gray. Right panel: The weighted synthetic aperture response for $\gamma = 10$ and the negative eigenvalues masked out with gray.

5.5 Conclusion

Lowering the noise and extracting more of the signal from the reservoir is important for CSEM where the diffusive fields contain only a small portion of information from the reservoir. With less uncertainty, CSEM may be employed in applications where high accuracy and repeatability are required. We used the theory of error propagation to design a weighted synthetic aperture source that decreases additive noise but also amplifies the anomaly from the reservoir. We demonstrated the benefits of this new optimization scheme with synthetic electromagnetic responses from a model with large separation between the sources and receivers in the crossline direction. Incorporating the norm of the variance of the synthetic aperture response into our optimization scheme reduces the additive noise in electromagnetic responses. The impact of this reduction is slight when compared to the synthetic aperture response with $\gamma = 0$, but there are changes to the noise floor and noise streaks when the error term is included in the objective function. We demonstrate the trade-off between reducing the noise and increasing the signal by displaying the amplitudes of the

optimal weights, which shows the reasons for the changes to the anomaly, the level of the noise floor, and the presence of noise streaks. Examining the negative eigenvalues is useful for identifying the responses that are too dominated by noise, allowing them to be removed before performing inversion. We caution against utilizing the synthetic aperture response that has negative eigenvalues because there is negligible information about the reservoir in those synthetic aperture signals. However, it is difficult to quantify the full impact of our new optimization method with just one synthetic model. We do not know how reducing the error propagation with synthetic aperture affects the results of inversion. With the application of optimally weighted synthetic aperture, we are able to extract valuable information about the reservoir from electromagnetic responses with towlines that are several kilometers away from the receivers. Without synthetic aperture, the noise from these responses obscures the signal from the reservoir. Optimally weighted synthetic aperture enables the side-looking capability of CSEM which may be useful in areas where the towlines cannot be directly over the reservoir.

5.6 Acknowledgments

We thank the Shell EM Research Team for research suggestions, industry perspective, and the synthetic data. We acknowledge the use of synthetic data generated from INTEM3D, a modeling code developed by the CEMI consortium at the University of Utah. We are grateful for the financial support from the Shell Gamechanger Program of Shell Research.

CHAPTER 6

THE SENSITIVITY OF SYNTHETIC APERTURE FOR CSEM

6.1 Introduction

Synthetic aperture for CSEM is often limited by the amount of signal in the responses from the reservoir. If there is no signal from the reservoir in the electromagnetic fields then there is nothing for synthetic aperture to amplify. There may also be situations where an interpreter believes the increase in the electromagnetic response is from a hydrocarbon reservoir but may actually be from basalts, salt, or other resistive bodies. As with any geophysical method, results from synthetic aperture should be compared with other available information, such as seismic or interpreted geology cross-sections. We show the benefits of applying synthetic aperture to electromagnetic responses from CSEM surveys in previous chapters. Chapter 4 details the optimization method we use to find the optimal weights for each synthetic aperture source array location. Chapter 5 explains how synthetic aperture reduces the error propagation in CSEM fields.

In this chapter, we address the possible limits of synthetic aperture from uncertainties in the responses by testing the sensitivity of synthetic aperture to uncertainties in the models of the subsurface. The optimization scheme relies on these models to calculate the optimal weights for each synthetic aperture source location. The weights that steer and/or focus the synthetic aperture response are determined by responses simulated from models of the subsurface with the reservoir present and without the reservoir present. The models may contain errors that would affect the response when the weights are applied to the real electromagnetic fields; these errors include inaccurate placement of the target and over-estimates of the overburden resistivity or of the level of anisotropy.

To test how sensitive synthetic aperture is to errors in the models, we calculate optimal weights from models that differ from the true subsurface and apply them to the responses

from the correct subsurface model. First we analyze the sensitivity of 2D and crossline only synthetic aperture to changes in the overburden resistivity and level of anisotropy. Then we test the sensitivity to the location of the target. We demonstrate that even with weights calculated from models with large perturbations, the synthetic aperture response still highlights the anomaly from the reservoirs in the correct location.

6.2 Testing sensitivity

We test two different types of errors in the modeling: perturbations in the background physical properties and a shift in the location of the target. Both types of uncertainties affect the strength and location of the signal from the target. Weighted synthetic aperture increases the anomaly from the reservoir by virtually increasing the aperture of the source and steering or focusing the energy toward the reservoirs. The optimization method calculates the optimal weights that maximize the difference between the response from the model with the reservoir present (the pay field) and the model without the reservoir (the wet field). If the models do not accurately present the expected electromagnetic response, then the optimal weights may decrease the anomaly from the reservoir or highlight an undesired signal.

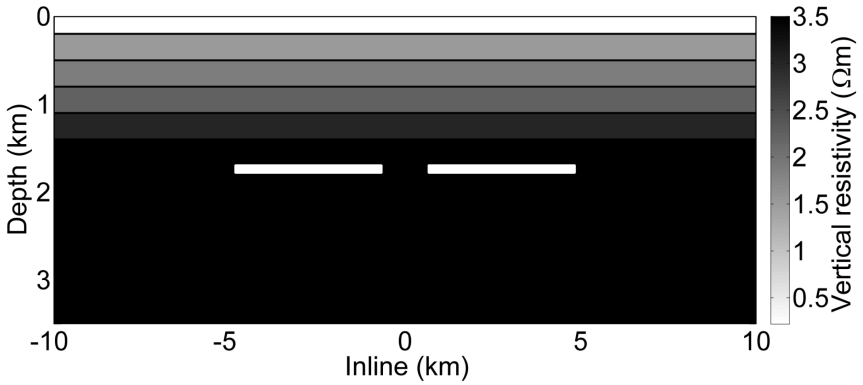

Figure 6.1: An inline cross-section of the model used to generate the electromagnetic fields. The first layer is water with a depth of 200 m. There are five sediment layers with varying resistivity. The reservoirs are shown as the white rectangles. The vertical scale is exaggerated.

For both of the tests, we use a shallow water synthetic model with two reservoirs separated laterally. The synthetic electromagnetic fields are generated by a 3D modeling code, IBCEM3D (Endo & Zhandanov, 2009). An inline cross-section of the model is shown in Figure 6.1. It is a layered anisotropic earth model with a water depth of 200 m. The color of each layer shows the vertical resistivity. The ratio of the vertical resistivity to the horizontal resistivity is 1.5 for the original model. The two reservoirs are 1.5 km below the seafloor, 50 m thick, and extend laterally 4 km in both the inline and crossline directions. They are 1.5 km apart and both have a resistivity of 50 Ωm.

Figure 6.2 displays a map view of the survey geometry, which follows a traditional CSEM survey setup with five parallel towlines, each with 186 source locations centered over the reservoirs. There is a single line of 61 receivers which are 500 m apart. The source is a 270 m horizontal electric dipole. We have the simulated electromagnetic fields for the model with the reservoirs present and without the reservoirs present.

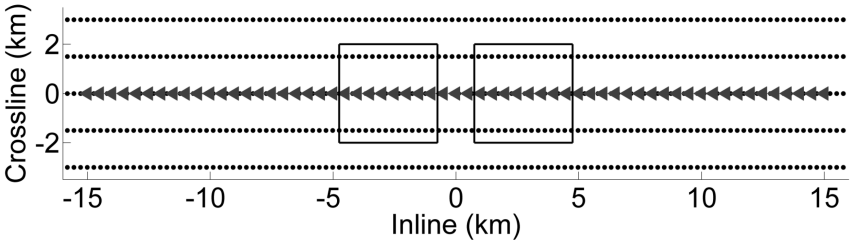

Figure 6.2: The survey geometry used to create the synthetic CSEM data. The sources are shown as black dots and the receivers are the gray triangles. The locations of the reservoirs are outlined with black squares.

6.2.1 Perturbing the model

Two of the largest sources of error in CSEM surveys are uncertainty in the resistivity of the overburden and uncertainty in the anisotropy, the measure of the ratio between the vertical resistivity and the horizontal resistivity (Chen & Dickens, 2009; Hesthammer *et al.*, 2010; Newman *et al.*, 2010; Sasaki & Meju, 2009). These uncertainties cause the estimates of the physical properties of the target to be larger or smaller than the true value (Chen &

Dickens, 2009; Newman *et al.*, 2010). Understanding the geologic setting of the survey area is a key parameter in determining the success of the application of CSEM (Hesthammer *et al.*, 2010). If the uncertainties in the physical properties are not analyzed, then the anomaly from the target may be misleading in magnitude or location (Newman *et al.*, 2010). For synthetic aperture, the optimal weights for each synthetic aperture source location are calculated from models constructed from the assumed subsurface geometry and physical parameters. These models are built from interpretations of other data sources such as seismic or well logs (Chen & Dickens, 2009). Errors that affect the electromagnetic signals from the models used in the optimization scheme could create weights that decrease the anomaly from the reservoir or highlight part of the signal coming from a source other than the reservoir.

To test how these errors affect the improvements from weighted synthetic aperture, we perturbed two different parameters of the model. The first perturbation is to the resistivity of the subsurface, which in the original model ranges from 1.5 Ωm to 3.5 Ωm. We increase the vertical and horizontal resistivities by 50%, which is a realistic level of uncertainty in the background field (Chen & Dickens, 2009). The vertical resistivity of the subsurface after the increase ranges from 2.25 Ωm to 5.24 Ωm. We refer to this model as the higher resistivity model. For the second perturbation, we increase the anisotropy by 33%; the vertical resistivity becomes two times the horizontal resistivity and ranges from 2 Ωm to 4.66 Ωm. We refer to this model as the higher anisotropy model.

We first examine the differences between the anomalies from the reservoirs for the three models. We display the normalized difference in a pseudo cross-section created by plotting the responses by common midpoint versus offset. The normalized difference is defined as the absolute value of the difference between the wet and pay fields divided by the absolute value of the wet field. We plot the inline electric field response from all receivers and all sources in the towline centered over the reservoirs for each model: unperturbed (Figure 6.3(a)), higher resistivity (Figure 6.3(b)), and higher anisotropy (Figure 6.3(c)). The maximum normalized difference for the unperturbed model is 0.20 or a 20% increase from the presence

of the reservoirs. The maximum normalized difference for the higher resistivity model is 12.5%. The increase in the background resistivity reduces the magnitude of the anomalies because there is less contrast between the subsurface resistivity and the reservoir resistivity (Figure 6.3(b)). The maximum of the normalized difference of the response from the higher anisotropy model is 8.8%. The magnitude of the anomalies is less with the higher anisotropy model because there is a larger difference between the vertical and horizontal resistivities causing the difference from the presence of the reservoirs to be very small when compared to the reference field (Figure 6.3(c)) (Newman *et al.*, 2010). The location of the anomalies also changes for both of the perturbation models. The signal from the reservoirs appears at larger source-receiver offsets for both perturbed models, which locates the anomalies deeper in the pseudo cross-section.

We simulate a situation where the optimal weights are calculated from models that do not represent the true subsurface and are applied to the acquired electromagnetic fields (i.e. the model with no perturbation). We test both 2D and crossline only weighted synthetic aperture. We use the optimization method that we explained previously in Chapter 4 to find the optimal weights for the sources in the synthetic aperture array, which maximizes the anomaly from the reservoir. Because the anomalies for the different models have different strengths and locations, the optimal weights found by the optimization differ for each model. For the 2D synthetic aperture source, we choose to use a synthetic aperture source that is 5.4 km-long in the inline direction (21 sources) and 6 km-long in the crossline direction (5 sources). Figure 6.4(a) shows the 2D weighted synthetic aperture response for the weights calculated from the unperturbed model and applied to the electromagnetic fields from the unperturbed model. As we have previously described (in Chapter 4), the magnitude and spatial area of the anomaly increase from the application of synthetic aperture.

We next use the optimization scheme to find the optimal weights from the model with higher resistivity. We apply the optimal weights from the higher resistivity model to the electromagnetic responses from the unperturbed model, shown in Figure 6.4(b). If the er-

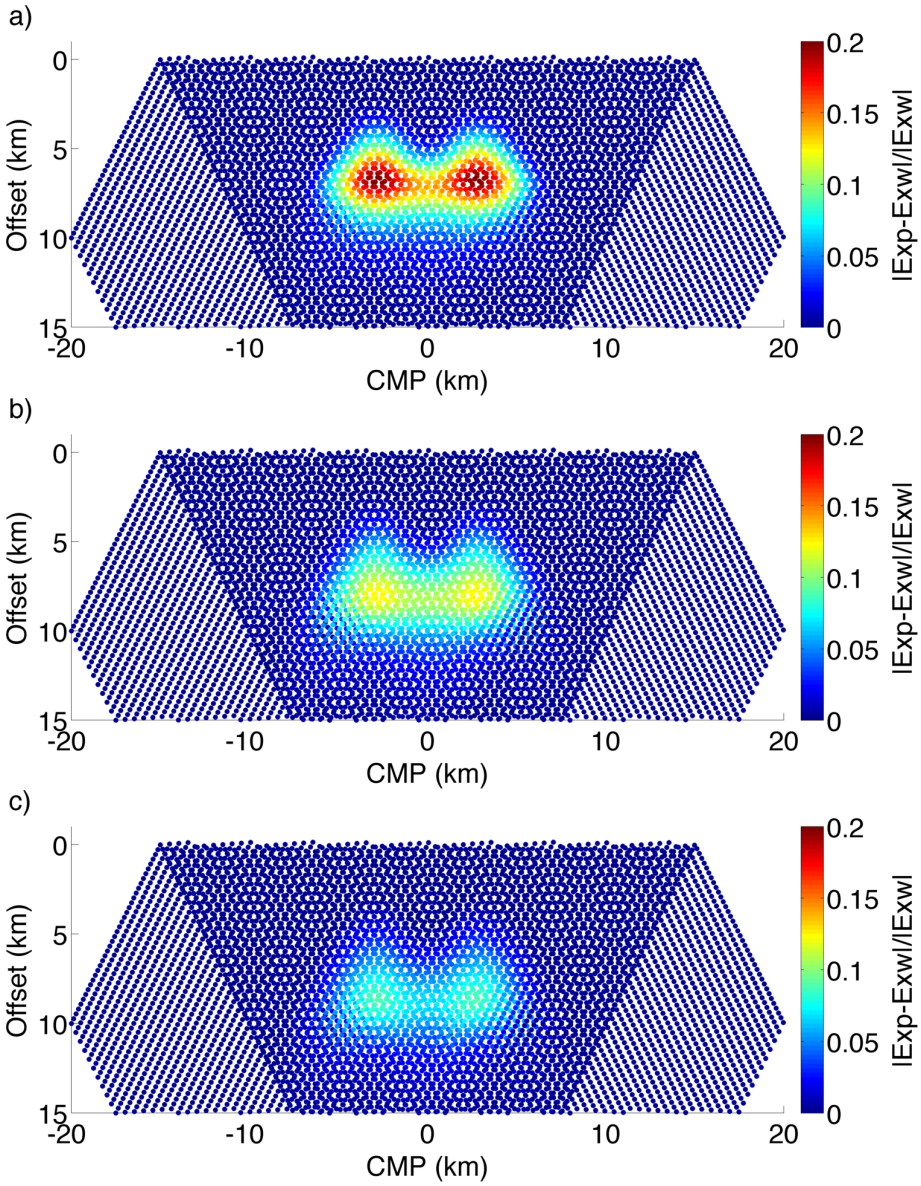

Figure 6.3: The normalized difference of the inline electric pay field and the inline electric wet field for the original data (panel a), the model with 50% increase in overburden resistivity (panel b), and the model with a 33% increase in anisotropy (panel c).

ror in the model had no effect on the optimal weights then the response with the weights from the higher resistivity model (Figure 6.4(b)) would appear identical to the response with the correct weights (Figure 6.4(a)). This is not the case because there are some differences between the two responses. The anomaly from the reservoirs has nearly the same spatial location but a slightly lower magnitude compared to the anomaly from the correct model. For the higher anisotropy model, we use the same process we earlier used for the higher resistivity model to find and apply and apply the incorrect weights to the unperturbed electromagnetic fields. The response from the 2D weighted synthetic aperture source with the incorrect weights from the higher anisotropy model is shown in Figure 6.4(c). The anomaly from the incorrect weights is located at the same offset as the anomaly but with a smaller spatial area from the unperturbed response (Figure 6.4(a)). This anomaly has a lower magnitude than the unperturbed anomaly. Neither the higher resistivity model nor the higher anisotropy model decrease the anomaly, and for both models the anomaly is in the correct location and is detectable. The differences would not effect interpreting the presence of a target in the subsurface.

To examine the differences between the weights calculated from each model, we show contour maps of the phase and amplitude of the optimal weights for a single synthetic aperture location shown in Figure 6.5 and Figure 6.6, respectively. For all models, the phase shifts of the optimal weights steer the energy toward the reservoirs in the inline direction and focus the energy in the crossline direction. The differences between the phase of the optimal weights from the unperturbed model (Figure 6.5(a)) and the higher resistivity model (Figure 6.5(b)) are subtle. The phase of the weights for the higher resistivity model steers at a lower angle in the inline direction but has very similar focusing in the crossline direction. The phase of the optimal weights from the higher anisotropy model has the largest difference (Figure 6.5(c)). The steering has a smaller angle farther away from the reservoirs, and the curvature of the focusing is smaller in the crossline direction.

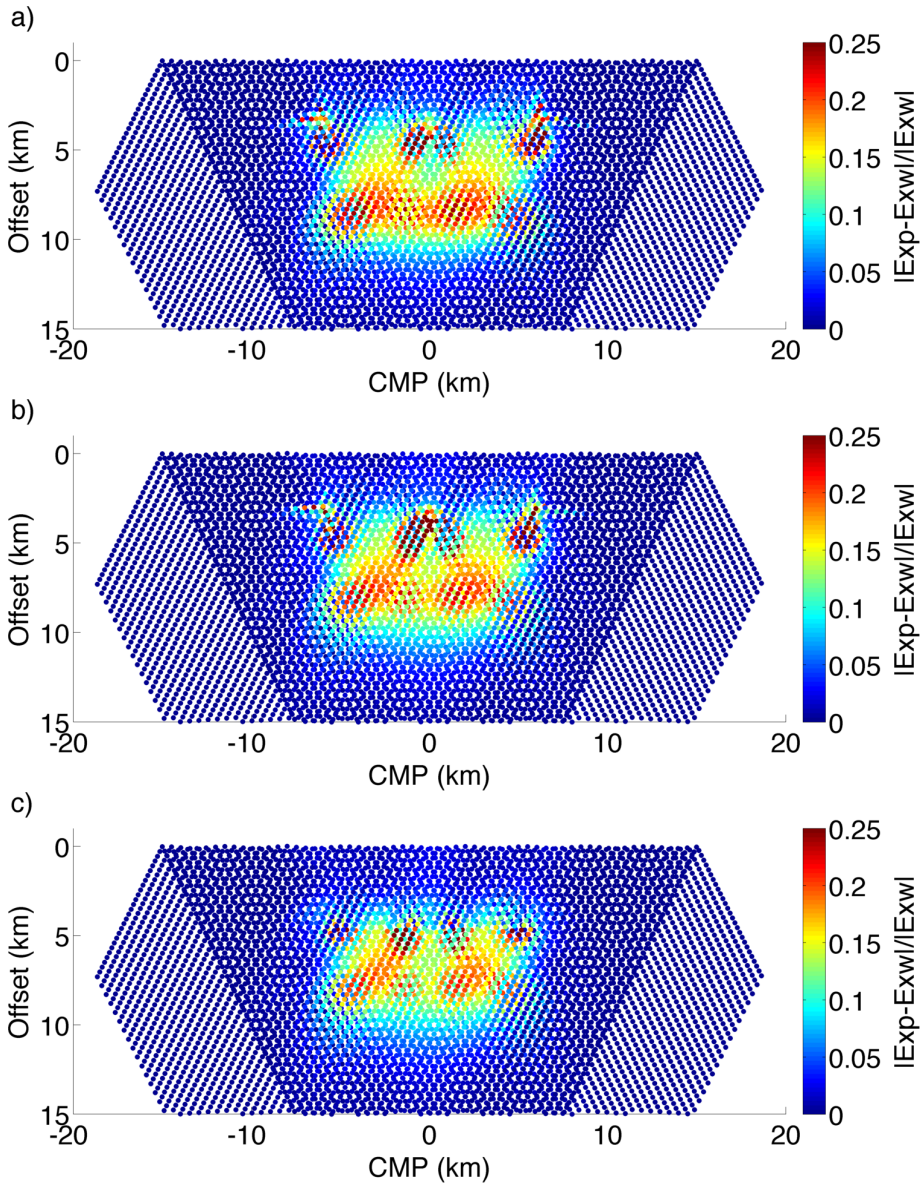

Figure 6.4: The normalized difference of the inline electric pay field and the inline electric wet field for the 2D weighted synthetic aperture response for the original data (panel a), the model with 50% increase in overburden resistivity (panel b), and the model with a 33% increase in anisotropy (panel c).

The amplitudes of the optimal weights indicate which of the sources in the source array contain more information about the target; the sources that receive larger amplitudes are more valuable for maximizing the response from the reservoirs. The weights for the unperturbed model utilize, for this source array location, the sources located about one kilometer away from the reservoir in the inline direction with slightly larger amplitude for the sources farthest away from the reservoir in the crossline direction (Figure 6.6(a)). The weights for the higher resistivity model give larger amplitude to sources farther away from the reservoir, around -7.5 km inline, and give the largest amplitude to two sources in the long offset towlines (Figure 6.6(b)). The weights for the higher anisotropy model place larger amplitude on the sources farthest away from the reservoir in the inline and crossline directions (Figure 6.6(c)). The changes to the angle of steering, the curvature of focusing, and the amplitude of the optimal weights produce the differences in the weighted synthetic aperture responses. Even with these changes, the weighted synthetic aperture response still highlights and increases the anomaly from the reservoirs.

We next implement crossline only synthetic aperture, which forms a synthetic aperture source array in the crossline direction. We previously applied crossline only synthetic aperture in Chapter 4 to demonstrate the benefits for improving the resolution for laterally separated reservoirs; this improvement highlights the signal from each individual reservoir without averaging them together. We form the synthetic aperture source with sources at the same inline position but from each towline, which creates a 6 km-long source in the crossline direction. To find the optimal weights for crossline only synthetic aperture, one implements the same optimization scheme, as used for the 2D synthetic aperture, with the sources from the crossline synthetic aperture source array. The crossline only synthetic aperture responses created with optimal weights calculated from the three different models are shown in Figure 6.7. The responses are nearly identical with two anomalies from the two reservoirs appearing at an offset of 7 km. There are some minor differences in the magnitude of the anomaly and in the presence of artifacts at small offsets. The reason for the

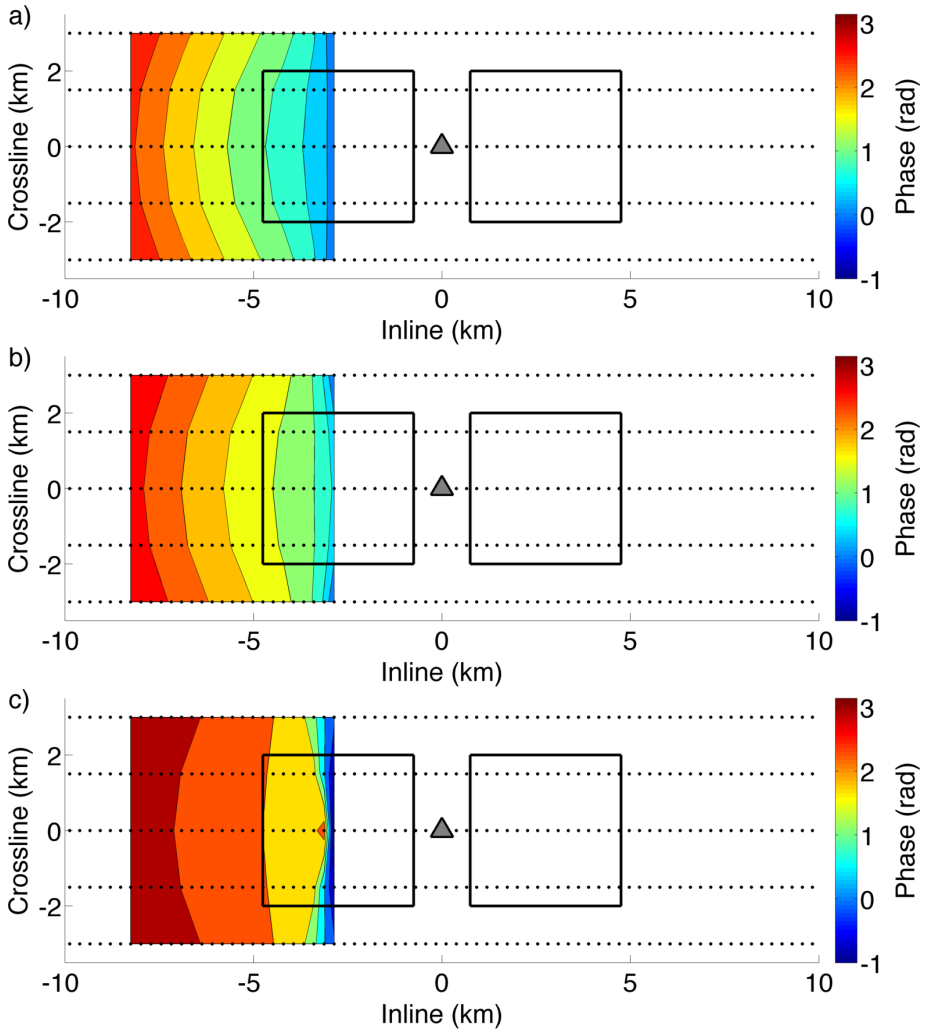

Figure 6.5: A contour of the phase of the optimal weights overlaid on a map of the survey geometry for the original data (panel a), the model with 50% increase in overburden resistivity (panel b), and the model with a 33% increase in anisotropy (panel c).

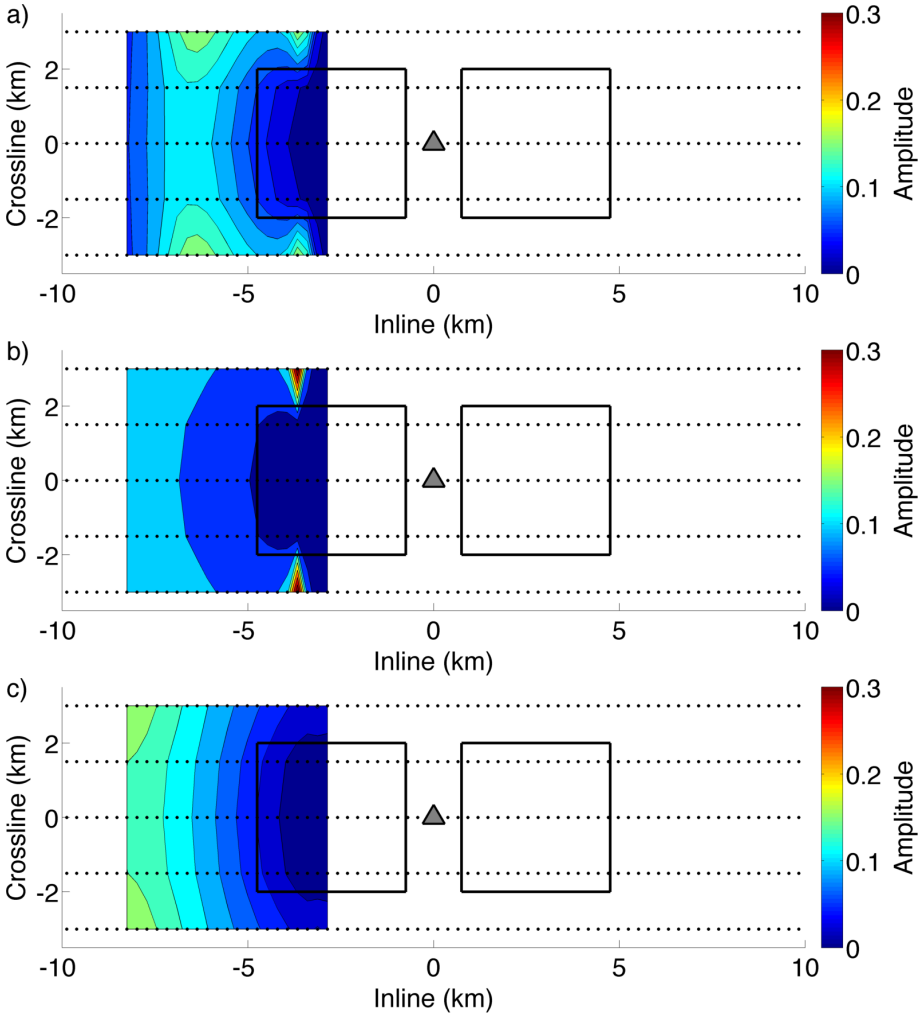

Figure 6.6: A contour of the amplitude of the optimal weights overlaid on a map of the survey geometry for the original data (panel a), the model with 50% increase in overburden resistivity (panel b), and the model with a 33% increase in anisotropy (panel c).

resemblance across the images comes from the similarities in the optimal weights. We show the phase and amplitude of the optimal weights for a single crossline synthetic aperture location in Figure 6.8 and Figure 6.9. The phase shifts of the optimal weights for all models are parabolic in shape, which creates focusing in the crossline direction and sends energy toward the reservoirs (Figure 6.8). The two perturbed models have slightly smaller phase shifts than the unperturbed model (which changes the focus point), but these shifts are not large enough to lower the magnitude of the anomalies. The amplitudes of the optimal weights for the sources from the unperturbed model are almost equal (Figure 6.9). Also, the amplitudes of the optimal weights for each model are almost identical. The similarities in the optimal weights for the unperturbed, higher resistivity, and higher anisotropy models result in synthetic aperture responses that locate the anomalies in the same positions with the same magnitude.

The CSEM response from an optimally weighted synthetic aperture is not greatly affected by changes in the physical properties of the models. The incorrect weights could have decreased the magnitude of the anomaly or incorrectly located the anomaly. However, for both the higher resistivity and higher anisotropy models, the detectability of the anomaly increases versus the original response. In the next section, we test the sensitivity of synthetic aperture to changes in the location of the target.

6.2.2 Uncertainty in the location of the target

The location of a hydrocarbon reservoir is typically well constrained by seismic data and geologic models for derisking applications. However, if CSEM is employed for exploration then it is possible that there may be no information, or only a broad estimate, about where the target may be located. Gabrielsen *et al.* (2009) demonstrate the ability of CSEM to reveal the location of new hydrocarbon targets but the application is limited to areas with small or low-saturated targets. Buland *et al.* (2011) analyze the value of CSEM for exploration and conclude that while the positive outcomes of implementing CSEM in exploration settings are growing, there is still a need for more accurate modeling and inversion to allow for better

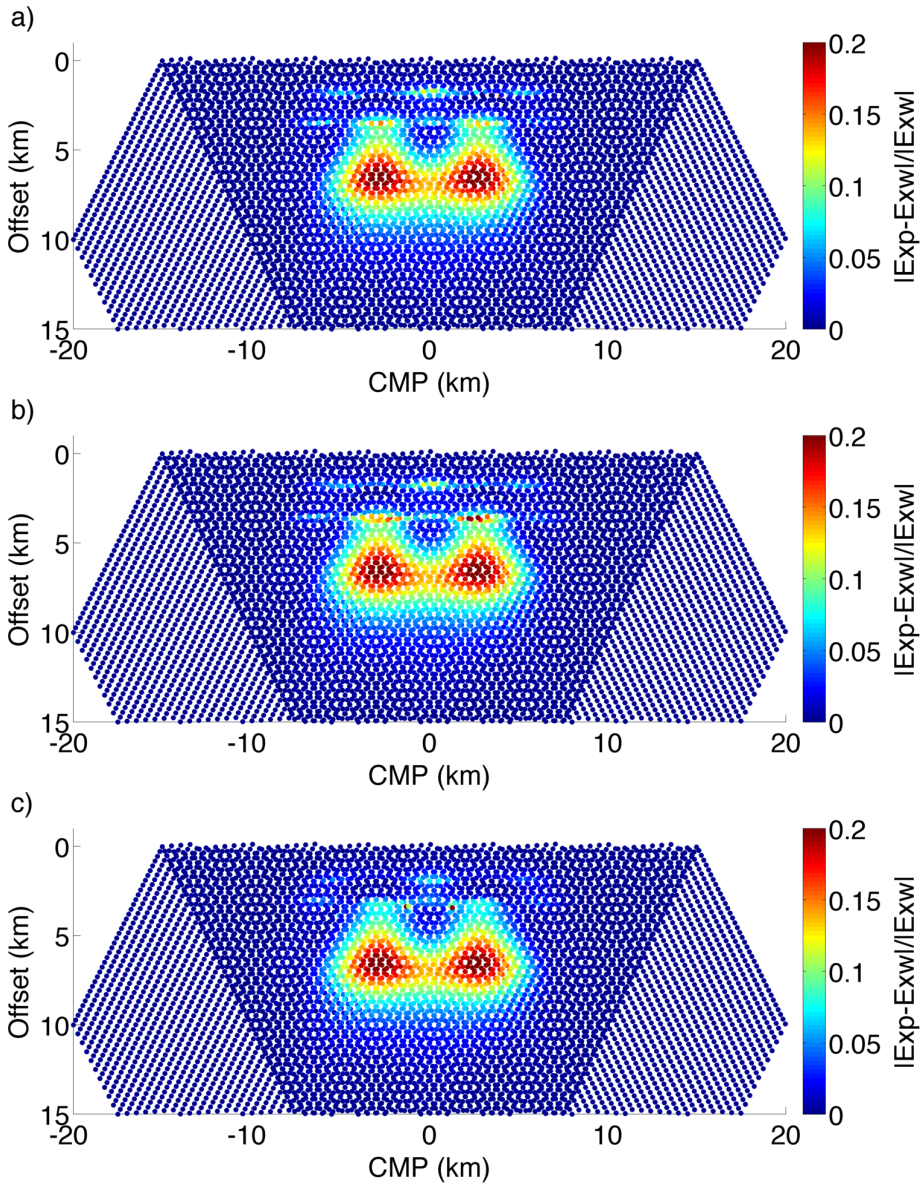

Figure 6.7: The normalized difference of the inline electric pay field and the inline electric wet field for the crossline weighted synthetic aperture response for original data (panel a), the model with 50% increase in overburden resistivity (panel b), and the model with a 33% increase in anisotropy (panel c).

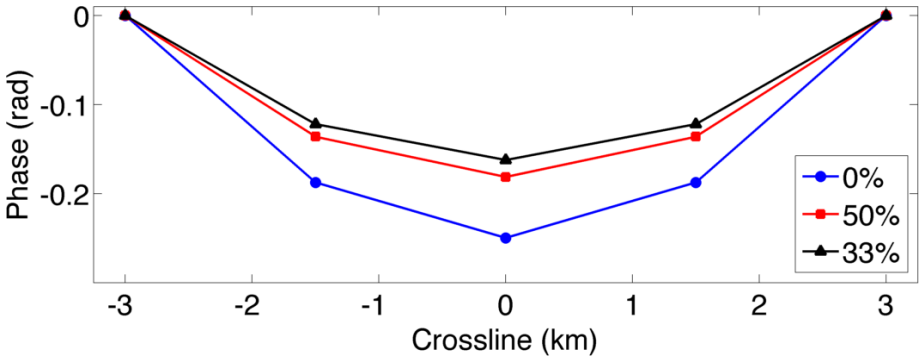

Figure 6.8: The phase of the optimal weights for crossline synthetic aperture for the source array centered at -12.85 km and the receiver at 0 km for the unperturbed model, the 50% increase in overburden resistivity, and the 33% increase in anisotropy.

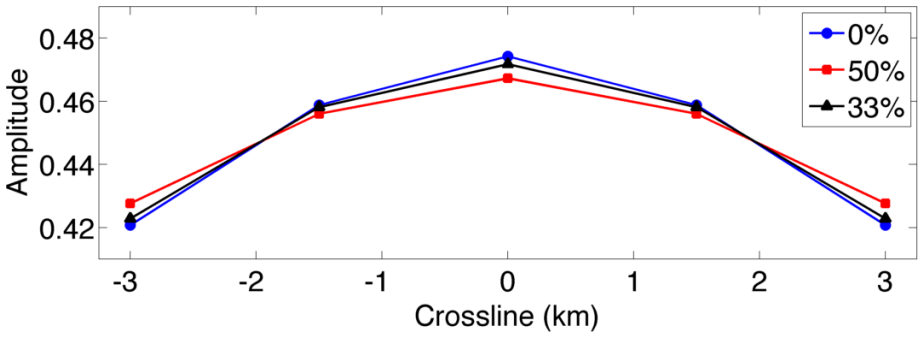

Figure 6.9: The amplitude of the optimal weights for crossline synthetic aperture for the source array centered at -12.85 km and the receiver at 0 km for the unperturbed model, the 50% increase in overburden resistivity, and the 33% increase in anisotropy.

detection and delineation of reservoirs. We investigate the benefits of weighted synthetic aperture for CSEM in an exploration setting where the location of the reservoir is unknown.

To understand how uncertainty about the location of the reservoir could affect the improvements from the application of synthetic aperture, we calculate the weights from a model with the reservoir shifted in the inline direction from the true location. We then apply those weights to the response from the model with the reservoir in the correct location. We use the same shallow water model with two reservoirs as the in the previous section but with a frequency of 0.2 Hz. We shift the reservoir locations by 2.5 km and 4.5 km in the inline direction to understand how the locations affect the response from the weighted synthetic aperture response. These are large shifts that would only occur in an exploration setting. We also choose to use shifts this large to test the limits of the synthetic aperture method. Figure 6.10 displays the two reservoir positions for unshifted (panel a), shifted 2.5 km (panel b), and shifted 4.5 km (panel c). We refer to these models as the unshifted model, 2.5 km shifted model, and 4.5 km shifted model, respectively.

We calculate the optimal weights by implementing the optimization scheme discussed in previously in Chapter 4. We apply 2D and crossline only synthetic aperture to understand how the reservoir misplacement affects the anomaly in the response. The anomaly from the reservoirs, if not affected by the incorrect weights, should appear in the same location as the image from the correct weights. We use the same 2D synthetic aperture source as the source we applied to the perturbation models in the previous section. We calculate the optimal weights for the model with the reservoir shifted and apply them to the original unshifted data. The 2D weighted synthetic aperture responses for the unshifted, 2.5 km shifted, and 4.5 km shifted models are shown in Figure 6.11. The normalized difference from the two reservoirs creates a single, large anomaly. The magnitude of the anomaly is created equally by the presence of the two reservoirs and is centered around 0 km CMP because of the survey geometry (Figure 6.11(a)). When the weights from the 2.5 km shifted reservoirs are applied to the unshifted data, the magnitude of the left side of the anomaly (around -4.5 km CMP)

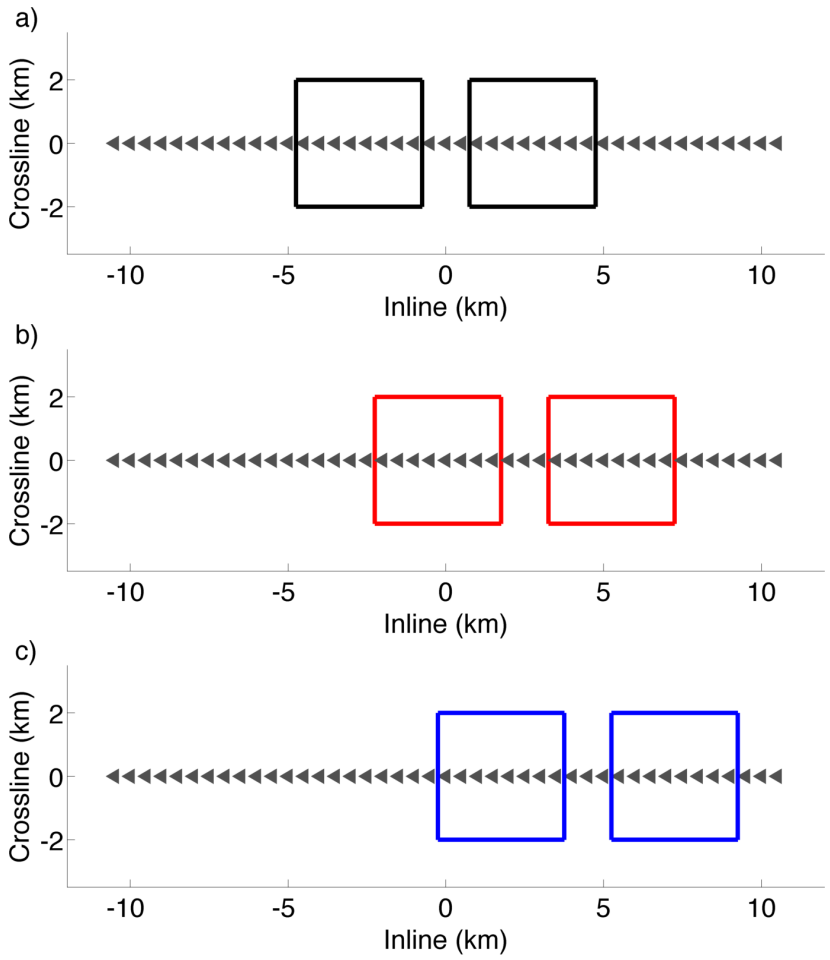

Figure 6.10: A map view of the location of the reservoirs outlined as squares with the receivers shown as gray triangles for the original model (panel a), the reservoirs shifted 2.5 km to the right (panel b), and the reservoirs shifted 4.5 km to the right (panel c).

becomes larger than the right side (Figure 6.11(b)). There is also a change to the spatial coverage of the left side of the anomaly with signal from the reservoir occurring at smaller offsets, which does not occur to the anomaly on the right side. However, the location of the anomaly is still centered around 0 km CMP and extends to cover the true location of the reservoirs. When the weights from the 4.5 km shifted reservoirs are applied to the unshifted data, the magnitude of the left side of the anomaly (around -5 km CMP) is larger than the right, as with the 2.5 km shifted response (Figure 6.11(c)). Also, the coverage of the anomaly becomes more uneven at small offsets, but the spatial coverage of the anomaly is still in the correct location. The difference between the left and right sides of the anomaly is a result of applying the weights from an incorrect model. Even with the application of incorrect weights, the anomaly from the reservoirs appears in only a slightly different location than the original anomaly. The strength of the anomaly changes but it remains centered around 0 km CMP.

We examine the optimal weights for the different reservoir locations to understand the differences in the responses. The phase and amplitude of the optimal weights for the three reservoir locations are shown in Figure 6.12 and Figure 6.13, respectively. The amplitude of the optimal weights for the unshifted reservoirs, for the source array centered at -7.5 km, is larger for the sources closer to the reservoir and the largest amplitude is given to sources in the large offset towlines (Figure 6.12(a)). The amplitudes of the optimal weights for the reservoirs shifted 2.5 km are nonzero for the sources closest to the reservoir (Figure 6.12(b)). The amplitudes of the weights for the reservoirs shifted 4.5 km are similar to the amplitude of the 2.5 km shifted reservoirs but with more sources receiving nonzero values (Figure 6.12(c)). The phases of the optimal weights for the unshifted reservoirs steer towards the reservoirs in the inline direction and focus in the crossline direction (Figure 6.13(a)). Similar phase shifts are given to the same sources for the 2.5 km shifted reservoir model but with a steeper steering angle and a smaller curvature for the focusing in the crossline direction (Figure 6.13(b)). The phase shifts of the 4.5 km shifted weights have a smaller steering angle in the inline direction

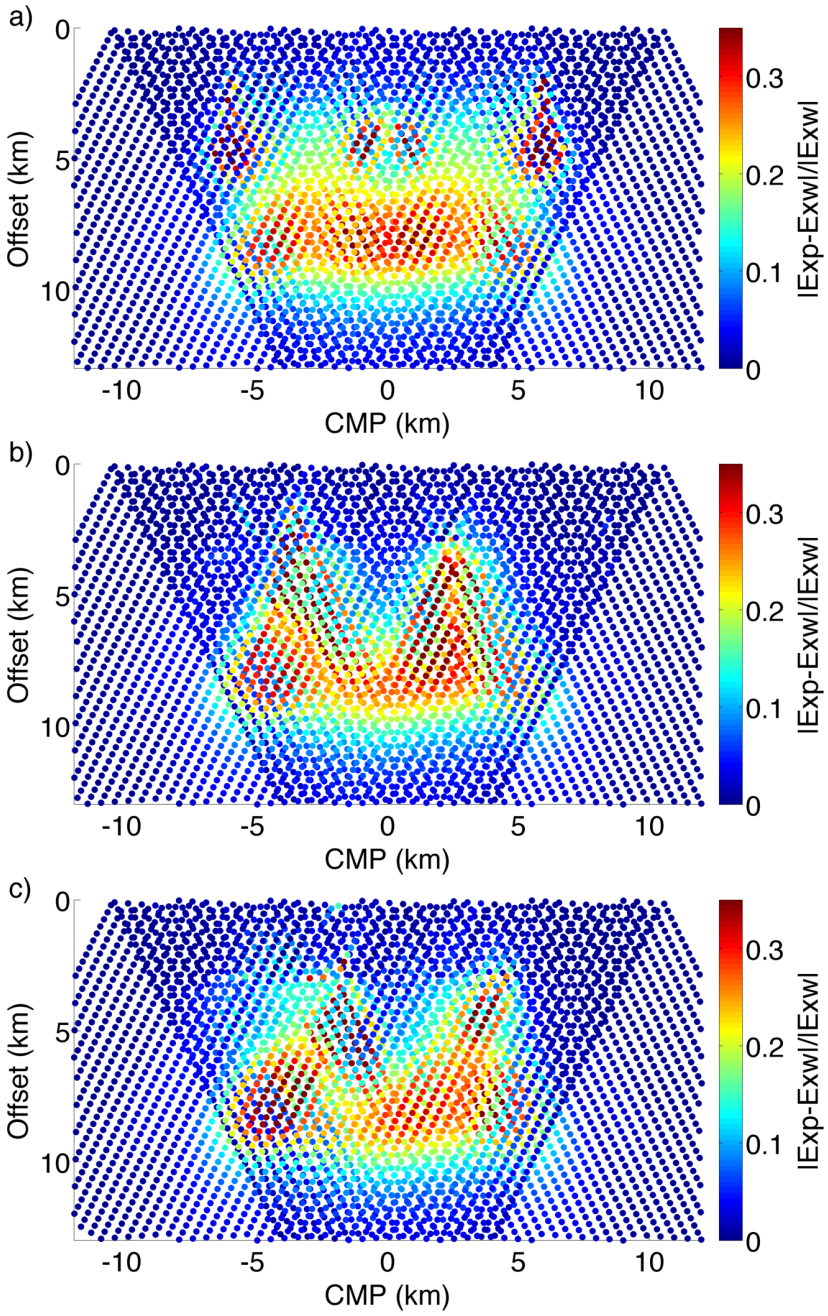

Figure 6.11: The normalized difference of the inline electric pay field and the inline electric wet field for the 2D weighted synthetic aperture response for no shift in the reservoir position (panel a), the response for the reservoir shifted 2.5 km to the left (panel b), and the response for the reservoir shifted 4.5 km (panel c).

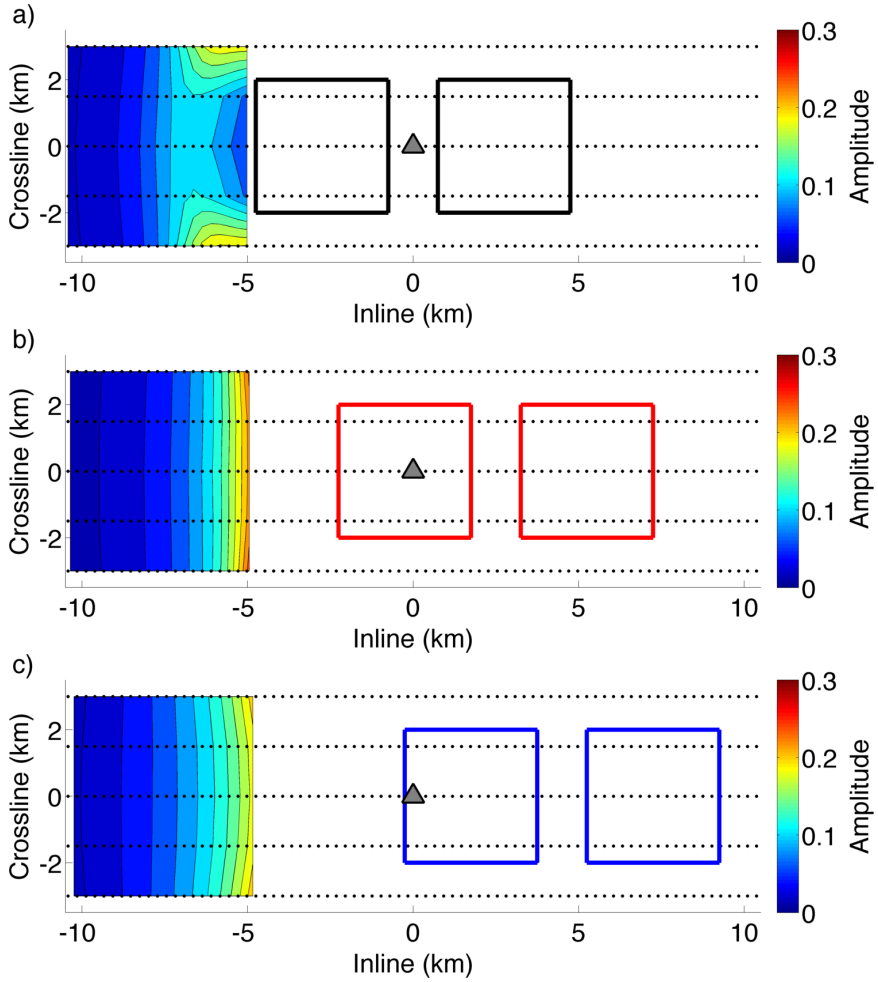

Figure 6.12: A contour of the amplitude of the optimal weights for the 2D synthetic aperture source centered at -7.5 km and the receiver at 0 km inline overlaid on a map of the survey geometry for the unshifted reservoirs (panel a), the reservoirs shifted 2.5 km (panel b), and the reservoirs shifted 4.5 km (panel c).

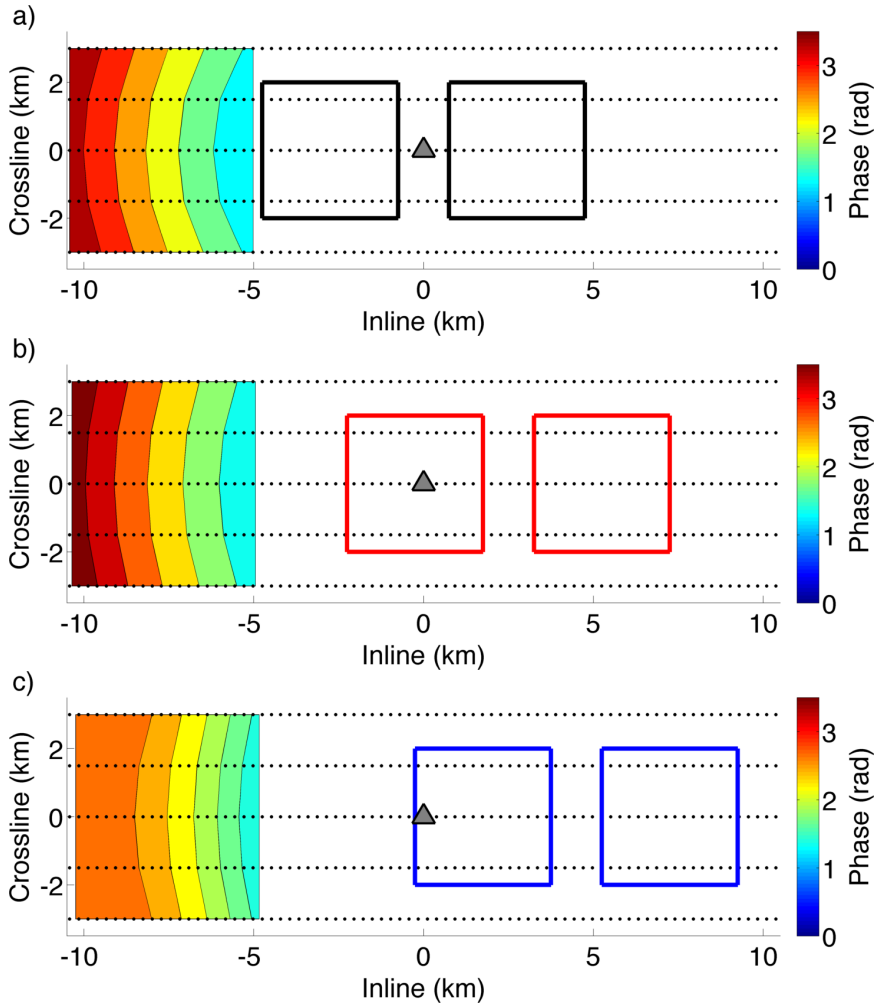

Figure 6.13: A contour of the phase of the optimal weights for the 2D synthetic aperture source centered at -7.5 km and the receiver at 0 km inline overlaid on a map of the survey geometry for the unshifted reservoirs (panel a), the reservoirs shifted 2.5 km (panel b), and the reservoirs shifted 4.5 km (panel c).

but still focus in the crossline direction (Figure 6.13(c)).

We next implement crossline only weighted synthetic aperture to the three different reservoir locations. We create the same crossline only synthetic aperture source as in the previous section, implement the optimization method to calculate the optimal weights for every receiver and source array location for each model, and then apply the optimal weights to the unshifted electromagnetic fields. The responses are shown in Figure 6.14. For the unshifted response, there are two anomalies (from the two reservoirs), one located at -3 km CMP and the other at 3 km CMP with equal magnitudes, which is what we expect because of the survey geometry (Figure 6.14(a)). We discuss in Chapter 4 that the crossline only synthetic aperture differentiates the two reservoirs more than 2D synthetic aperture because the crossline synthetic aperture does not blur the anomalies in the inline direction. When the optimal weights for the reservoirs shifted by 2.5 km are applied to the unshifted response, the anomalies are still centered around 0 km CMP, but the magnitudes of the two anomalies are no longer equal (Figure 6.14(b)). The reservoir located at -3 km CMP has a slightly larger magnitude. These changes also occur in the response with the weights from the 4.5 km shifted reservoirs (Figure 6.14(c)). The difference in the strength of the two anomalies is larger. However, the differences from the shifted reservoir weights are not large enough to obscure the true location of the reservoirs or the fact that there are two anomalies present.

We examine the optimal weights for a single source array location to view the differences caused by the shift in the reservoir location. The phase and amplitude of the optimal weights for the three different models are shown in Figure 6.15 and Figure 6.16, respectively. The phase shifts of the optimal weights for all reservoir locations are parabolic indicating that the synthetic aperture array focuses toward the center of the survey geometry. The curvature of the phase shifts decreases as the reservoirs are shifted farther away. This shows that the focusing point of the weights adjusts to the location of the reservoirs. The amplitudes of the optimal weights for the 2.5 km shifted and the 4.5 km shifted models are almost identical and equally weigh all sources in the synthetic aperture source array. The amplitude of the

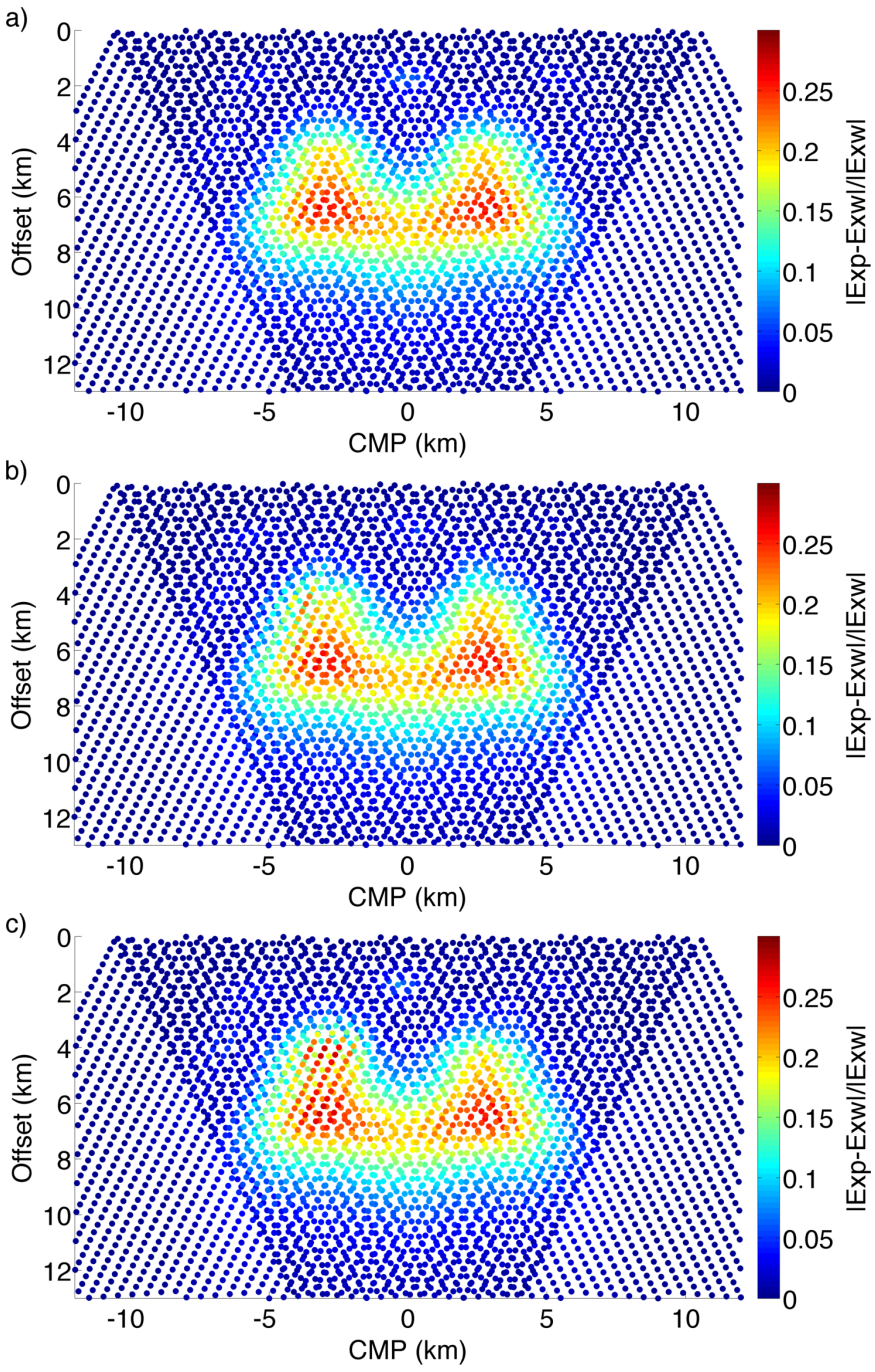

Figure 6.14: The normalized difference of the inline electric pay field and the inline electric wet field for the crossline weighted synthetic aperture response for no shift in the reservoir position (panel a), the response for the reservoir shifted 2.5 km to the left (panel b), and the response for the reservoir shifted 4.5 km (panel c).

optimal weights for the unshifted reservoir places a larger weight on the sources in the outer towlines. These differences account for the changes in the synthetic aperture response from the optimal weights for the three different models applied to the unshifted electromagnetic fields. The uncertainty in the position of the reservoirs for the crossline synthetic aperture response creates fewer differences in the images than the 2D synthetic aperture response because all the weights have a similar parabolic shape, which similarly focus the energy toward the reservoirs even with an inline shift.

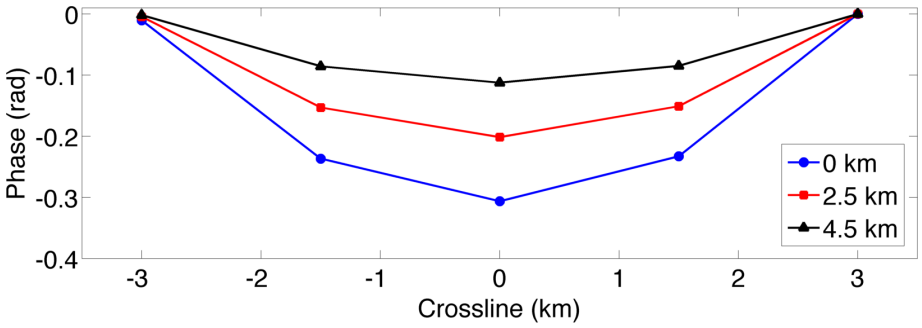

Figure 6.15: The phase of the optimal weights for crossline synthetic aperture for the source array centered at -7.5 km and the reservoirs shifted 0 km, 2.5 km, and 4.5 km.

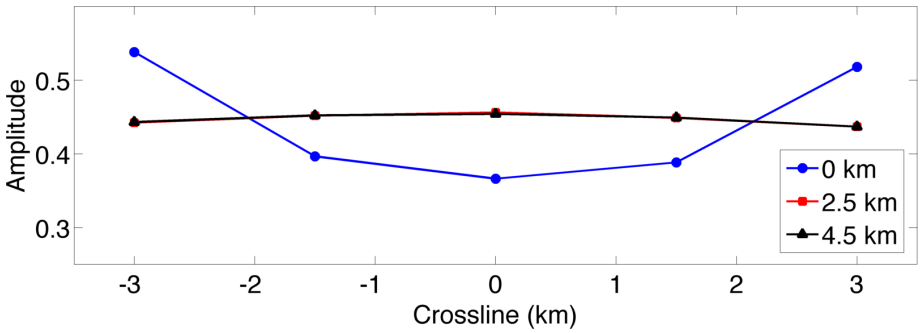

Figure 6.16: The amplitude of the optimal weights for crossline synthetic aperture for the source array centered at -7.5 km and the reservoirs shifted 0 km, 2.5 km, and 4.5 km.

6.3 Conclusion

Locating hydrocarbon reservoirs with CSEM is difficult with uncertainties in the subsurface properties and in the location of the reservoir. We demonstrate, with the use of

erroneous models, that weighted synthetic aperture for CSEM still increases the signal from the target when the weights are calculated from incorrect models. We show that with a 50% increase to the resistivity of the layered background, weighted synthetic aperture is still able to highlight the anomalies from the reservoirs and they appear in the correct location. This is also true when the anisotropy is increased by 33% and when the reservoir location is shifted by 4.5 km. The true physical properties of the subsurface, from which the optimal weights for synthetic aperture are calculated, cannot always be accurately modeled. However, synthetic aperture amplifies the signal from the reservoir in electromagnetic fields even with incorrect weights. None of our perturbations to the physical properties or our shifting of the reservoir resulted in a decrease to the magnitude of the anomaly when compared to the correct response, which demonstrates the robustness of the synthetic aperture technique to changes in the subsurface models.

6.4 Acknowledgments

We thank the Shell EM Research Team, especially Liam Ó Súilleabháin, Mark Rosenquist, and Yuanzhong Fan, for research suggestions, industry perspective, and the synthetic data. We acknowledge the use of synthetic data generated from IBCEM3D, a modeling code developed by the CEMI consortium at the University of Utah. We are grateful for the financial support from the Shell Gamechanger Program of Shell Research.

CHAPTER 7

FRACTURED ROCK, PUBLIC RUPTURES: THE HYDRAULIC FRACTURING DEBATE

Allison Knaak[1] and Jen Schneider[2]

7.1 Introduction

The amount of energy consumed by the world population is increasing and the need for generated power, oil, and natural gas is escalating. To meet the rising demand, we are finding new ways to extract energy from new sources. The quick expansion into new resources has led to controversy over the safety and sustainability of these energy sources, as seen in debates over hydraulic fracturing, clean coal, and wind power. The hydraulic fracturing debate is one example of how a controversy can erupt, even when industry advertises something as a safe procedure. Hydraulic fracturing, or "fracking," is a process used by the oil and gas industry to facilitate the extraction of significant amounts of natural gas and oil using expanded subsurface technologies. Controversy initially erupted in the middle of 2010 after it appeared that hydraulic fracturing had contaminated drinking water. Proponents countered that these claims were the result of an uneducated public misunderstanding the mechanics of the technology. The controversy has since escalated with both sides making contrasting claims about the risks, economic impact, and effects on the environment.

The hydraulic fracturing debate is important especially from a policy perspective because of the large role of natural gas in the United States. Hydraulic fracturing is one technology that has enabled access to previously inaccessible shale gas, also known at tight gas, which is natural gas trapped in thin, impermeable layers of shale formations. As much as 60% of 1,744 trillion cubic feet (tcf) of technically recoverable gas is unconventional, requiring the

[1]Center for Wave Phenomena, Colorado School of Mines, Golden, CO
[2]Department of Public Policy and Administrative, Boise State University, Boise, ID

use of expanded subsurface processes for extraction (DOE, 2009). The increase in production of natural gas has led to a decreased reliance on coal and foreign sources of energy in the U.S. Some argue that natural gas is a "bridge fuel," allowing for an easier transition to more sustainable energies.

The debate is also interesting from a scholarly perspective because the hydraulic fracturing debate is not just about the possible dangers posed by a single technology; rather it encompasses all of the processes involved when one extracts natural gas from shale gas regions. The outcome of policies on hydraulic fracturing will affect the economy, environment, jobs, energy futures, and the day-to-day lives of those who live in tight gas regions. But no major regulatory adjustments or slowing of the debate has occurred since the beginning of the controversy in the early 2000s. The average citizen who is impacted by fracking has few options for action the face of energy exploration and production. To broaden and deepen discourse on hydraulic fracturing issues by all stakeholders, the previous standard procedures for conducting research, delivering conclusions to policy-makers, and formulating policies based solely on research conclusions must be replaced with a different framework that engages all stakeholders. The motivation for implementing an engagement approach to hydraulic fracturing is that the current dialogue on fracking issues overlooks key stakeholders and the voices of those with less power. We address and analyze the topic of hydraulic fracturing from a middle ground, neither opposing nor supporting the technology. To better advise how to reduce the controversy, we stand back to gain a perspective of the interfaces between the technical and nontechnical experts.

The first step to achieving a more democratic decision-making process is to recognize that the hydraulic fracturing controversy belongs to a different, more complex category of debates. This chapter's argument about stakeholder engagement rests on the premise that hydraulic fracturing is a post-normal technology. The term "post-normal" is used here to refer to a case in which both sides are able to marshal evidence in the form of scientific data to support their opposing arguments (Funtowicz & Ravetz, 1993). The uncertainty about the

use of hydraulic fracturing in the new shale plays, the diverse values held by those affected, and the large role natural gas plays in the energy portfolio of the U.S necessitates action regarding the debate over fracking. However, there is such a diversity of options and opinions that it is almost impossible for a consensus to emerge on the extent to which fracking should be implemented or regulated. The decision stakes are high because whatever course of action is chosen will result in significant repercussions for all stakeholders including industry, shale gas communities, consumers, and energy policy or environmental advocates, internationally. The debate over fracking, as a post-normal technology, calls for an altered type of inquiry and decision-making, which the "normal" procedures of the past are inadequate to handle. Ideally, as research is conducted and new technologies are developed, these new methods are then tested to ensure they are safe and, when needed, new rules or regulations are drafted based on the results of testing. But hydraulic fracturing has not followed this scenario; instead, the technology was billed as an established and familiar process despite the current situation where many questions have emerged around the current practice of fracking in many communities.

Evidence that hydraulic fracturing qualifies as a post-normal technology is found in the high complexity, uncertainty, and stakes of the debate. The recent succession of advocacy documentaries for and against fracking demonstrates hydraulic fracturing's post-normal status. The first film on hydraulic fracturing is *Gasland*, a 2010 documentary that debuted at the Sundance Film festival, which won multiple awards from several international and environmental film festivals (IMDb, 2011). The attention the film received at the festivals brought it into the spotlight and spurred a "fact war" between the industry, media, and nation. Subsequent documentaries including *Truthland*, *Gasland II*, and *FrackNation* further support our claim that hydraulic fracturing is different from other technologies and cannot be adequately addressed with "normal" policies and procedures because of the conflicting uncertainties and values expressed within the films. *Gasland* first raised the question of whether the industry's implementation of hydraulic fracturing and natural gas drilling was

democratic, a reasonable concern and one this paper expands on. Democracy ensures that procedures are in place that protect citizens' due process, role in deliberation, and rights (Liberatore & Functowicz, 2003). The chapter explores how the voice and dialogue from the average citizen, in some cases, has been obscured by the goals of industry and government. All the films reveal the high complexity of the fracking debate with many diverse stakeholders, issues, and benefits, which are currently not adequately addressed.

Instead of trading "facts" back and forth, the industry, regulators, and the general public have an obligation to move toward an approach that involves democratic discussion from all the stakeholders. This chapter argues that there will need to be significant amounts of public engagement in order to develop sound, ethical energy policy options to move forward. The hydraulic fracturing debate needs to be approached in a different manner for fair, sustainable solutions to be crafted. We rely on numerous theories and models developed by social scientists to find a democratic dialogue model for hydraulic fracturing. As energy consumption continues to increase, so will the conflicts over extracting more energy and ensuring it is done safely. An effective and just approach to the fracking debate could set the tone for future energy issues. We outline how an extended participation model, modified specifically for hydraulic fracturing, could serve as a framework for how to involve all stakeholders in determining the quality of the process and negotiating multiple policy pathways. This framework may serve as an example for how other energy controversies could be handled.

We first give an overview the field of participatory models, then review the history of hydraulic fracturing and describe beginnings of the debate. We then go on to argue why hydraulic fracturing qualifies as a post-normal technology, and describe a democratic, fair approach for negotiating policy solutions.

We think it is important to acknowledge that we use the terms "hydraulic fracturing" and "fracking" interchangeably in this text. Members of the oil and gas industry prefer to use the term "hydraulic fracturing" because it is a description of the technological process used. We therefore use this term in our paper, though we would also suggest that "hydraulic

fracturing" creates a scientific or technical rhetorical distance between the industry and citizens. We alternate our use of this term with the term "fracking," the preferred term of anti-hydraulic fracturing activists (and, often, the media). We believe opponents of fracking prefer this term because it is simpler and more accessible, and also because the sound of the word itself implies a form of violence or profanity, as in "What the Frack?," the name of a group that opposes hydraulic fracturing (see http://what-the-frack.org/). In short, we endeavor to acknowledge that words – with all of their connotations, definitions, sounds, and contexts – have meanings, and that we are aware of those meanings. We purposefully define and use these words to avoid the miscommunication already rampant in the discussion and in an effort to explore the many sides of this controversy.

7.2 Participatory models

We call for a more effective, fair approach to decision-making in the fracking debate that engages all stakeholders; such models have been applied to a variety of other controversies, including environmental ones, and could be applied effectively here. There have been calls for a more democratic process for approaching decision-making for decades (Fischer, 2003; Rowe & Frewer, 2000). A large body of work exists on the implementation and function of discourse models from the social sciences (see Depoe *et al.* 2004 and Hajer 2003 for a general overview). These frameworks for open dialogue on policy issues are defined as participatory or engagement models. Public participation "encompasses a group of procedures designed to consult, involve, and inform the public to allow those affected by a decision to have input into that decision" (Rowe & Frewer, 2000). The stakeholders in an issue are directly involved in "the agenda-setting, decision-making, and policy-forming activities" (Rowe & Frewer, 2005).

Calls for nonexpert participation in science, technology, and policy emerged in the 1970's along with the environmental movements such as antinuclear protests (Lengwiler, 2008). Previously, the association between science, politics, and nonexpert knowledge involved only communication between scientists and politicians, excluding the public (see Lengwiler 2008 for a brief history). It was traditionally believed that technical issues should be left to experts

and scientists. However, many recognized the limits of the experts in the presence of high uncertainties and that developing policy without public input is undemocratic and unpopular (Rowe & Frewer, 2000). The goal of public participation is to first provide the relevant information about an issue to all stakeholders, then to allow all parties to deliberate the possible policy options through two-way communication, and finally to ensure the adjustments or modifications to actions or policies are at least considered and possibly implemented (Rowe & Frewer, 2005). Laird (1993) describes how these models require more than just informed sharing between the participants. Instead, all participants in these models must "learn how and when to challenge the validity of the asserted facts, where new data would be useful, and how the kinds of policy questions being asked influence the type of data they seek."

There is a broad range of nonexpert involvement, from merely acknowledging the existence of impacts to society to direct participation of citizens in research or policy (Lengwiler, 2008). Public participation methods can include public opinion surveys, public hearings, focus groups, consensus conferences, and citizen juries (Rowe & Frewer, 2000). There are many informative texts outlining theories about how to apply these types of dialogue frameworks, which address the need for structure, facilitators, and well-defined goals to create successful programs (Fischer, 2003; Rowe & Frewer, 2005). Many issues with engagement models have been defined such as the lack of trust and imbalance of power between stakeholders. Kinsella (2004) outlines how the knowledge barrier between technical experts and laypersons can affect policy discussions and that there is a need to view public expertise on local issues as substantive. Researchers have also repeatedly noted that engagement models "suffer from hierarchical power relations among the actors involved" (Lengwiler, 2008). Evaluations of common participatory models reveal that while public opinion surveys and focus groups satisfy the public, they typically do not provide concentrated modifications to the issue (Rowe & Frewer, 2000). Models that involve a facilitator and more direct interaction with stakeholders are more successful; however, the success of a participatory program will depend on designing the model to fit the specifics of each unique situation (Rowe & Frewer, 2000). In a

later section, we describe what we believe will be a successful model of public participation for hydraulic fracturing. Even given complications resulting from an imbalance of power, lack of transparency, and mistrust, we optimistically propose that an approach which involves all stakeholders negotiating toward policy options is possible.

One parallel to the participatory model development in the oil and gas industry is corporate social responsibility (CSR), which is a business approach intended to address the social and environmental impacts of company activities (Frynas, 2009). CSR is an "umbrella term" that describes the responsibility companies have for their impacts on the public and the environment, for the other companies they do business with, and for giving value back to society (Frynas, 2009). Oil and gas companies promote and enact CSR more than other industrial sectors, but the implementation of CSR has occurred very unevenly and the programs differ from company to company (Frynas, 2009).[3] Stakeholder engagement, for large multinational companies, is a key element of CSR. Several high-profile environmental protests in the 1990's brought stakeholder engagement to the attention of oil and gas companies and proved that CSR activities were not addressing all stakeholders (Holzer, 2008).

Since these events, oil and gas companies have individually developed stakeholder engagement programs that typically outline the principles the company follows. For example, ConocoPhillips lists six key principles of their stakeholder engagement program: identify key stakeholders early, include these key stakeholders in the design and implementation of the engagement process, listen in order to understand stakeholders' concerns, communicate openly, seek solutions that create mutually beneficial business and engagement approaches, and follow through on commitments (ConocoPhillips, 2014). The level of detail and topics covered in the stakeholder engagement plans vary by company but the main components are similar. Oil and gas companies began hydraulic fracturing with principles developed from a CSR approach, which does not equate to a participatory approach. The communi-

[3]Frynas (2009) makes this statement because of the large growth of codes of conduct and social reporting seen broadly over the entire oil industry. See the article for tables listing the environmental information reported and the money spent on community improvements for several major oil companies across the world.

cation involved in these CSR-type programs may be one-way (only from the industry) or two-way (from both industry and the local community) but still lacks a true democratic process, where all voices are valued equally. CSR-based engagement can still ignore some stakeholders because the businesses determine how and when to contact the communities. The companies may choose to not interface with groups that do not directly impact their business (or even groups that do) (Holzer, 2008). As we will show, the rapid implementation of hydraulic fracturing in new areas caused some key stakeholders to be overlooked and communication to be dominated by those with power, creating controversy.

Before we outline the participatory model that could assist in crafting policy for hydraulic fracturing in a democratic manner, we first introduce the process of fracking, describe the controversy, and detail why hydraulic fracturing needs to be treated as a post-normal technology.

7.3 Background

The oil and gas industry uses hydraulic fracturing because the process substantially increases natural gas extraction and enables industry to reach otherwise hard-to-get natural gas. If a well is decreasing in production or is in an area of "tight gas," then fracking will greatly increase the flow of gas. Hydraulic fracturing is a treatment applied to an existing oil or natural gas well where a carefully crafted fluid containing chemicals and proppant, a medium to hold open the fractures, is pumped down the well at high pressures to fracture the rock, creating new pathways for the product to reach the well and therefore increasing the amount of oil or gas produced from the well.

7.3.1 Entrance of hydraulic fracturing and regulations

During the 1950s, an increase in vehicle production and the passing of the Federal Highway Act, which authorized the construction of highways, resulted in a surge in American fuel consumption (Holder, 2008). The method of hydraulic fracturing had just been tested in an experimental well with outstanding results for increasing the production of oil (Brady

et al., 1992). The public reacted positively to this development, which on average caused around a 75% increase in oil production per well (Montgomery & Smith, 2010). Within five years, thousands of wells had been hydraulically fractured (Brady *et al.*, 1992). These were rural, vertical wells that required lower pressures than the hydraulic fracturing treatments that would later be applied to modern horizontal wells. The early technology began by trial-and-error, with many unknowns about how the subsurface rock was breaking or how the fluid was travelling. It took several years before the mechanics of hydraulic fracturing were explained by theories from rock and fluid mechanics. Initially, operators believed the rock fractured horizontally until key research by Hubbert & Willis (1957) found that subsurface fractures are predominately vertical because they form perpendicular to the minimum amount of stress. The design of a treatment plan in the days of a low-volume, vertical well fracture was based more on estimation and intuition than on a well-researched, scientific strategy; as hydraulic fracturing was applied to more complicated reservoirs, tools for fracture estimation and fluid propagation were developed (Brady *et al.*, 1992).

Many of the main guiding practices for hydraulic fracturing were established before any environmental regulations were in place. The move toward regulation of water use and disposal did not begin until the 1970's with the emergence of the Environmental Protection Agency (EPA) and the creation of many new safety procedures concerning waste, water, and air (Farrah, 1992). Attempting to retroactively control the activities surrounding natural gas drilling may have created confusion and regulatory gaps that have been exploited with the application of modern hydraulic fracturing.

The guidelines for regulating hydraulic fracturing have constituted a gray area from the beginning of environmental regulation. One of the most important federal acts connected to concerns about natural gas drilling is the Safe Drinking Water Act (SDWA), enacted in 1974. Even though the original purpose of the SDWA was not to regulate oil and gas drilling but to protect the drinking water of American citizens, many stakeholders maintain there is a risk that hydraulic fracturing could contaminate water sources. Especially significant for

natural gas activities, the law requires the EPA to establish "minimum regulatory programs that will prevent underground injections that endanger drinking water" and this resulted in the establishment of the Underground Injection Control (UIC) program which regulates the disposal of wastewater from industrial activities (EPA, 2014; Hall, 2011). Hall (2011), an environmental lawyer, states that the definition of "underground injection" in SDWA is "the subsurface emplacement of fluids by well injection." Fracking activities appear to fall under this definition because fluid is pumped down the well; however, hydraulic fracturing has never been explicitly regulated under the SDWA. The reasons for this exclusion are that the process of hydraulic fracturing does not involve disposal, and almost all of the fluid is brought back to the surface so the fluids are not "emplaced". Also, the time required for the fracking fluid to create fractures and then be pumped out is relatively short when compared to the time that the well will produce oil (days versus decades). Regulators and industry perceived the risk from a short-term process like hydraulic fracturing as low compared to the risk from disposal of wastewater that remains in the ground indefinitely. Explicit instructions on how to govern fracking with respect to water contamination have yet to emerge. Thus, regulation of hydraulic fracturing under the SDWA has remained a gray area and has received renewed attention with the surge of fracking in new areas, where the combination of hydraulic fracturing and horizontal drilling have spurred concerns about the risks of contaminating drinking water aquifers.

7.3.2 Key new technology

Horizontal drilling – a new technology that combined with hydraulic fracturing to enables the production of complex, unconventional gas – opened up new areas with natural gas activities, which then brought the attention of the public to the impacts of fracking in the early 2000s. The use of this new technology, horizontal drilling, combined with hydraulic fracturing, enabled the production of complex, unconventional shale gas, which was the initiator for hydraulic fracturing to come to the public's attention. Previously, oil and gas wells were drilled down vertically into the subsurface. The invention of horizontal drilling

allows operators to first drill vertically to the depth of the oil or gas, then to deviate at an angle, and eventually to drill completely horizontally (Helms, 2008). It is this combination of horizontal drilling and hydraulic fracturing that allows access to the natural gas trapped in shale plays located through out the U.S. Horizontal drilling was invented in the 1800's, but it was not until the 1980's that drilling motors and precision drill bits allowed for horizontal drilling to become commercially efficient (Helms, 2008). The technology developed even more in the past decade to reach greater distances and depths within complex media, areas in the subsurface that contain multiple layers, rock types, and structures (Helms, 2008).[4] Horizontal drilling reduces the surface impact of natural gas drilling because one well pad, the area where the well initiates, can support multiple wells that extend horizontally in different directions (Arthur *et al.*, 2008b). Horizontal drilling created a new environment for hydraulic fracturing and thus, the technical practices of hydraulic fracturing changed to adjust to the new, longer, horizontal wells.

7.3.3 Current practices

A modern form of hydraulic fracturing, different in many ways from the technology used in previous decades, has been rapidly implemented on longer, horizontal wells for natural gas extraction. The pressure used to fracture the rock is much higher in current procedures, the duration of the frack is greater, and significantly more water is used. Furthermore, the types of chemicals used are different than in past practice. However, the oil and gas industry now describes fracking as a common, well-established, routine procedure employed worldwide on all types of wells (gas, oil, vertical, and horizontal).[5]

The process of hydraulic fracturing begins with designing a treatment plan, which is specific to each individual well. The plan details the amount of water, as well as the types and amounts of chemicals and proppant (typically sand). Also, the pressures needed to

[4] A horizontal well is able to extend from 1,000 to 5,000 feet which drains an area of rock that is 4000 times larger than a conventional vertical well (Arthur *et al.*, 2008b; DOE, 2009).

[5] Industry experts estimate that 50,000 fracture stages were completed worldwide in 2008, including anywhere from eight to 40 stages per well and the Society of Petroleum Engineers estimates that around 60% of all wells in the United States are fracked (Montgomery & Smith, 2010).

crack the rock are determined from modeling (Brady *et al.*, 1992; DOE, 2009). After the treatment plan is developed, initial water and chemicals are pumped down to prepare the well, and fracture locations are created by perforating the well casing, a protective lining that is meant to that ensure the well does not leak and holds pressure (DOE, 2009). Then a mixture of water, chemicals, and sand are pumped down the well at high pressures.[6] The liquid goes through the holes in the casing, fractures the rock, and fills the fractures (Brady *et al.*, 1992). The proppant is forced into the fractures and when the liquid is pumped out of the well, the fractures (which would close under the pressure of the earth above) remain open because of the presence of the sand (DOE, 2009). This process of pumping down fluid and fracturing is repeated for every perforation in the well casing. Each repetition is called a fracture stage, and multiple fracture stages are performed on one well. The liquid pumped out of the well is called flowback (containing water, chemicals, and contaminants from the subsurface), which is typically toxic and sometimes results in slightly radioactive material (Chen *et al.*, 2014). The flowback is put into holding ponds at the well site until a truck comes to take it to a wastewater treatment plant or to be recycled (Chen *et al.*, 2014). After the flowback has been evacuated from the well, the process of hydraulic fracturing is completed. A well may be fractured multiple times over its lifetime when the production of oil or gas decreases (Chen *et al.*, 2014).

7.3.4 Shale gas and major plays

The combination of hydraulic fracturing and horizontal drilling has allowed industry to reach resources in areas previously thought too difficult and costly to develop, but which may also be much more populated, environmentally sensitive, or otherwise developed. "Shale gas," or gas that is trapped in thin layers of massive slabs of shale, is one of the resources that has only recently been accessed with hydraulic fracturing and horizontal drilling.[7] Hydraulic

[6]The chemicals in the fracturing fluid have many different purposes, from etching the rock to preventing corrosion of the pipe; some of the common additive types are shown in Table Table 7.1 (DOE, 2009).

[7]Shale is a type of sedimentary rock that has an extremely low vertical permeability, which typically keeps the gas (found in these rocks) from naturally migrating from lower depths to higher depths (or vice versa) (DOE, 2009).

Table 7.1: A table detailing some of the common hydraulic fracturing fluid additives, their compounds, purposes, and common uses. Taken from DOE (2009).

Fracturing Fluid Additives, Main Compounds, Purposes and Common Uses			
Additive type	**Main Compound(s)**	**Purpose**	**Common Use**
Diluted Acid (15%)	Hydrochloric acid or muriatic acid	Help dissolve minerals and initiate cracks in the rock	Swimming pool chemicals and cleaner
Biocide	Glutaraldehyde	Eliminates bacteria in the water that produce corrosive byproducts	Disinfectant; sterilize medical and dental equipment
Breaker	Ammonium persulfate	Allows a delayed break down of the gel polymer chains	Bleaching agent in detergent and hair cosmetics, manufacture of household plastics
Corrosion inhibitor	N,n-dimethyl formamide	Prevents corrosion of the pipe	Used in pharmaceuticals, acrylic fibers, plastics
Crosslinker	Borate salts	Maintains fluid viscosity as temperature increases	Laundry detergents, hand soaps, and cosmetics
Friction Reducer	Mineral oil	Minimizes friction between the fluid and the pipe	Make-up remover, laxatives, and candy
Gel	Guar gumor hydroxyethyl cellulose	Thickens the water in order to suspend the sand	Cosmetics, toothpaste, sauces, baked goods, ice cream
Iron Control	Citric acid	Prevents precipitation of metal oxides	Food additive, flavoring in food and beverages; Lemon juice $\sim 7\%$ citric acid
KCl	Potassium chloride	Creates a brine carrier fluid	Low sodium table salt substitute
Oxygen Scavenger	Ammonium bisulfite	Removes oxygen from the water to protect the pipe from corrosion	Cosmetics, food and beverage processing, water treatment
pH Adjusting Agent	Sodium or potassium carbonate	Maintains the effectiveness of other components, such as crosslinkers	Washing soda, detergents, soap, water softener, glass and ceramics
Proppant	Silica, quartz sand	Allows the fractures to remain open so the gas can escape	Drinking water filtration, play sand, concrete, brick mortar
Scale Inhibitor	Ethylene glycol	Prevents scale deposits in the pipe	Automotive antifreeze, household cleansers, and deicing agent
Surfactant	Isopropanol	Increases the viscosity of the fracture fluid	Glass cleaner, antiperspirant, and hair color
Note: The specific compounds used in a given fracturing operation will vary depending on company preference, source water quality and site-specific characteristics of the target formation. The compounds shown above are representative of the major compounds used in hydraulic fracturing of gas shales.			

fracturing creates new pathways (fractures) for the shale gas to travel to the well, and horizontal drilling allows the well to remain in the same gas rich horizontal layer, which enables the extraction of the gas previously too costly to access.

There are several regions in the United States that contain massive amounts of shale gas, as shown in Figure 7.1. The Marcellus Shale is the most extensive shale gas area or "play;" it is located beneath six states including Pennsylvania and New York (DOE, 2009). The amount of natural gas located in the Marcellus Shale and three other large shale plays is said to be about 50-60% of the total natural gas reserves in the United States (DOE, 2009).[8] Unlike in Texas, where drilling of the Bakken Shale has been occurring for years among a relatively dispersed population, the Marcellus Shale exists under one of the most populous areas of the United States, and most residents had never seen oil or gas wells and were probably not familiar with processes like hydraulic fracturing.

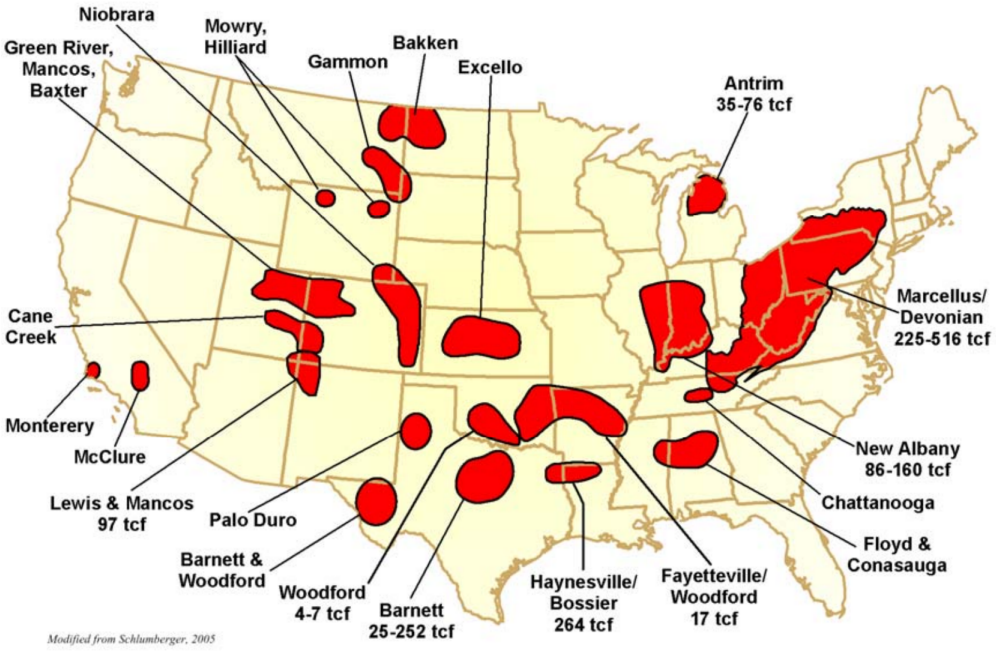

Figure 7.1: The locations of all the shale basins in the United States. Taken from Arthur *et al.* (2008b).

[8]The increase in drilling of the Marcellus Shale began in 2003 when Range Resources-Appalachia, LLC drilled a new well, applying techniques of horizontal drilling and fracking with great results (Arthur *et al.*, 2008a). From that point forward, the amount of well permits issued increased significantly.

The U. S. Energy Information Administration (EIA) reports that natural gas production and consumption in the United States has steadily risen since 2009 and this increase is predicted to continue because of the extraction of natural gas from shale plays (EIA, 2014b). Most energy analysts acknowledge that these shale gases will play an important role in the energy future of the United States. Shale gases take on this predicted prominent role particularly if and when coal production – which fluctuates between providing 45 and 50% of domestic electricity generation (depending on various factors) – is regulated or priced according to its contributions toward climate change and pollution (Brown, 2007). The amount of natural gas that is technically recoverable from these unconventional plays is estimated to last the United States around 90 years (DOE, 2009). Many believe natural gas is less harmful in terms of greenhouse gas production than coal, and so natural gas has been billed as a "bridge fuel" that will ease the transition to sustainable energies. However, as we shall see below, some experts challenge this belief about the relatively benign impact of natural gas emissions.

7.3.5 Current regulations

Currently, natural gas drilling and all the activities surrounding it, including hydraulic fracturing, are regulated individually at the state level through the state's environmental departments. The EPA ensures that each state's regulatory body follows the federal regulations, but the state is in charge of drafting rules, inspecting well sites, enforcing regulations, and imposing fines, which leads to a diversity of regulations from state to state. To list all of the regulations by state would not benefit the reader here; instead, we direct the reader to each state's webpage for more information or to the reports generated by the State Review of Oil and Natural Gas Environmental Regulations (STRONGER), which grade each state on the strength of their oil and natural gas regulations and suggest improvements (STRONGER, 2014).

When the use of hydraulic fracturing increased in the early 2000s, the government revisited issue of whether the process should be regulated under the SDWA. The Energy Policy

Act of 2005 specifically excludes hydraulic fracturing from the definition of "underground injection" (Hall, 2011). This section of the Energy Policy Act is nicknamed the "Halliburton loophole" to refer to the large role the oil and gas industry played in the committee that made the suggestion to have hydraulic fracturing excluded from SDWA. Fracking remains unregulated under federal regulations, but the states have attempted to keep up with the rapid implementation of hydraulic fracturing by amending other regulations surrounding natural gas drilling. The changes focus on the newest issues that have arisen such as: a call for disclosure of chemicals, the proximity of wells to residential areas, and baseline testing of water (Pless, 2012). Presently, 15 out of 29 states that practice hydraulic fracturing have some type of chemical disclosure rule, which requires operators to post a list of the chemicals placed down the well (Chen *et al.*, 2014). Trade secrets, a combination of chemicals that set a company's fracking formula apart from others, are exempt. Limitations to the placement of wells near homes and schools are now written into many regulations (COGCC, 2013). While there have been modifications to the regulations which have concentrated on dealing with immediate issues, there is still a need for a larger, broader overhaul to the regulations that addresses the concerns and values of a variety of stakeholders as hydraulic fracturing is carried out at a higher rate and in increasingly sensitive environments.

The oil and gas industry calls attention to fracking as both a historic and accepted practice, while at the same time presenting it as a new technology that can recover vastly more gas than in the past. The current use of the technology uses larger amounts of water and chemicals at much higher pressures and is carried out in new (some more populated) areas. Some members of the public and the media in these areas have reacted to the drilling of wells with a mix of anger, confusion, and distrust because of the sudden appearance of trucks and industrial equipment in shale-rich regions that had previously not experienced natural gas extraction. The introduction of fracking, an arguably "old" technology, to new areas such as the Marcellus Shale, has resulted in a national debate on the safety of hydraulic fracturing.

7.4 The fracking debate

There are many elements still unknown about fracking, but the different sides in the debate claim to know "the facts." The opposing sides have contrasting answers to questions about the risks to drinking water aquifers, the effects of the chemicals in the hydraulic fracturing fluid, the reasons for the increase in seismicity, and the extent of the air pollution caused by the process. As is the case with many controversial energy-related topics – such as climate change, nuclear power, or renewable energy – it can be both confusing and frustrating for an individual to make sense of competing claims and to try to discover the "facts" about hydraulic fracturing. To better understand the complexities of the fracking debate, we first introduce some of the stakeholders and present the main issues of concern.

The hydraulic fracturing debate, from a distant perspective, may seem to have only two sides: pro-fracking and anti-fracking. However, we need to recognize that there is a spectrum of positions on hydraulic fracturing held by a variety of stakeholders. There are stakeholders on every scale, from the large oil and gas industry down to the individuals who experience fracking on their land. There are those who are directly impacted by fracking such as the oil and gas industry, landowners, local communities, and governmental agencies regulating the practice. But also, there are those indirectly impacted, such as nongovernmental organizations, the media, and American citizens in general.

The main categories of stakeholders – which include many individuals, groups, and small companies within the hydraulic fracturing debate – are the oil and gas industry, government, and the average citizen who is impacted in some way by fracking. The oil and gas industry is an aggregate of multiple large and small companies – huge companies like BP and Shell, but also smaller companies whose primary purpose is to extract natural gas such as EnCana or Range Resources. There are also service companies that engage in a variety of activities to support the drilling such as surveying or transporting wastewater. The governmental stakeholders come from every facet of government from the President, Congress, and the EPA to the individual state regulatory agencies such as the Colorado Oil and Gas Conserva-

tion Commission (COGCC) or the Pennsylvania Department of Environmental Protection (DEP). Local and town governments are also stakeholders; they act as a conduit for information about fracking for the local citizens. Knowing the category of general public is a broad, in this chapter we focus on members of the interested public, which encompasses all those with natural gas drilling in their backyards, citizens indirectly affected through employment or locality, and individuals who have only heard of fracking from the media or documentaries. Some landowners have lease contracts with gas companies but some do not receive any benefits from the extraction on their land because someone else owns the mineral rights.

Other stakeholders exist that do not fit easily into the three main categories. There is an abundance of nongovernmental organizations on both sides that ensure important issues get attention. Some stakeholders are unable to speak for themselves, such as children and future generations. The stakeholders in the hydraulic fracturing debate encompass more than just proponents and opponents, however they include individuals and groups who value part of the benefits of hydraulic fracturing while maintaining concerns about the risks to their health, safety, and the environment. They are both sympathetic to and skeptical of the various claims, which add more complexity and controversy to the situation.

Many of the issues that are being debated in hydraulic fracturing are those pertaining to risks to health, safety, and the environment. The first issue raised by landowners was the potential for the fractures created by the technology to cause unintended harm by fracking fluid or gas entering water wells. One mechanism that those not technically familiar with hydraulic fracturing originally thought responsible for contamination was a fracture propagating upward and breaching a drinking water aquifer, allowing gas to enter (Osborn *et al.*, 2011). Industry states that the occurrence of this is highly unlikely, but there is still a small chance a hydraulic fracturing could fracture a water aquifer in some unique situations (Davies, 2011). There is higher probability for water contamination to come from failure of

the integrity of the well casing and cement.[9] The casing can corrode, crack, or leak and the concrete can crack – both of which create pathways for the gas to migrate into the subsurface and possibly into nearby water wells (Brufatto *et al.*, 2003). There are tests to monitor for these issues, but the problem is not always caught before the gas migration has occurred (Brufatto *et al.*, 2003).

Another issue is the amount of water needed to hydraulically fracture a single well, which is around 2.3-3.8 million gallons (Chen *et al.*, 2014). Without careful regulation, this large amount of water withdrawal could advance the water shortage for certain states like Colorado or California, which are currently in a severe drought (Chen *et al.*, 2014). A large percentage of the liquid put down the well is water, but the amount of chemicals used for hydraulic fracturing is also significant.[10] Residents are concerned about the increased health risks that could result from the interface between these chemicals and where they live and work, such as the potential for a higher incidence of cancer (Rafferty & Limonik, 2013). In addition, the air emissions from all the activity surrounding drilling and extracting natural gas could have dangerous side effects, as studies have shown that these emissions might create a greater health risks for residents living close to drilling sites (McKenzie *et al.*, 2012). Compounding worries about chemicals and air emissions is the placement of wells near residential areas and schools.[11]

Also, geoscientists have investigated concerns about the possibility of drilling practices increasing the number of earthquakes, ranging from small earthquakes created by fracturing the earth to larger earthquakes triggered by an increase in wastewater disposal through injection into the subsurface (Ellsworth, 2013; van der Elst *et al.*, 2013). There are no

[9] Several layers of casing (metal pipe placed down the well) and cement (placed between the casing and the rock) are what protects the shallow subsurface from the liquids pumped into and extracted from the well (DOE, 2009).

[10] For example, gas wells in the Marcellus Shale will use around 3.8 million gallons of water in the fracturing fluid (DOE, 2009). One gas well in Susquehanna county, PA, fractured in 2011, reported Hydrochloric acid, a chemical that etches the rock face, composed only 0.08% of the total fracturing fluid (FracFocus, 2011). This amounts to around 35,000 gallons of acid.

[11] Drilling activities, depending on the state, can occur within 500 to 1,000 feet of homes and schools (Richardson *et al.*, 2013).

regulations designed to assess the seismic dangers of the practices involved in the extraction of natural gas (Ellsworth, 2013). The likelihood for these various negative incidents to occur and the range of impacts and benefits surrounding drilling practices are contested by opposing sides in the fracking debate; the issues are further captured and explored in the documentary films about hydraulic fracturing.

The counterpoints to all the concerns about the risks to health and safety from hydraulic fracturing are the benefits of the process to the economy and energy independence. The impact to the local economy from natural gas drilling is large. A 2011 study found that drilling in the Marcellus shale generated around $11.2 billion for the Pennsylvanian economy in the year 2010; this number includes value generated from leasing, surveying, drilling, pipeline construction, and other services connected to the industry (Considine *et al.*, 2011). Much of the economic benefits come from a severance tax, a tax placed on all gas production, which is typically a percentage of value of the gas extracted (Richardson *et al.*, 2013). Fracking also creates more jobs in new areas. In Pennsylvania, hydraulic fracturing supported almost 140,000 direct, indirect, and induced jobs in 2010 (Considine *et al.*, 2011). The direct jobs account for a large portion of the total number with the most jobs coming from construction, mining, retail, and wholesale trade (Considine *et al.*, 2011). The jobs and economic value generated by hydraulic fracturing have revived struggling towns and communities where previously there was no source of income (Griswold, 2011).

Hydraulic fracturing affects the economies locally, but it also has a large effect on the imports of resources from other countries. Production of domestic natural gas decreases our reliance on foreign sources of energy. The demand for natural gas exceeds domestic production and if U. S. unconventional gas was not extracted, the gap between U.S. gas production and demand could increase requiring more foreign sources to be imported (DOE, 2009). Natural gas represents around 27% of total energy consumption (EIA, 2014a). As much as 60% of 1,744 trillion cubic feet (tcf) of technically recoverable gas is unconventional, requiring the use of expanded subsurface processes for extraction (DOE, 2009). There is

uncertainty in the scientific community about whether natural gas can claim to be a low-cost "bridge" fuel that would allow a transition to more sustainable energies. A study by Howarth *et al.* (2011a) recently argued that the greenhouse-gas footprint from natural gas drilling was substantially more than previously thought, particularly as a result of methane leaks over the lifetime of a well. Still the economic and energy future values are significant which, for some, outweigh the risks to health and safety.

Proponents and opponents of hydraulic fracturing contest each of these risks and benefits. As we will show, both sides give contrasting evidence to support their position relying on scientific studies and experts. The diversity of issues and stakeholders has created a highly complicated debate that has moved past the confines of simply determining how to implement a normal technology.

7.4.1 Hydraulic fracturing documentaries

The ability of both sides to marshal evidence in the form of scientific data to support their opposing arguments suggests that fracking has now become what Funtowicz & Ravetz (1993) call "post-normal science", what Sarewitz (1996) might call "controversial science", and what Pielke Jr (2007) might refer to as "high-values, high-uncertainty" science. In post-normal science, the separation between scientific information and the values of the stakeholders disappears (Funtowicz & Ravetz, 1994). The traditional systems employed to evaluate options and arrive at a valid solutions, such as peer review in the science community or best practices in industry, no longer apply because the uncertainty is too high and the values are too diverse (Funtowicz & Ravetz, 1993). More deliberation on all the issues and uncertainties by all stakeholders is needed before the scientific community can come to a consensus about the issue.

We argue that the realm of the post-normal is always in the political realm: where discussions over ethics, responsibilities, rights, futures, and justice occur and that such decisions must be made. Changing the framework for discussion about energy choices to include public voices and expertise will strengthen the decision-making process altogether, making it more

robust to dramatic shifts over time.

We demonstrate how hydraulic fracturing qualifies as a post-normal technology through several documentaries about fracking. This chapter focuses on the release of *Gasland*, a documentary about the impacts of hydraulic fracturing, the "fact war" that erupted after, the subsequent documentaries created to challenge *Gasland*: *Truthland* and *FrackNation*, and the sequel to *Gasland*: *Gasland II*.

Gasland tells the story of how filmmaker Josh Fox was approached by oil and gas companies wishing to lease his land in upstate New York for natural gas drilling. As Fox tells it, he refused, but then became involved in the issue as he saw his neighbors agreeing to lease their land, which he felt could affect his property values, the intrinsic value of the forests around his home (including their beauty), and the quality of the air and water around the wells and in regional watersheds that could affect human, animal, and plant life. The documentary follows Fox as he visits individuals and families across the United States who either did not own the mineral rights on their properties or who signed leases with oil and gas companies interested in fracking, and who felt they had suffered significant health and environmental damage as a result of poor drilling practices. The most memorable scenes feature Fox with homeowners in Colorado and elsewhere lighting their tap water on fire because of the high methane content. *Gasland* paints a dreary, scary picture of hydraulic fracturing using dramatic tone and dark imagery.

Conversely, *Truthland* is a short 35-minute film produced by Energy In Depth and the Independent Petroleum Association of America, two groups that represent and promote the views and actions of the oil and gas industry, as a reaction to *Gasland*. Shelly DePue – a mom, dairy farmer, teacher, and Pennsylvanian – makes a similar journey as Fox around the U.S. to determine if hydraulic fracturing is safe to use on her farm. DePue visits Texas, Colorado, and Louisiana, but unlike Fox, speaks mostly with experts to discover of the "truth" and "facts" about hydraulic fracturing. The goal of the film is clearly to convince the general public that fracking is a safe, routine practice that does not need more regulation or scrutiny.

DePue narrates the film and attempts to answer questions, such as "Is the U.S. gas industry good or bad?" This type of vague, black-and-white, simplistic question is answered with seemingly hard facts from experts. One example includes John Hanger, the former secretary of the Pennsylvania DEP, stating that fracking fluid has never contaminated drinking water through hydraulic fracturing. A critical viewer recognizes that even if this "fact" is true, it does not answer the broad question of whether or not the industry is "good." In summary, DePue claims that Fox unfairly presented the gas industry in *Gasland*. At the end of the film, DePue heads home feeling assured that fracking is safe to be used on her farm. The overly simplistic manner of the argumentation in *Truthland* represents industry's attempt at convincing the public that hydraulic fracturing is safe and needs to continue. The industry believed the controversy over hydraulic fracturing occurred only because of an uninformed public, so they created *Truthland* to give the "facts" about the process to the public directly while at the same time kicking the "folksy," down-to-earth approach used in *Gasland*.

Another documentary attempting to establish the "facts" about hydraulic fracturing is *FrackNation*. In this film, Phelim McAleer, an Irish journalist, travels around the U.S., like Fox and DePue, to discover his own "truth" about gaslands. The documentary was funded with a Kickstarter campaign, a crowdsourcing platform that allows anyone can make a monetary contribution to a proposed project, but it is not exactly clear what motivated McAleer to look into fracking other than his reputation as an independent "journalist," who has produced other documentaries on controversial topics. McAleer travels to the same towns and cities that Fox visited in *Gasland*. However, McAleer finds and speaks with other community members who have different perspectives on the issue of hydraulic fracturing. One particular group that *FrackNation* addresses, which is absent in the other films, are Pennsylvanian dairy farmers, who argue that they will lose their ancestral lands without the extra income from allowing their lands to be leased. McAleer focuses on the contaminated water shown in *Gasland* and finds contradictory evidence apparently to demonstrate how *Gasland* does not show the "truth." *FrackNation* broadens the scope of issues to consider in

the hydraulic fracturing debate by addressing the international use of natural gas and how the restriction of gas has led to domination of some nations by those (mostly Russia) who control the energy source. Overall, *FrackNation* has an upbeat tone and presents hydraulic fracturing in a positive light. The film ends with a montage of images depicting what is made possible by energy, which is almost everything in industrialized society.

Gasland II is a continuation of the first *Gasland* film, which was released soon after *FrackNation*. In this newest film, Fox focuses on the role of the government and industry in allowing the pollution of the environment and the endangerment of people directly impacted by hydraulic fracturing. Fox discusses the influence of different political figures that have close ties with the natural gas industry. In this film, the government and industry are rolled into one villainous entity. However, Fox portrays the EPA as somewhat of a good guy, although controlled by tainted higher-ups. Fox is still maintains his populist approach by interviewing local folks in Dimock, PA, Pavillion, WY, and Dish, TX, but (similarly to *FrackNation*) also visits with farmers in Australia demonstrating the global impact of hydraulic fracturing. The film covers many of the issues that have occurred since the first film including air pollution, water use, induced seismicity, and cement failure. Fox broadens the scope of this film to include the Macondo well disaster. He shows dramatic images of the oil on the surface of the ocean and speaks to citizens living on the coast, who were directly affected. There are scenes of water set ablaze in diverse locales and at a larger scale. One farmer in Australia demonstrates how he could light a whole pond of water on fire. The tone of *Gasland II*, similar to *Gasland*, is unsettling and dismal, which is emphasized with dark scenes and graphics. Fox calls for a dramatic shift or revolution in the treatment of hydraulic fracturing by the government and industry, which appears insurmountable.

The main goal of all the hydraulic fracturing documentaries is to reveal some unbiased, pure "truth." However, this effort to find an impartial truth is futile because the hydraulic fracturing debate is past the point of being resolved using only scientific data. We show in the next section that the value of the films is not how well they proved their claims but the

evidence they show of a technology that is past "normal" practices.

7.5 Fracking as a post-normal technology

Hydraulic fracturing is a post-normal technology because it fits the two main traits of post-normal science. The two characteristics that identify post-normal science are what Funtowicz & Ravetz (1993) define as high system uncertainties and high decision stakes or what Pielke Jr (2007) defines as a high uncertainty and low values consensus. Some of the uncertainties in the fracking debate, which are highlighted in the documentaries, are how or whether fracking causes an increase in diseases like cancer, causes pathways for methane to enter drinking water aquifers, or endangers the community through the use of chemicals in the fluid. The documentaries focus on the diverse values of the stakeholders involved in the hydraulic fracturing debate, from rural Pennsylvanians to pensioners in Ukraine. There are those who value the jobs, energy independence, and economic benefits that fracking produces. But there are also those who value their health, safety, clean rivers, and pristine forests. And there are still others who are trying to balance some of these competing values. In the next two sections, we present some of the evidence from the documentaries that characterize hydraulic fracturing as a post-normal technology.

7.5.1 System uncertainties

System uncertainties are defined by Funtowicz & Ravetz (1993) as uncertainties found across the realm that the issue encompasses. Pielke Jr (2007) defines uncertainty as when "more than one outcome is consistent with expectations." Hydraulic fracturing has many incidences where expectations do not meet with the actual outcome but also where the outcome is unknown – such as the environmental impacts to river basins. For a system to be truly understood, we would need to comprehend the entire "complex reality" of the issue, which is impossible for a complicated situation like hydraulic fracturing (Funtowicz & Ravetz, 1993). Every possible pathway for contamination and every possible risk to the population and environment would need to be understood and quantified. Often uncertainty

remains in a complex issue, even with multiple stakeholders working to reduce it, because the stakeholders have different agendas (Pielke Jr, 2007). For example, local citizens will push for more studies to qualify the risks of water contamination from hydraulic fracturing, while the industry will invest resources in better qualifying the amount of natural gas that hydraulic fracturing could extract, which gives better profit analyses to their stockholders. The efforts work against each other and uncertainty remains for both areas. Examples of the system uncertainties in fracking exist throughout all four documentaries on hydraulic fracturing.

The height of the uncertainty within the fracking debate is captured in the "fact war" that erupted after the first *Gasland* documentary. Energy In Depth, Colorado Oil and Gas Conservation Commission (COGCC), and several others drafted "debunking" documents outlining all the "facts" Fox got wrong in his documentary. In a letter written in response to industry rebuttals to his film, Fox quotes an industry executive who feared the documentary could "block our industry" (Fox, 2010). According to Fox, the American Petroleum Institute hired the public relations firm Energy in Depth to help respond to the claims made in Gasland and to manage public perceptions of natural gas and particularly of planned drilling projects of the Marcellus Shale. One result of that effort was the documentary *Truthland*. The industry was particularly concerned with how the public might react to Fox's documentary.

Energy in Depth's rebuttal of *Gasland*, titled "Debunking *Gasland*," is the most in-depth of the many industry responses to the film. The document pulls out minute-by-minute statements made in the film and offers the industry's explanations or corrections by bullet point. The main corrections are to Fox's statements about the regulation of fracking under SDWA, details about hydraulic fracturing, and the contamination of specific sites. The document discredits the authority of Fox and states that industry practitioners are the most qualified experts to be trusted on the subject and that fracking is a heavily regulated, standard industry practice. A number of other "Debunking-Gasland"-type documents exist from other industry sources. For example, the Barnett Shale Energy Education Council features a short

list of rebuttals to *Gasland's* primarily claims, arguing that hydraulic fracturing is heavily monitored by local, state, and federal regulations. More telling than this brief rebuttal of Fox's documentary is an extensive "frequently asked questions" (FAQ) list following the "Debunking Gasland" points. Here, drilling in the Barnett Shale, located in West Texas, is defended as having a proven safety record, a record of protecting local landowners, and a history of heavy regulation by the Railroad Commission of Texas. The tone of the responses to the FAQs is intended to soothe anxious landowners who may have seen *Gasland*, in particular framing fracking as a long-time practice having a proven safety record. Similarly, the COGCC argues that "an informed public debate on fracking depends on accurate information" (COGCC, 2014). However, the document does not acknowledge that the uncertainty in the information is too high. There is not a way to know how all the chemicals affect the environment or how methane travels in the subsurface to a high level of accuracy.

The COGCC fact sheet focuses largely on the issue of methane contamination of drinking wells. A highly visual example of this uncertainty occurs when Fox in *Gasland* shows how a resident in Colorado can light his water on fire. The claim Fox makes is that hydraulic fracturing has caused methane to migrate and leak into the drinking wells. However, experts in *Truthland* and *FrackNation* claim that in methane-rich areas, the gas can migrate on its own. The COGCC relies in particular on distinguishing between biogenic (naturally occurring shallow methane) and thermogenic methane (naturally occurring methane, buried deeper in rock or shale formations). The two forms of methane can be scientifically distinguished from one another, and "[i]n Colorado, thermogenic methane is generally associated with oil and gas development, while biogenic methane is not" (COGCC, 2014). This distinction is significant, argues the COGCC, because the methane that causes the residents in *Gasland* to be able to light their water on fire is actually biogenic methane, not thermogenic methane, and therefore was not the result of oil and gas drilling. McAleer supports this claim in *FrackNation* when he speaks with a resident of Dimock, PA, who had to re-drill their drinking water well three times because of contamination by methane before any gas

drilling or fracking occurred. However, as Fox and others put it, just because there was biogenic rather than thermogenic methane in some of the wells inspected by COGCC does not mean that the presence of biogenic methane in the wells was not created by drilling activities. According to Fox (2010), ". . . gas fingerprinting simply identifies the gas. It does not identify the migratory pathway of the gas." *Gasland II* shows more water lighting on fire in more places including Australia, all of which have experienced fracking. Without being able to trace every pathway created in the subsurface from hydraulic fracturing, we cannot know if it is natural processes or fracking that causes the gas to migrate.

The uncertainty in the "facts" also creates doubt in the "experts." A common problem for high-uncertainty debates is the discrepancy between experts in the same technical field. This is shown many times throughout the documentaries. One example of experts disagreeing is presented in both *Truthland* and *Gasland II* when scientists from the same field have two different opinions on hydraulic fracturing. The first scientist, Terry Engelder, a professor at Pennsylvania State University, appears in *Truthland* and assures Sherry that hydraulic fracturing is safe. However, in *Gasland II*, Robert Howarth and Anthony Ingraffea, both professors at Cornell University, speak about their concerns about hydraulic fracturing causing contamination to water from leaks in the well casing. Who should the viewer believe? The confusion continues into the scientific community itself. In 2011, the selective, peer-reviewed journal *Nature* published an article titled "Natural gas: Should fracking stop?" presenting two perspectives on the risks of hydraulic fracturing (Howarth *et al.*, 2011b). Howarth and Ingraffea, representing one side, answer by stating, "Yes, it's too high risk" and Engelder answers with "No, its too valuable." All the authors are esteemed scientists whose individual work is published in peer reviewed literature, but they have different opinions about the safety versus benefits of hydraulic fracturing. The uncertainty from the scientific community shows how decision-makers cannot rely solely on information from the "experts."

7.5.2 Decision stakes

The second characteristic of a post-normal technology is the high decision stakes, which are decisions that will have a large impact on those involved. Funtowicz & Ravetz (1993) state that the decision stakes of an issue pertain to the "conflicting purposes among stakeholders." When the decision stakes are high, there is a large discrepancy in the desires and values of the stakeholders and making a decision becomes more difficult. Pielke Jr (2007) calls this trait the decision context, which depends on the degree of consensus among the stakeholders. If there is a consensus on what is valued, then making a decision is a fairly simple task, such as deciding to send federal aid to disaster areas. But if everyone values a different aspect of the issue then the decision stakes become higher. Decision stakes include "all the various cost, benefits, and value commitments" involved in the issue (Funtowicz & Ravetz, 1993). For fracking, these commitments include money, jobs, preserving the environment, clean drinking water, and many more. With conflicting values, benefits, and costs, the unbalanced division of power for each position plays an important role in determining which stakeholders' voices are heard (Pielke Jr, 2007). The industry holds the most power in the hydraulic fracturing debate, while the individual citizens have the least; some have none at all, such as future generations (Funtowicz & Ravetz, 1993). The diversity of values and imbalance of power cause a situation where the traditional process to assess the valid options for actions cannot accommodate the high discrepancy of positions fairly.

For the industry and government, the decision stakes of hydraulic fracturing appeared to be straightforward. The industry values an increase in profits while operating in a quick but safe manner that extracts the natural gas from the ground with minimal costs. The local government values smooth permitting, adherence to the rules and regulations, well sites that pass safety checks, and effortless collection of taxes. If there is an issue with a regulation or process then the government and industry work together to develop methods that reduce errors but do not interfere with drilling time. The multinational oil corporations hold a large portion of the market force, which gives industry a disproportionate amount of power

in determining energy policy. The industry values policy that will allow them to continue profiting from the increase in production of natural gas. The industry and government cannot and should not represent the values for all the stakeholders. The documentaries show the perspective of some of the other stakeholders.

In *Gasland*, Fox details his own personal story with hydraulic fracturing when a company wanted to lease the land where he grew up. The story is accompanied by images of his family home in Pennsylvania. After, Fox travels around the U.S. telling the stories of others, who without Fox's film may not have received much attention. For example, in one scene of *Gasland* featuring Coloradoan Renee McClure, whose water supplies were supposedly adversely affected by hydraulic fracturing, she tells of contacting the COGCC and being frustrated by their inattention to her concerns: "I thought that the Colorado Oil and Gas Conservation Commission was there for the people. They are not there for the people, they are there to work and help the oil and gas companies. And I asked them 'who's there for the people?' And he told me, 'NOBODY, call an attorney!'" This is a view echoed by many citizens that Fox speaks to across the nation. The landowners or families who confront the oil and gas companies about possible contamination sometimes sign nondisclosure agreements to reach a settlement, but then the family is not allowed to speak about any part of the contamination or agreement.

There are also those who support hydraulic fracturing but still do not have a loud voice in the fracking debate. McAleer, in *FrackNation*, also brings new voices to the debate – mainly the Pennsylvanian dairy farmers – that want hydraulic fracturing to continue. The farmers would benefit from being able to lease their lands for natural gas drilling, which would enable them to keep the land that has been in their family for generations. This group of citizens feels that their voice has been obscured by the large anti-fracking movement that began after the release of *Gasland*. DePue in *Truthland* speaks with a couple steel workers in Ohio who describe how the increase in natural gas drilling brought their jobs back because they produce the steel pipe used to case the well.

The films highlight the different values of the stakeholders involved in the hydraulic fracturing debate – from rural Pennsylvanian farmers to pensioners in Ukraine. Many value the increase in jobs, energy independence, and economic benefits that fracking produces, but they also value their health, safety, clean rivers, and pristine forests. The hydraulic fracturing documentaries represent stakeholder voices and values that were overlooked by others in the debate. An important role of the documentaries is telling the story of the local people – a side of technological debates that is often missing or obscured by factual information. The wide interest in *Gasland* and the other films allow the local stories and concerns to overpower the technical information held by industry and the government. However, the balancing of stakeholder voices should not be left to filmmakers, instead engagement models need to be established for these types of controversies to allow discussion and negotiation by all parties.

We argue that the value of the documentaries lies not as much in detailing and discussing all of the uncertainties in hydraulic fracturing (which they do to a great extent), but more in pointing out that the typical American who is affected by fracking has little recourse to action in the face of energy exploration and production. There are significant debates to be had about the system uncertainties of hydraulic fracturing, such as risks to public health and environmental impacts of fracking. But of equal concern is the fact that hydraulic fracturing as it is currently being carried out constitutes an undemocratic practice. New technologies are being developed and implemented quickly, by industry, and demand for inexpensive electricity production is growing steadily. All of this amounts to little opportunity for meaningful or thoughtful public debate over the choices made. It is also possible that, by focusing the debate around the facts, the oil and gas industry and the opponents to fracking are missing an important opportunity to engage citizens in meaningful discussion and decision making about how to proceed. More citizens may begin to oppose drilling, partly because they resent being excluded from making choices about their health, economy, and environment. Not engaging citizens is an inequitable approach, one unbefitting a nation with democratic ideals toward deliberation and decision-making. The difficulty of invoking scientific facts

in support of particular policy options is further problematized by the fact that systems of public accountability in the case of hydraulic fracturing seem to have broken down.

7.6 Importance of Deliberation

The present controversy over hydraulic fracturing demands fair, sustainable solutions negotiated through dialogue between all stakeholders. The documentaries demonstrate the conflict between the industry, government, and public over attempting to determine the "facts." The lack of a consensus on the risks and benefits of hydraulic fracturing caused the relations between industry, landowners, and the government to sour. The stories depicted in the documentaries are only a few out of countless other, similar situations (see National Geographic (2014) for more personal stories). The commonality among these stories is the lack of two-way communication, exchange of information, and fruitful discussion from all parties – in general, the normal practices do not adequately address the concerns and uncertainties of the stakeholders. The industry would like to continue "business-as-usual" by allowing the experts to handle policy decisions without creating a space for deliberation with all parties to address broad concerns. Opponents of hydraulic fracturing also ignore a subset of the stakeholders by advocating for all fracking activity to stop. Both the anti-fracking and pro-fracking documentaries advocate for a single solution that completely fits with their version of the "truth."

De Marchi (2003) outlines the two extremes of controversial debates: "On the one hand, there are those who claim that the scientific analysis of risks can control uncertainty, defeat ignorance and provide indisputable input for appropriate regulation. On the other hand, there are those who maintain that uncertainty and ignorance in risk issues have not been tamed by scientific research and possibly never will." This describes only two positions out of numerous views in the hydraulic fracturing debate. Those absolutely opposed to hydraulic fracturing want all fracking activities to completely stop because of the unacknowledged risks. Those who fully support fracking want the resistance to cease so hydraulic fracturing can continue unimpeded, because they believe hydraulic fracturing is regulated enough to

ensure it is a safe process. Both of these extremes must be abandoned to move toward a fair process that includes all stakeholders and allows for arbitration of policies. In the next section, we acknowledge the challenges of democratic dialogue for fracking and outline an approach to negotiating equitable policies that ensures all stakeholders have a voice and all information is considered.

7.6.1 Challenges to a democratic approach

The modified framework that we believe will benefit the hydraulic fracturing debate is broadly outlined by Funtowicz & Ravetz (1993) as an "extended peer community" but it is also called the "extended participatory model" by Liberatore & Functowicz (2003). Others including Sarewitz (1996) and Pielke Jr (2007) have called for new models that increase democracy by public participation. The industry has made efforts to address the stakeholders through engagement – even creating pathways for two-way communication. However, these are motivated by CSR efforts and typically do not result in significant modifications to actions taken by industry. The theories about the function and implementation of participatory models are well developed, as we discussed at the beginning of this chapter. However, there is a gap between the theories and the practices that occur in the oil and gas industry.

After hydraulic fracturing was found to be economically feasible in 2003, there was a rush to purchase leases in the shale plays.[12] Oil and gas companies, focused on securing leases and acquiring more knowledge about how to fracture shale rock in horizontal wells, did not properly prepare for all of the impacts this drilling boom might have on local communities. The companies also underestimated the health and environmental impacts of the drilling.

A major part of business for the natural gas industry is getting the land with the best locations, and therefore the process of leasing is very secretive. Some companies will even buy land under different names to avoid identification and therefore to secure the greatest profits (Jaffe, 2011). Traditionally, the first contact a natural gas or oil company will make

[12] A study of the impact of gas extraction in Pennsylvania states that from 2005 to 2006, the number of permitted natural gas wells jumped by almost a thousand (Considine *et al.*, 2011).

with the community is through a letter in the mail or a landman (an industry representative) knocking on their door to obtain a lease (AAPL, 2014). The secretive nature extends to the fracking fluid components discussed above. The industry and public will need to work around these secrets to build trust that the industry is not hiding any crucial information.

We also argue that one of the biggest challenges is to move all stakeholders away from responding to concerns or issues with "facts." Each side of the hydraulic fracturing debate views the use of the technology as a black or white situation. The vast majority of oil and gas professionals truly believe hydraulic fracturing is an efficient, safe, and useful process, and is an integral part of our energy future. The opponents believe that hydraulic fracturing will always cause contamination and health risks. However, as we have seen from the documentaries, simplifying the issues down to only hard facts does not work. There will always be someone to refute the purportedly unquestionable statement. Solving technological controversies through data alone is ineffective. Hydraulic fracturing is past the point of being able to be resolved through fact trading. For ethical reasons, fair and democratic representation and debate should not be circumvented, but there are also practical reasons for the industry to slow down and revisit their typical procedures. The negative response from the public could be detrimental to more than just the local operations and begin to affect their broader profits.

Another problematic assumption frequently held by industry is that technocratic decision making – scientistic decision-making by a few, educated elite – is the best way to determine policy. Put another way, technocracy is the belief that all policy issues can be resolved by quantifying and separating facts from values to find the best solution, while ignoring citizens voice. All issues are processed by means of scientific research methods, which actually limit the suitable solutions that can be found, rather than expanding them (Pielke Jr, 2007).

Despite these challenges, there have been many attempts to implement some form of engagement model in areas with hydraulic fracturing by the industry. These efforts come from the individual oil and gas companies, sometimes under the banner of CSR. Depending

on the company the approach may include only a low-level of community participation, such as public hearings or town hall meetings. These are approaches that utilize one-way communication (Rowe & Frewer, 2005). In recent years though, there has been an emergence of more two-way communication programs.

In July 2014, the American Petroleum Institute (API) released "Community Engagement Guidelines" to "promote the safe and responsible development of the nation's oil and natural gas resources by engaging and respecting the communities where these operations occur" (API, 2014). The guidelines define engagement considerations for each stage of oil and gas projects: entry, exploration, development, operations/production, and exit (API, 2014). The main points for each phase are to identify and engage relevant stakeholders and establish clear communication pathways to ensure a dialogue can occur (API, 2014). The guidelines serve as a list of best practices for the oil and gas industry but also for what the communities can expect from the companies (API, 2014). These guidelines are a step toward ensuring a more democratic process.

However these best practices still fall short of the needed level of engagement that will lead to effective changes. The role of the industry as the sponsor for engagement programs creates a conflict of interest. Because the individual company determines the level of engagement with the stakeholders, the type of program and overall goal will vary. The same area may have several different operators that do not communicate with each other on the information given to stakeholders or how to reach them for comments. Many companies recognize the benefits of dialogue with stakeholders and make a good effort to create areas for communication. Some states also mandate a certain amount of public communication through public hearings or public notices (COGCC, 2014).[13] However when unfortunate events occur, the line of communication from the company to the community stakeholders may break. For example, if a well casing leaks, the company may not choose to disclose this information with the

[13]These types of hearings typically focus on the facts relayed by experts and largely ignore the anecdotes from the community. Endres (2009) describes an occurrence of this during the public hearings on the nuclear waste depository in Yucca Mountain.

greater community in order to protect their profits (although it would be reported to the state regulatory agency). There may also be situations where the gas company has a landowner sign a nondisclosure agreement after contamination has been found and a settlement made.

The balance of power must be restored for any type of engagement of stakeholders to be successful at qualifying and discussing policy options. The private actors (oil and gas companies) of hydraulic fracturing use their large amount of power and money to ensure policy is enacted that benefits their businesses. If only the industry is charged with creating places for engagement then this only increases the imbalance of power. Liberatore & Functowicz (2003) recognize this by stating, "The increased influence of private actors (from multinational corporations to local lobbies of various types) influencing public policy is widely recognized; thus a main question is whether such influence can be made more balanced, transparent and regulated."

The current industry engagement programs focus on how to make current practices safer and on increasing communication with stakeholders. But these programs do not discuss broader changes to regulations or procedures that would affect all fracking operators. Discussions about larger policy changes need to occur because there will always be more challenges to address in the hydraulic fracturing debate. If an effective engagement program is established, then new concerns can be discussed quickly and without controversy. Some of the current issues that are still being resolved are: induced seismicity (Ellsworth, 2013; van der Elst *et al.*, 2013), proximity of wells to residential areas, water use/supply, disclosure of chemicals, air emissions, and the fluctuation in natural gas prices.

In the next section, we offer suggestions for how a fair, democratic model might be structured but the fine details have to be fleshed out as this type of framework is implemented. We know there are many questions about the implementation of a democratic engagement model, which need to be addressed. These questions include the following: How would the power be distributed to participants from different backgrounds? Or would the new participants only play an advisory role? Who chooses the peer community? How is a

facilitator selected? Some of these questions we elaborate on below.

7.6.2 Extended peer communities/extended participation model

One concept that accommodates the complexities of the hydraulic fracturing debate is engagement/participation approaches to policy, which instead of limiting information, requires multiple perspectives and emphasizes citizen involvement (Fischer, 2003). The goal of engagement is to encourage participatory policy analysis, make data and analyses accessible to the public, and heighten the interaction between the public, decision makers, and policy analysts (Fischer, 2003). This policy method ensures that a suggested program is quantitatively verified, situationally relevant, societally approved, and ideologically supported. In other words, this method encompasses the views and opinions of those impacted at every level: scientists, engineers, industry, local residents, society as a whole, and particular communities (Fischer, 2003). Democracy is a large part of the motivation to approach policy debates with citizen participation because democracy ensures that procedures are in place that protect citizen's due process, role in deliberation, and rights (Liberatore & Functowicz, 2003). One version of participatory models is the extended participation model, which involves more than just participants with expert knowledge or accreditation. The extended participation models include any legitimate, competent participant who wants to resolve the issue (Funtowicz & Ravetz, 1993).

The group of participants is called the extended peer community and the goal is to determine the quality of information, expose underlying assumptions, and negotiate a policy solution (De Marchi, 2003; Funtowicz & Ravetz, 1993). Sarewitz (1996) states, "The policy goal is not to substitute 'common sense' for technical knowledge but to allow democratic dialogue to play its appropriate role in decision making that is inevitably dominated not by authoritative data but by subjective criteria and social norms." The extended peer community includes new participants from broader institutions including social and cultural movements (Funtowicz & Ravetz, 1993). For hydraulic fracturing, these new peers would be community members, landowners, leaders of environmental advocacy groups, regulators,

and industry employees from multiple operators. There should be different extended peer communities for each state because the regulations differ in each, and it may actually be more productive to develop small-extended peer communities by county.

An important factor of using the extended participatory model is establishing the validity and competence of participants (Funtowicz & Ravetz, 1993). True dialogue can only occur when the voice from all participants is valued equally. De Marchi (2003) warns that "[t]he most vociferous protestors are not necessarily those who represent the largest number of people, or those who are genuinely interested in going beyond mere activism." Those asked to join the extend peer community will need to focus on assessing the information and finding a solution instead of trumpeting their position. Accepting information from nonexperts may pose a challenge for the technical scientists, but it will be essential for the engagement program to be gainful (Kinsella, 2004).

For this type of model to be successful for the hydraulic fracturing debate, there needs to be a person in the margins that selects participants and assists with communication between the main stakeholders. This is someone who has a "vantage point" that allows them to see the numerous positions and diversity in knowledge but also to see how these may come together to find a policy solution (Foss *et al.*, 2002). Funtowicz & Ravetz (2001) call this person a facilitator who needs "to see [the] partial systems from a broader perspective, and find or create some overlap among them all." This person would ideally come from the government or some other impartial body to avoid the conflict of interest that occurs with an industry representative. A team of two facilitators, one with the technical knowledge and one well versed in the social science theories of participation, would make an excellent team. Their responsibilities would be to assist in determining appropriate participants, ensuring equal access to information, and moderating the discussion.

The group will need to allow for acceptance of a "plurality of knowledge" (Ravetz & Funtowicz, 1999). Exploring the interrelationships between the assumptions that make the core of each participant's position will allow the group to gain what Healy (1999) defines

as "mutual intersubjective sensitivity." Traditional information, such as scientific studies, are considered along with anecdotes and informal surveys which Funtowicz & Ravetz (1993) call "extended facts." This is in contrast to searching for some universal or impartial truth (as shown in the documentaries and fact war) to determine the policy direction (Ravetz & Funtowicz, 1999). The perspective from locals is valuable because they have local knowledge and greater concern about the quality of information (Funtowicz & Ravetz, 1993). Examples of valuable local knowledge are found in the documentaries. McAleer interviews a resident of Dimock, PA whose family had to stop using two of their wells in the 1970's, before the introduction of fracking to the area, because of high levels of iron and methane. Fox mentions how residents know the details of the local environment, such as the locations of streams and ponds. Anecdotes and narratives, which provide information only known to locals, play a larger role in negotiating towards a solution (Pielke Jr, 2007).

Another important aspect is ensuring that there is trust between all participants. Healy (1999) states, "Trust is both a rationale and a key requirement for extended peer communities. The taken-for-granted bond of trust that decision makers still regularly assume between science and the general community can no longer be relied upon." Those in the extended peer community will need to be transparent, open, and have a willingness to communicate (Healy, 1999). This may prove to be especially difficult for the industry because they hold much of the process of fracking a secret. Special provisions may need to be established to allow industry representatives to share the relevant information without losing their competitive edge.

The general theory of extended peer communities is well defined, such as who should participate and how to build trust, but the mechanism for the deliberation is not. We offer an insight of how to structure the dialogue to create successful interactions. The participatory engagement model has been put into practice under the name of "citizen's juries" or "focus groups" (Funtowicz & Ravetz, 2001). The Jefferson Jefferson Center (2014) defines a citizen's jury as a "randomly selected and demographically representative panel of citizens" that

meets over a period of days to discussion "an issue of public significance." This may offer an established set of rules that could be translated to a hydraulic fracturing extend peer community; the selection of participants and the time period would be modified to accommodate the extended peer community and the long-term implementation needed. Rowe & Frewer (2005) analyzed numerous participatory models and ranked them with respective to several different characteristics. The models that will be most successful for hydraulic fracturing are those with face-to-face contact, flexible input, controlled selection of the participants, and facilitation of the information and opinions (Rowe & Frewer, 2005). A mechanism that has all of these traits is deliberation opinion polls, which brings together a representative subset of participants to receive information, hear others opinions, and then discuss together the policy options (Fishkin & Luskin, 1999). Then participatory community is polled twice, before and after discussion on the issue (Rowe & Frewer, 2005). In 1996, this engagement model was put into practice for the National Issues Convention, where a national sample of about 400 Americans went to Texas to read prepared material and discuss issues for three days. Then the group questioned candidates for the Republican presidential nomination in person, with some parts broadcast on PBS (Fishkin & Luskin, 1999). The success of this model with broad, complex issues and diverse stakeholders from across the nation demonstrates that a similar model may be successful for hydraulic fracturing, although at a smaller scale and a higher frequency.

The hydraulic fracturing debate needs a long-term participatory-based approach to spread information, listen to opinions, and assess policy options. This effort would be most successful if a governmental regulatory body, such as the EPA or a state body such as the COGCC, spearheads the program. The engagement model should be crafted specifically for each state (because of the diversity of regulations) and possibly even for individual counties or towns. The goal should be to establish a program that will exist during the period of active well sites in the local area, which could be decades or years depending on the region. Funding this level of participation may be outside the realistic amount from only the government. If

several local oil and gas companies (who operate in the region) sponsored the effort, then a more effective program could be developed that could have a larger impact. Participants should be chosen for their willingness to hear all sides and discuss options. These participants should be selected through a structured process from the local community, the governmental regulatory bodies, and the local oil and gas operators. The discussion should include information about the risks and benefits of hydraulic fracturing – from the increase in jobs to the water contamination risk. The facilitators should work to ensure that all relevant information (technical and nontechnical) is shared and understood by all. The discussion should push the participants to extract where broader policies are needed and where better practices should be enacted.

7.7 Summary

We argue that the high uncertainties and diverse values of the stakeholders qualify hydraulic fracturing as a post-normal technology. The fracking documentaries demonstrate how hydraulic fracturing has not followed the standard scenario, and that significant amounts of stakeholder engagement are needed to develop sound, ethical energy policy options. Developing a fair engagement approach for hydraulic fracturing will not be simple. We acknowledge that there is no clear formula for stakeholder engagement that is guaranteed to work to the satisfaction of all involved but that is not the goal. However, we outline several key characteristics of the engagement model needed for hydraulic fracturing. The rapidly rising energy needs threaten to increase the number of future energy controversies. Thus, it is vital to establish models for democratic deliberation now.

CHAPTER 8

GENERAL CONCLUSIONS

This chapter contains a summary of the general conclusions of the overall thesis and future research suggestions. For more detailed conclusions, please refer to the conclusions given in Chapters 2 through 6.

In this thesis, I expand the application of optimally weighted synthetic aperture to controlled-source electromagnetics, which increases the detectability of hydrocarbon reservoirs, better defines the lateral position and extent of these reservoirs, and reduces independent, random noise within the response. In Chapter 2, I first demonstrate the inclusion of crossline sources in the synthetic aperture array, which creates a 2D source. I test the 2D synthetic aperture source on modeled diffusive fields and show that coherent steering is possible even with sources 2 km apart. I also introduce a new visualization tool to view the direction and propagation of a frequency-domain field. The phase-binned gradient allows one to analyze the changes caused by the application of synthetic aperture. The direction of the phase-binned gradient of the diffusive field from the 2D steered synthetic aperture source shows that there is more upgoing energy, indicating the application of synthetic aperture enables more energy to reach the seafloor.

In Chapter 3, I apply 2D synthetic aperture to simulated electromagnetic fields from a modeled CSEM survey over a typical deep-water situation with a single reservoir. I use exponential weighting, with a phase shift and energy compensation term, to steer the 2D synthetic aperture source in both the inline and crossline directions. The best steering parameters are determined by defining a range of possible combinations of angles and amplitudes, and then searching for the combination that maximizes the detectability ratio. For the synthetic deep-water model, I show that the application of 2D steered synthetic aperture increases the detectability of the reservoir from barely detectable for a single source to

unquestionably detectable for the 2D steered synthetic aperture source. An examination of the Poynting vectors (the energy flux density of the electromagnetic field) shows that more energy travels down towards the reservoir with the 2D steered synthetic aperture response than with the single source response. The Poynting vector is a useful visualization tool to determine if the steered synthetic aperture response favorably changes the direction of the energy.

In Chapter 4, I introduce a new optimization method to find the optimal weights for synthetic aperture. The exponential weighting that I used previously in Chapter 3 restricts the radiation pattern of the synthetic aperture source to a plane wave at a fixed angle. Using a single complex number as the weight for each source in the synthetic aperture array allows one to steer and focus the source array. The optimization method relies on the information encoded in the reservoirs to determine the optimal weights, instead of requiring the user to determine the steering or focusing direction. For each synthetic aperture source array location, the optimal weights adjust to maximize the anomaly from the reservoir. With synthetic electromagnetic responses from a model with two reservoirs laterally separated, I show that the application of optimally weighted synthetic aperture increases the magnitude of the anomaly from the reservoir, decreases random, independent noise, and better defines the lateral position and extent of the two reservoirs. The optimal weights found by the optimization are verified with an analytic focusing equation. The optimization method works with any survey geometry and any size of synthetic aperture array.

In Chapter 5, I show how to design the synthetic aperture source to maximize the anomaly from the reservoir and decrease the presence of random, independent noise. The inclusion of a term to minimize the variance of the noise in the objective function allows for one to reduce the presence of the noise while maximizing the anomaly from the reservoir. I demonstrate the ability of optimally weighted synthetic aperture to recover the signal from the reservoir even when the original responses are dominated by noise. With this technique, there is a lower noise floor, less noise streaks, and a stronger anomaly from the reservoir, which enables

CSEM to be implemented in situations where the towlines must be positioned kilometers away from the receivers.

Chapter 6 shows results from sensitivity tests of the calculation of the optimal weights for synthetic aperture. I show that the synthetic aperture response from incorrect weights is robust to changes in the overburden resistivity, overburden anisotropy, and location of the target. One can use subsurface models, built from only estimates of the geologic structure and physical properties, to determine a set of weights for synthetic aperture that will increase the anomaly from the target.

There are several areas of potential future research that may answer questions raised by the above conclusions. The first is how synthetic aperture affects the inversion results of CSEM data. Typically, the electric and magnetic responses of CSEM surveys are inverted to solve for a resistivity model of the subsurface. From an inversion perspective, synthetic aperture is a data transform, where the responses are combined to reduce the overall amount of data. However because of the non-linearity of electromagnetic inversions, the influence of synthetic aperture on inversion is not clear. Synthetic aperture may combine the data in a way that allows the inversion to better define the resistivities of the structures. To quantify the full impact of synthetic aperture, the method must be applied to real electromagnetic fields and then inverted. Synthetic aperture has been applied to real data with success. Most recently Engelmark *et al.* (2013) and Mattsson *et al.* (2013) acquired data with a towed EM system and applied synthetic aperture to increase detectability. Especially with towed systems, noise is significant. Synthetic aperture could be designed to reduce the correlated noise that often occurs in CSEM surveys, such as from tides and swells. The framework detailed in Chapter 5 could be extended to include the minimization of correlated noise.

Synthetic aperture also needs to be tested in more complicated settings, such as a reservoir near salt or a deep reservoir underneath shallow gas hydrates. For the case where there are gas hydrates present above a reservoir, there may be benefits of applying synthetic aperture with multiple frequencies. The electromagnetic responses from a higher frequency ($\sim$5–12

Hz) characterize shallow anomalies, while the responses from a lower frequency (∼0.1–1 Hz) characterize deeper targets. One could apply synthetic aperture to reduce the presence of the shallow anomaly and highlight the deeper anomaly by optimally weighting sources in synthetic aperture arrays for each frequency, and then optimally combining the synthetic aperture responses. Yoon & Zhdanov (2014) demonstrate the reduction of the airwave with the application of synthetic aperture. Implementing different detectability measures may allow the synthetic aperture source to be designed specifically for reducing undesired signals like the airwave. The full contribution of synthetic aperture for CSEM is still not completely understood, and more research on this topic could expand the application of CSEM to new areas.

REFERENCES CITED

AAPL. 2014. *About Landmen*. http://www.americaslandman.com/about-landmen.

API. 2014. *Community Engagement Guidelines*. http://www.api.org/news-and-media/news/newsitems/2014/july-2014/~/media/Files/Policy/Exploration/100-3_e1.pdf.

Arthur, J. D., Bohm, B., & Layne, M. 2008a. *Hydraulic Fracturing Considerations for Natural GasWells of the Marcellus Shale. The Ground Water Protection Council Annual Forum*. http://www.dec.ny.gov/docs/materials_minerals_pdf/GWPCMarcellus.pdf.

Arthur, J. D., Langhus, B., & Alleman, D. 2008b. *An overview of modern shale gas development in the United States*. http://www.all-llc.com/publicdownloads/ALLShaleOverviewFINAL.pdf.

Aster, R. C., Thurber, C. H., & Borchers, B. 2005. *Parameter estimation and inverse problems, v. 90*. International geophysics series. Amsterdam, Boston: Elsevier Academic Press.

Avery, T. E., & Berlin, G. L. 1985. *Interpretation of aerial photographs*. 4th edition edn. Minneapolis, Minn: Burgess Pub. Co.

Barber, B. C. 1985. Theory of digital imaging from orbital synthetic aperture radar. *International Journal of Remote Sensing*, **6**(7), 1009–1057.

Bellettini, A., & Pinto, M. A. 2002. Theoretical Accuracy of Synthetic Aperture Sonar Micronavigation Using a Displaced Phase-Center Antenna. *IEEE Journal of Oceanic Engineering*, **27**(4), 780–789.

Bevington, P., & Robinson, D. K. 2002. *Data Reduction and Error Analysis for the Physical Sciences*. 3rd edition edn. Boston: McGraw-Hill Science/Engineering/Math.

Boas, M. 1983. *Mathematical methods in the physical sciences*. 2nd edn. New York: Wiley.

Brady, B., Elbel, J., Mack, M., Morales, H., Nolte, K., & Poe, B. 1992. Cracking Rock: Progress in Fracture Treatment Design. *Oilfield Review*, **4**(4), 4–17.

Brown, M. 2007. Energy myth one – Today's energy crisis is "hype". *Pages 23–50 of:* Sovacool, B., & Brown, M. (eds), *Energy and American Society: Thirteen Myths*. New York: Springer.

Brufatto, C., Cochran, J., Conn, L., Power, D., El-Zeghaty, S., Fraboulet, B., Griffin, T., James, S., Munk, T., Justus, F., Levine, J., Montgomery, C., Murphy, D., Pfeiffer, J., Pornpoch, T., & Rishmani, L. 2003. From mud to cement - Building gas wells. *Oilfield Review*, 62–76.

Buland, A., Lseth, L. O., Becht, A., Roudot, M., & Rsten, T. 2011. The value of CSEM data in exploration. *First Break*, **29**(4), 69–76.

Chen, J., & Dickens, T. A. 2009. Effects of uncertainty in rock-physics models on reservoir parameter estimation using seismic amplitude variation with angle and controlled-source electromagnetics data. *Geophysical Prospecting*, **57**(1), 61–74.

Chen, J., Al-Wadei, M. H., Kennedy, R. C. M., & Terry, P. D. 2014. Hydraulic Fracturing: Paving the Way for a Sustainable Future? *Journal of Environmental and Public Health*, **2014**(Mar.), Article ID e656824, 10 pages.

Cheney, M., & Borden, B. 2009. *Fundamentals of Radar Imaging*. Philadelphia: Society for Industrial and Applied Mathematics.

COGCC. 2013. *Series Safety Regulations*. `https://cogcc.state.co.us/RR_Docs_new/rules/600Series.pdf`.

COGCC. 2014. *Colorado Oil and Gas Conservation Commission*. `http://cogcc.state.co.us/`.

ConocoPhillips. 2014. *Stakeholder Engagement Principles*. `http://www.conocophillips.com/sustainable-development/people-society/engaging-stakeholders/Pages/stakeholder-engagement-principles.aspx`.

Considine, T., Watson, R., & Blumsack, S. 2011. *The Pennsylvanian Marcellus Natural Gas Industry: Status, Economic Impacts and Future Potential. Pennsylvania State University*. `http://marcelluscoalition.org/wp-content/uploads/2011/07/Final-2011-PA-Marcellus-Economic-Impacts.pdf`.

Constable, S. 2010. Ten years of marine CSEM for hydrocarbon exploration. *Geophysics*, **75**(5), 75A67–75A81.

Constable, S., & Srnka, Leonard J. 2007. An introduction to marine controlled-source electromagnetic methods for hydrocarbon exploration. *Geophysics*, **72**(2), WA3–WA12.

Davies, R. 2011. Methane contamination of drinking water caused by hydraulic fracturing remains unproven. *Proceedings of the National Academy of Sciences of the United States of America*, **108**(43), E871.

De Marchi, B. 2003. Public participation and risk governance. *Science and Public Policy*, **30**(3), 171–176.

Depoe, S. P., Delicath, J., & Aepli Elsenbeer, M. 2004. *Communication and Public Participation in Environmental Decision Making*. SUNY Press.

DOE. 2009. *Modern Shale Gas Development in the United States: A Primer*. `http://energy.gov/fe/downloads/modern-shale-gas-development-united-states-primer`.

Edwards, N. 2005. Marine Controlled Source Electromagnetics: Principles, Methodologies, Future Commercial Applications. *Surveys in Geophysics*, **26**(6), 675–700.

EIA. 2014a. *Primary Energy Consumption by Source. Monthly Energy Review*. `http://www.eia.gov/totalenergy/data/monthly/pdf/sec1_7.pdf`.

EIA. 2014b. *Short-Term Energy Outlook: Natural Gas*. `http://www.eia.gov/forecasts/steo/report/natgas.cfm`.

Ellingsrud, S., Eidesmo, T., Johansen, S., Sinha, M., MacGregor, L., & Constable, S. 2002. Remote sensing of hydrocarbon layers by seabed logging (SBL): Results from a cruise offshore Angola. *The Leading Edge*, **21**(10), 972–982.

Ellsworth, W. L. 2013. Injection-Induced Earthquakes. *Science*, **341**(6142), 1225942.

Endo, M., & Zhandanov, M. 2009. *IBCEM3D: www.cemi.utah.edu/soft/index.html*.

Endres, D. 2009. Expanding Notions of the Scientific Argument: A case study of the use of scientific argument by American Indians. *Pages 187–208 of:* Kahlor, L, & Stout, P (eds), *Understanding and Communicating Science: New agendas in communication*. Routledge.

Engelmark, F., McKay, A., & Mattsson, J. 2013. Application of synthetic aperture concepts to Towed Streamer EM data. *23rd International Geophysical Conference and Exhibition, ASEG Expanded Abstracts*, 1–4.

EPA. 2014. *Regulation of Hydraulic Fracturing Under the Safe Drinking Water Act*. `http://water.epa.gov/type/groundwater/uic/class2/hydraulicfracturing/wells_hydroreg.cfm`.

Fan, Y., Snieder, R., Slob, E., Hunziker, J., Singer, J., Sheiman, J., & Rosenquist, M. 2010. Synthetic aperture controlled source electromagnetics. *Geophysical Research Letters*, **37**(13), L13305.

Fan, Y., Snieder, R., Slob, E., Hunziker, J., & Singer, J. 2011. Steering and focusing diffusive fields using synthetic aperture. *Europhysics Letters*, **95**(3), 34006.

Fan, Y., Snieder, R., Slob, E., Hunziker, J., Singer, J., Sheiman, J., & Rosenquist, M. 2012. Increasing the sensitivity of controlled-source electromagnetics with synthetic aperture. *Geophysics*, **77**(2), E135–E145.

Farrah, R. 1992. *Origins of EPA. The Guardian.* `http://www2.epa.gov/aboutepa/guardian-origins-epa`.

Fischer, F. 2003. Beyond empiricism: policy analysis as deliberative practice. *Pages 209–227 of:* Hajer, M, & Wagenaar, H (eds), *Deliberative policy analysis: Understanding governance in network society.* Cambridge: Cambridge University Press.

Fishkin, J., & Luskin, R. 1999. Bringing Deliberation to the Democratic Dialogue. *Pages 3–37 of:* Mccombs, M., & Reynolds, A. (eds), *The Poll With A Human Face: The National Issues Convention Experiment in Political Communication.* Mahwah, NJ: Lawrence Erlbaum Associates.

Foss, S., Foss, K., & Trapp, R. 2002. *Contemporary perspectives on rhetoric.* Waveland Press.

Fox, J. 2010. *Affirming Gasland.* `http://www.gaslandthemovie.com/whatisfracking/affirminggasland`.

FracFocus. 2011. *Hydraulic Fracturing Fluid Product Component Information Disclosure. Chemical Disclosure Search.* `http://www.fracfocusdata.org/DisclosureSearch/SearchResults.aspx`.

Frynas, J. G. 2009. Corporate social responsibility in the oil and gas sector. *The Journal of World Energy Law & Business*, **2**(3), 178–195.

Funtowicz, S., & Ravetz, J. 2001. Post-Normal Science. Science and Governance under Conditions of Complexity. *Pages 15–24 of:* Decker, M., & Wtscher, F. (eds), *Interdisciplinarity in Technology Assessment.* Wissenschaftsethik und Technikfolgenbeurteilung, no. 11. Springer Berlin Heidelberg.

Funtowicz, S. O., & Ravetz, J. R. 1993. Science for the post-normal age. *Futures*, **25**(7), 739–755.

Funtowicz, S. O., & Ravetz, J. R. 1994. Uncertainty, complexity and post-normal science. *Environmental Toxicology and Chemistry*, **13**(12), 1881–1885.

Gabrielsen, P. T., Brevik, I., Mittet, R., & Løseth, L. O. 2009. Investigating the exploration potential for 3D CSEM using a calibration survey over the Troll Field. *First Break*, **27**(6), 63–71.

Griffiths, D. J. 2008. *Introduction to electrodynamics*. San Francisco: Pearson.

Griswold, E. 2011 (Nov.). *The Fracturing of Pennsylvania. The New York Times*. http://www.nytimes.com/2011/11/20/magazine/fracking-amwell-township.html?pagewanted=all&_r=0.

Hajer, M. A. 2003. *Deliberative Policy Analysis: Understanding Governance in the Network Society*. Cambridge University Press.

Hall, K. 2011. Regulation of hydraulic fracturing under safe drinking water act. *Westlaw*, **31**(18), 1–7.

Healy, S. 1999. Extended peer communities and the ascendence of post-normal politics. *Futures*, **31**, 655–669.

Helms, L. 2008. Horizontal drilling. *North Dakota Department of Mineral Resources Newsletter*, **35**(1), 1–3.

Hesthammer, J., Stefatos, A., Boulaenko, M., Fanavoll, S., & Danielsen, J. 2010. CSEM performance in light of well results. *The Leading Edge*, **29**(1), 34–41.

Holder, D. 2008. *Founding principles guide "better business" publication through half century of change. American Oil & Gas Reporter*. http://www.aogr.com/about-us/history.

Holzer, B. 2008. Turning stakeseekers into stakeholders: A political coalition perspective on the politics of stakeholder influence. *Business & Society*, **47**(1), 50–67.

Howarth, R. W., Santoro, R., & Ingraffea, A. 2011a. Methane and the greenhouse-gas footprint of natural gas from shale formations. *Climatic Change*, **106**(4), 679–690.

Howarth, R. W., Ingraffea, A., & Engelder, T. 2011b. Natural gas: Should fracking stop? *Nature*, **477**(7364), 271–275.

Hubbert, M. K., & Willis, D. 1957. Mechanics of hydraulic fracturing. *Petroleum Transactions, AIME*, **210**, 133–168.

Hursán, G., & Zhdanov, M. 2002. INTEM3D. *www.cemi.utah.edu/soft/index*.

IMDb. 2011. *Gasland (2010) Awards*. http://www.imdb.com/title/tt1558250/awards?ref_=tt_awd.

Itoh, K. 1982. Analysis of the phase unwrapping algorithm. *Applied Optics*, **21**(14), 2470.

Jackson, J. D. 1999. *Classical electrodynamics*. New York: Wiley.

Jaffe, M. 2011 (Oct.). *Oil companies rushing to buy leases along Colorado's Front Range The Denver Post*. http://www.denverpost.com/ci_19169758?source=infinite.

Jefferson Center. 2014. *Citizens Juries*. http://jefferson-center.org/what-we-do/citizen-juries/.

Jensen, J., Ivanov, N. S., Gammelmark, K. L., & Pedersen, M. H. 2006. Synthetic aperture ultrasound imaging. *Ultrasonics*, **44**, e5–e15.

Kinsella, W. 2004. Public Expertise: Public Expertise: A Foundation for Citizen Participation in Energy and Environmental Decisions. *Pages 83–95 of:* Depoe, S. P., Delicath, J., & Aepli Elsenbeer, M. (eds), *Communication and Public Participation in Environmental Decision Making*. Albany, NY: State University of New York Press.

Knaak, A., Snieder, R., Fan, Y., & Ramirez-Mejia, D. 2013. 3D synthetic aperture and steering for controlled-source electromagnetics. *The Leading Edge*, **32**(8), 972–978.

Laird, F. N. 1993. Participatory Analysis, Democracy, and Technological Decision Making. *Science, Technology & Human Values*, **18**(3), 341–361.

Lengwiler, M. 2008. Participatory Approaches in Science and Technology Historical Origins and Current Practices in Critical Perspective. *Science, Technology & Human Values*, **33**(2), 186–200.

Liberatore, A., & Functowicz, S. 2003. 'Democratising' expertise, 'expertising' democracy: what does this mean, and why bother? *Science and Public Policy*, **30**(3), 146–150.

Løseth, L. O., Pedersen, H. M., Ursin, B., Amundsen, L., & Ellingsrud, S. 2006. Low-frequency electromagnetic fields in applied geophysics: Waves or diffusion? *Geophysics*, **71**(4), W29–W40.

Maaø, F., & Nguyen, A. 2010. Enhanced subsurface response for marine CSEM surveying. *Geophysics*, **75**(3), A7–A10.

Mandelis, A. 2000. Diffusion Waves and their Uses. *Physics Today*, **53**(8), 29–34.

Mattsson, J., Lindqvist, P., Juhasz, R., & Bjrnemo, E. 2012. Noise reduction and error analysis for a Towed EM System. *82th Annual International Meeting, SEG, Expanded Abstracts*, 795–799.

Mattsson, J., Engelmark, F., & Anderson, C. 2013. Towed streamer EM: the challenges of sensitivity and anisotropy. *First Break*, **31**(6), 155–159.

McKenzie, L., Witter, R., Newman, L., & Adgate, J. 2012. Human health risk assessment of air emissions from development of unconventional natural gas resources. *Science of the Total Environment*, **424**(May), 79–87.

Mittet, R., & Morten, J. 2012. Detection and imaging sensitivity of the marine CSEM method. *Geophysics*, **77**(6), E411–E425.

Montgomery, C., & Smith, M. 2010. Hydraulic fracturing: History of an enduring technology. *Journal of Petroleum Technology*, **62**(12), 26–41.

Myer, D., Constable, S., Key, K., Glinsky, M., & Liu, G. 2012. Marine CSEM of the Scarborough gas field, Part 1: Experimental design and data uncertainty. *Geophysics*, **77**(4), E281–E299.

National Geographic. 2014. *The Great Shale Gas Rush News*. `http://news.nationalgeographic.com/news/energy/2010/10/101022-energy-marcellus-shale-gas-rush/`.

Newman, G., Commer, M., & Carazzone, J. 2010. Imaging CSEM data in the presence of electrical anisotropy. *Geophysics*, **75**(2), F51–F61.

Orange, A., Key, K., & Constable, S. 2009. The feasibility of reservoir monitoring using time-lapse marine CSEM. *Geophysics*, **74**(2), F21–F29.

Osborn, S., Vengosh, A., Warner, N., & Jackson, R. 2011. Methane contamination of drinking water accompanying gas-well drilling and hydraulic fracturing. *Proceedings of the National Academy of Sciences of the United States of America*, **108**(20), 8172–8176.

Parkhurst, J., Price, G., Sharrock, P., & Moore, C. 2011. Phase unwrapping algorithms for use in a true real-time optical body sensor system for use during radiotherapy. *Applied Optics*, **50**(35), 6430–6439.

Pielke Jr, R. A. 2007. *The Honest Broker: Making Sense of Science in Policy and Politics*. Cambridge University Press.

Pless, J. 2012. *Natural Gas Development and Hydraulic fracturing: A policymaker's guide. National Conference of State Legislatures*.

Rafferty, M. A., & Limonik, E. 2013. Is Shale Gas Drilling an Energy Solution or Public Health Crisis? *Public Health Nursing*, **30**(5), 454–462.

Ravetz, J., & Funtowicz, S. 1999. Post-Normal Science - an insight now maturing. *Futures*, **31**, 641–646.

Richardson, N., Gottlieb, M., Krupnick, A., & Wiseman, H. 2013. *The State of State Shale Gas Regulation. Resources for the Future.* `http://www.rff.org/rff/documents/RFF-Rpt-StateofStateRegs_Report.pdf`.

Rowe, G., & Frewer, L. J. 2000. Public Participation Methods: A Framework for Evaluation. *Science, Technology & Human Values*, **25**(1), 3–29.

Rowe, G., & Frewer, L. J. 2005. A Typology of Public Engagement Mechanisms. *Science, Technology & Human Values*, **30**(2), 251–290.

Sarewitz, D. 1996. *Frontiers Of Illusion: Science, Technology, and the Politics of Progress.* Temple University Press.

Sasaki, Y., & Meju, M. 2009. Near-surface effects on 3D marine CSEM responses: Implications for reducing uncertainty in energy resource exploration. *Proceedings of the 9th SEGJ International Symposium, Sapporo, Japan*, Jan., 1–4.

Schroeder, D. V. 1999. *An introduction to thermal physics.* San Francisco, CA: Addison Wesley.

Shanker, A. P., & Zebker, H. 2010. Edgelist phase unwrapping algorithm for time series InSAR analysis. *Journal of the Optical Society of America A*, **27**(3), 605–612.

Silva Crepaldi, J., Pereira Buonora, M., & Figueiredo, I. 2011. Fast marine CSEM inversion in the CMP domain using analytical derivatives. *Geophysics*, **76**(5), F303–F313.

STRONGER. 2014. *State Review of Oil and Natural Gas Environmental Regulations.* `http://www.strongerinc.org/`.

van der Elst, N. J., Savage, H. M., Keranen, K. M., & Abers, G. A. 2013. Enhanced Remote Earthquake Triggering at Fluid-Injection Sites in the Midwestern United States. *Science*, **341**(6142), 164–167.

Van Veen, B. D., & Buckley, K. M. 1988. Beamforming: a versatile approach to spatial filtering. *IEEE ASSP Magazine*, **5**(2), 4–24.

Wang, C., & Mandelis, A. 1999. Purely thermal-wave photopyroelectric interferometry. *Journal of Applied Physics*, **85**(12), 8366–8377.

Wang, H., Weaver, J. B., Perreard, I., Doyley, M., & Paulsen, K. D. 2011. A three-dimensional quality-guided phase unwrapping method for MR elastography. *Physics in Medicine and Biology*, **56**(13), 3935–3952.

Weitemeyer, K., Gao, G., Constable, S., & Alumbaugh, D. 2010. The practical application of 2D inversion to marine controlled-source electromagnetic data. *Geophysics*, **75**(6), F199–F211.

Yodh, A., & Chance, B. 1995. Spectroscopy and Imaging with Diffusing Light. *Physics Today*, **48**(3), 34–40.

Yoon, D., & Zhdanov, M. 2014. An optimal synthetic aperture method for the creation of directional sensitivity and removal of the airwave effect in MCSEM data. *84th Annual Internation Meeting, SEG Expanded Abstracts*, 685–690.

Ziolkowski, A., & Wright, D. 2010. Signal–to–Noise Ratio of CSEM data in Shallow Water. *80th Annual International Meeting, SEG, Expanded Abstracts*, 685–689.